AD-A255 791

(12)

DTIC
ELECTE
SEP 2 8 1992
S D
C

UNIVERSITY OF CINCINNATI
COLLEGE OF ENGINEERING

92 9 15 064

92-25239
42214
126
pg

Department of Electrical and Computer Engineering

Final Report
ONR Grant N00014-88-2035

LEVEL-MIXING ASSISTED TUNABILITY OF NUCLEAR RESONANCE LINEWIDTHS FOR GAMMA-RAY LASERS

Contractor: **Dr. P. Boolchand**
Professor, Electrical and Computer Engineering
University of Cincinnati
Phone: 513-556-4758 (office); 556-4790 (laboratory)
FAX: 513-556-7326

Subcontractor: **Dr. R. Coussement**
Professor, Katholieke Universiteit
Instituut Voor Kern En Stralingsfysika
3030 Heverlee
Belgium
Phone: 32-16-20-10-15
FAX: 32-16-29-19-59

Submitted to: **Dr. Paul Kepple**
Naval Research Laboratory
Code 4720, Building A50, Room #141****
Washington, DC 20375-5320
Phone: 202-767-3169

DTIC QUALITY INSPECTED 3

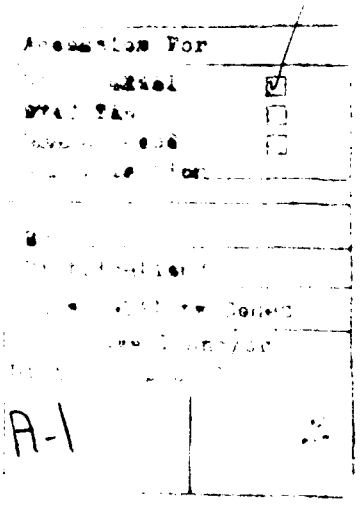

Statement A per telecon Dr. Kepple
NRL/Code 4720 Washington, DC 20375

JK 9/24/92

List of Contents

I. Overview

The present approach to a γ-ray laser is based on the use of a long-lived nuclear state (isomer $\tau > 1$ sec) acting both as the storage and lasing level. The present approach requires that nuclear resonant emission occur from long-lived states. We have examined the issue both theoretically and experimentally. Theoretically, as discussed in a recent paper, there are reasons to believe that for long-lived states ($\tau >$ few msec) the controlling width for nuclear resonance is not the natural linewidth (Γ_n) but the homogeneously broadened relaxation width (h/τ_r). This would make observation of the Mössbauer effect from long-lived states less stringent than previously believed.

Experimentally, our efforts have continued to focus on observing the Mössbauer effect with the 88 keV level in ^{109}Ag possessing a meanlife ($\bar{\tau}$) of 57.14 seconds. A facility dedicated to these experiments and based on a vibration-free He-closed cycle cryostat which can provide for T-variation and control at cryogenic temperatures was developed during the course of this grant. The first results on the resonant self absorption experiments on this facility are now available and are discussed in section II of the report.

During the course of these Mössbauer resonant self-absorption experiments, we began to suspect that the smallness of the effect could be due to the presence of a small (300 mGauss) but finite earths magnetic field on the ^{109}Cd/Ag source. This magnetic field actually leads to an enormous Nuclear-Zeeman splitting ($\sim 10^6\Gamma_n$) which reduces the resonant cross-section available in the self-absorption measurements by approximately a factor of 4. This is a point discussed later in section II. Furthermore, presence of this magnetic field on the source, in principle, also destroys partially the nuclear dipole-dipole coupling between the

Ag nuclei in Ag metal. This coupling, we believe, is needed to promote relaxation (τ_r) at the zero-field nuclear level-crossing (prevailing for cubic Ag) to produce homogeneous line broadening (h/τ_r). In the absence of this homogeneous line-broadening, the Mössbauer effect from the long-lived state may not be feasible. For these two specific reasons, experimental efforts towards reducing the ambient magnetic field on the source by four orders of magnitude were undertaken and successfully carried out. The underlying effort is discussed in section II.

The tunability of nuclear relaxation at level-crossings constitutes the second basic principle that must be unambiguously demonstrated for the present approach to a γ-ray laser to be feasible. The spin I=1, 29.4 ms mean-life level in ^{12}B produced in a spin polarized state and implanted in a crystalline host, provides an elegant atomic scale probe of nuclear relaxation in solids. The case of face-centered-cubic Al single crystal in an external magnetic field has been investigated by us in detail. At finite magnetic fields the ^{12}B hyperfine interaction (gap) can equal the ^{27}Al hyperfine splitting. At such fields the initial ^{12}B polarization can be resonantly transferred to the ^{27}Al nuclei. The ^{12}B spin polarization measured as a function of applied magnetic fields will display resonances at these special fields. These resonances have now been identified as multi-spin level-mixing resonances. Time-differential measurements of the asymmetry at level-crossing magnetic fields has for the first time permitted us to extract relaxation times (τ_r). These results discussed in section III clearly demonstrate the tunability of τ_r at nuclear-level crossings. These results constitute an important building block in realization of a γ-ray laser based on the present approach.

II. Status of Mössbauer Effect Experiments from Long-Lived States

a. Experimental Considerations

We designed a self-absorption experiment in which geometry changes of the cold finger upon cooling to He-temperatures are minimized. We have used a cold finger cooled by a He-closed cycle refrigerator (Model CS202 from APD, Inc.) in which the expander (DMX-20) vibrations are totally decoupled from the sample. The decoupling was confirmed by measuring the linewidth on the inner two lines of α-Fe in a conventional ^{57}Fe Mössbauer experiment and displayed evidence of no measurable line-broadening upon switching on the expander. In the ^{109}Ag experiment, we detected the gamma rays in a Ge detector, whose axis is perpendicular to the direction of contraction of the cold-finger. Because of this geometric configuration and also because of the comparatively shorter length of the cold-finger in these refrigerators (in relation to the length of liquid He dewars used by previous workers) our experimental arrangement is at least two-orders of magnitude less sensitive to geometry changes induced by cooling. Furthermore, we have the advantage that we can scan the full temperature range from 10K up to 300K, without touching the system.

b. Nuclear Zeeman Splitting in ^{109}Ag

Table I lists the relevant Mössbauer parameter of the 88 keV γ-resonance. Presently the most noteworthy parameter in this table, is the nuclear Zeeman splitting of 5.55×10^{-11}eV expected in a 1 Gauss field, which represents a 4.8×10^{6} Γ_n. The Zeeman splitting is illustrated in Fig. 1. In a 1 Gauss field the two outermost members of the 14 line multiplet structure are separated by 94.64 nm/s in velocity units. In a resonant self-absorption measurement since the emitting and absorbing nuclei are both present in the same magnetic field, the relevant hyperfine structure is the one shown in Fig. 2. It consists of a 21 line multiplet

TABLE I

MÖSSBAUER PARAMETERS OF THE
88 keV γ-RESONANCE IN ^{109}Ag

- 88.034 keV level, $I_e = 7/2^+$
- MEAN LIFE $\bar{\tau} = 57.14s$
- MULTIPOLARITY - E3 Transition $I_e = 7/2^+ \rightarrow I_g = 1/2^-$
- Natural Linewidth $\hbar/\bar{\tau} = \Gamma_n = \hbar/\bar{\tau} = 1.153x\ 10^{-17}$ eV
- NUCLEAR ZEEMAN SPLITTING in 1 Gauss Field:

  189.28 nm/s or $4.816 \times 10^6 \Gamma_n$ or 5.55×10^{-11} eV
- GRAVITATIONAL RED SHIFT over a 1μ fall:

  $0.83\ \Gamma_n$ or 0.96×10^{-17} eV
- SECOND-ORDER-DOPPLER SHIFT at T > 100K

  1.12×10^{-10} eV/K or Γ_n /μK

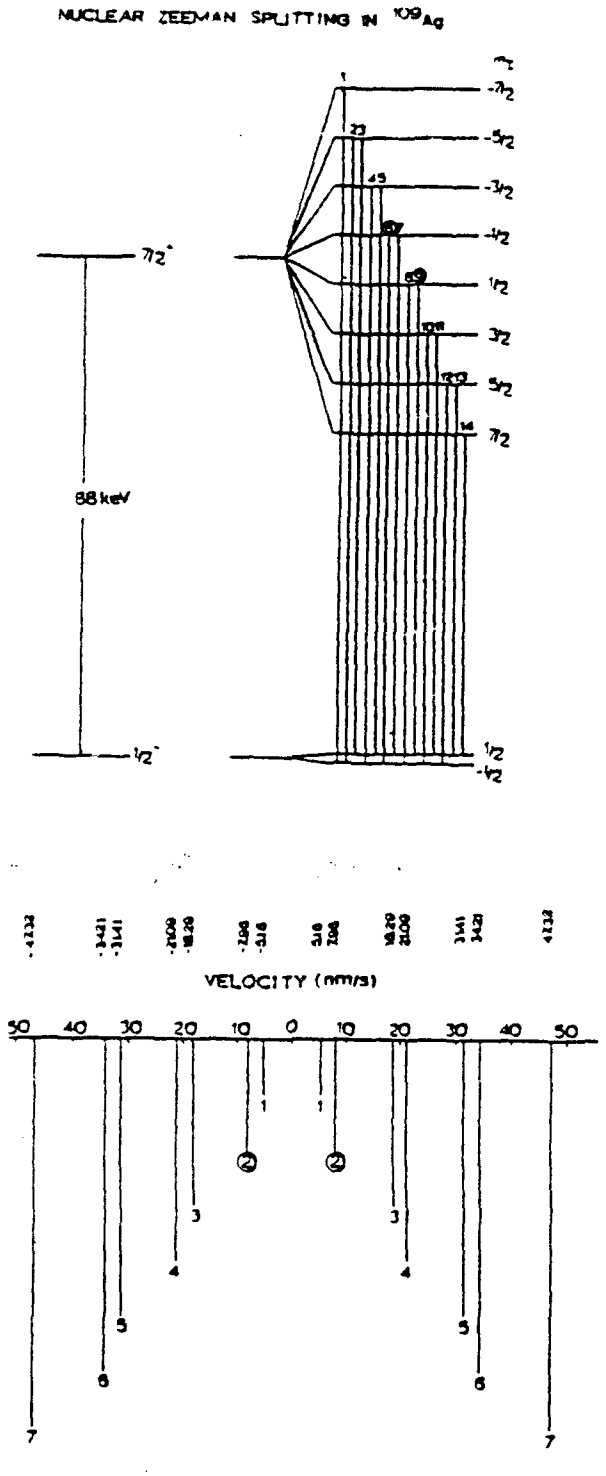

Fig. 1. Nuclear Zeeman splitting of the 88 keV γ-resonance in a 1 Gauss external magnetic field (top). Expected Mössbauer spectrum with a single line source and split absorber (bottom) would consist of a 14-line multiplet structure.

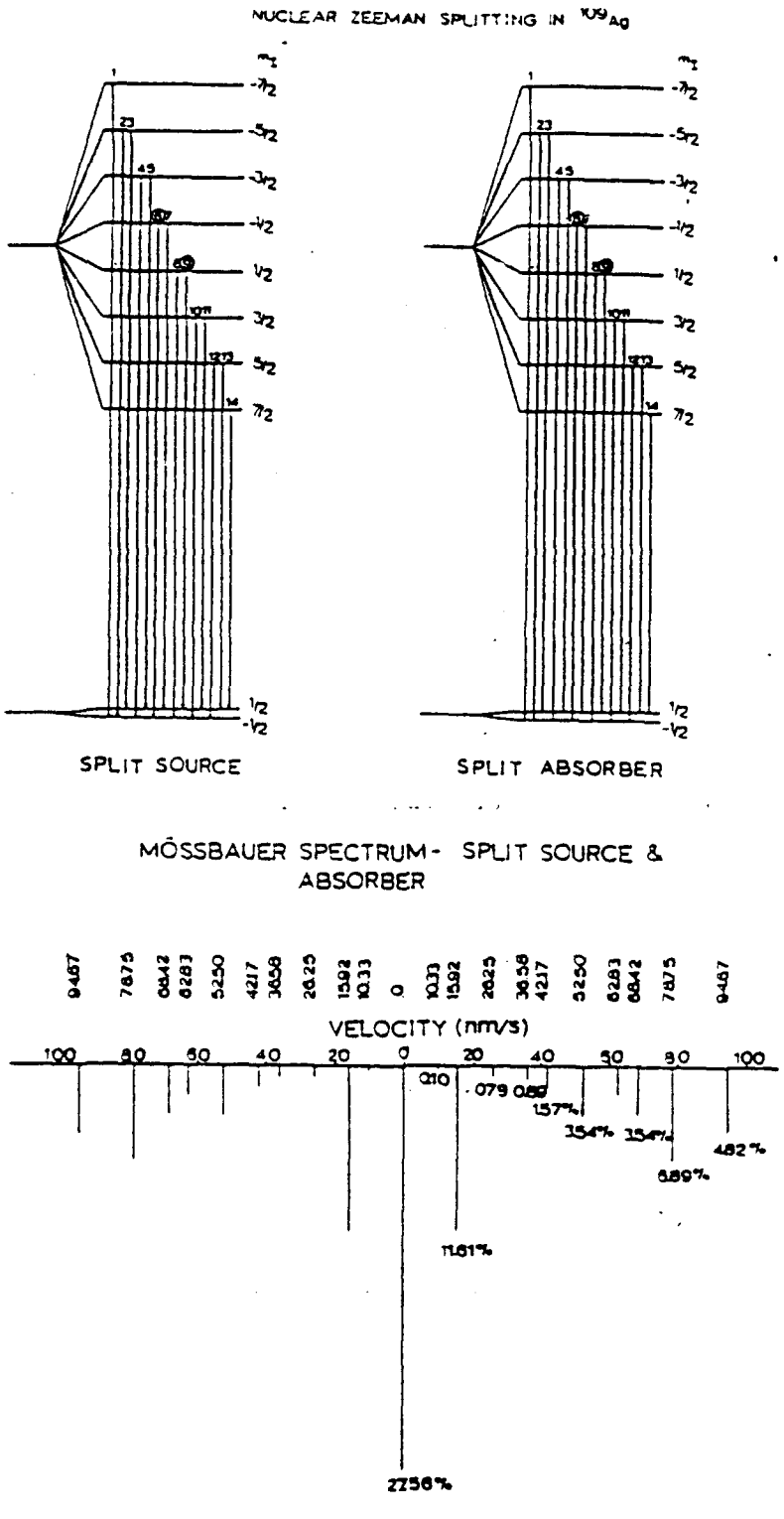

Fig. 2. ^{109}Ag Magnetic Hyperfine Structure expected for a magnetically split source and magnetically split absorber in a 1 Gauss field (top). The calculated hyperfine structure (bottom) consists of a 21-line spectrum, with the maximum cross-section (27.56% of σ_0) for the line at v=0 nm/s. This corresponds to the 14 emission-lines from the source resonantly absorbed with corresponding 14 transitions in the absorber.

structure. Because of the hyperfine splitting, only 27.56% of the resonant cross-section is actually at the centroid for the resonant self absorption measurement. We note that the splitting between the outermost lines represents ~ $10^6\,\Gamma_n$. Indeed if the observed linewidth happens to be the homogeneously broadened width (10^{-14}eV) rather than the natural width (10^{-18}eV), one would expect the whole hyperfine splitting to collapse at the centroid in a field of 10 mGauss. Such a collapse would increase the size of the resonant self-absorption by a factor of approximately four (27.56% → 100%). This constitutes one of the obvious factors why the ^{109}Ag measurements must be performed in a low-field.

To buck the earth's magnetic field on the ^{109}Cd source, we proceeded in two steps. First a system of four nested shields of 0.040" mu-metal with 1/4" spacers were designed by surrounding the Al vacuum shroud DMX-20 of the Dixplex (CS202) He cryostat. The shields were designed by Magnetic Shield Corporation, Bensenville, Illinois. Three of these shields were outside the vacuum shroud while the fourth one lined the inside of the vacuum shroud. Mu-metal is a high permeability magnetic material that essentially shields by rerouting magnetic flux-lines around the sample. The system lowered the magnetic field from about 300 mGauss to about 1 mGauss on the source location. The fields were measured by a triple-axis Applied Physics System 520 fluxgate magnetometer.

The second step consisted of sandwiching the dime-sized ^{109}Cd(Ag) source between a pair of superconducting thin films (0.5μ thick) of $Y_1Ba_2Cu_3O_7$ sputtered on thin-single crystal MgO substrates. Such films have been routinely grown and thoroughly characterized as part of the Ph.D. thesis of Chuck Blue (working with the contractor) on an NSF grant. These films display a T_c = 90K with a width ΔT ~ 2K, and are characterized by a $J_c \sim 10^6$ A/cm^2 at 10K, and a H_{c_1} that exceeds 100

Gauss. Given that the penetration depth of these superconducting films are typically $\lambda = 1200\text{Å}$ at $T < T_c$, one expects the reduction of the magnetic flux on the source to be about $e^{-t/x}$ (where t = film thickness), i.e. a factor of about 65. With the films in place, we thus estimate the magnetic field on the source to be down to 15μ Gauss.

d. Data Acquisition System and Results

Pulse height spectra of the source were taken with an intrinsic Ge detector (MAC portable detector) using an S-100 card multichannel analyzer (both from Canberra Industries) on an IBM-PS2 computer using a 400 MHz ADC. Figure 3 displays a typical pulse height spectrum of the ^{109}Cd source in which windows were set on the K_α, K_β x-rays and the 88 keV gamma photo peak. Integrated counts in these windows were accumulated every six hours in a task-mode of operation. The integrated counts under the x- and γ-ray peaks as well as the ratio of integrated counts was obtained and plotted as a function of time. Figures 4 and 5 display some of the results with the source cooled at 13K and 60K, respectively, with the superconducting thin-films inserted. Table II gives an overview of our results taken over a 6-month period on a $^{109}Cd/Ag$ source. These results clearly indicate the absence of any measurable change in the ratio $x/\gamma(T)$ between 14K and 60K either at H = 3 milligauss or H = 30 μGauss.

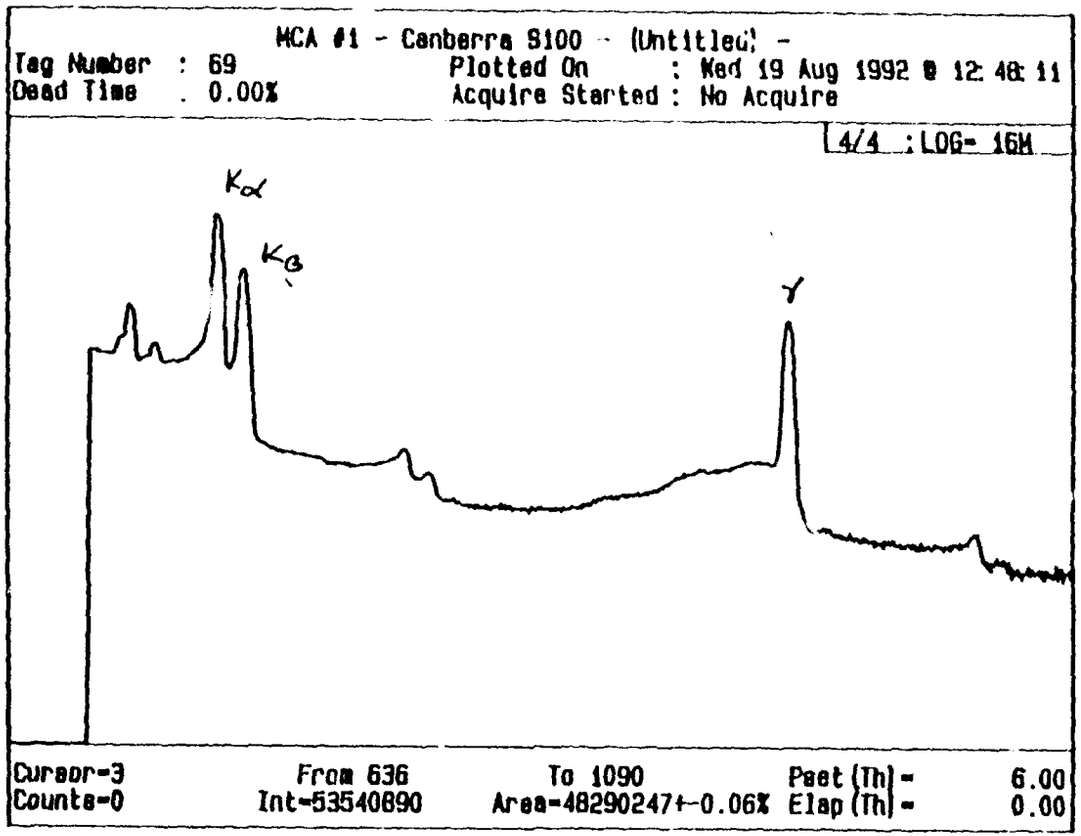

Fig. 3. Pulse height spectrum of $^{109}Cd/Ag$ source recorded with an intrinsic Ge detector. Integrated counts under the x-ray and γ-ray peaks were obtained by setting a window around the peak positions. The ratio of the integrated counts X/γ was calculated at various temperatures.

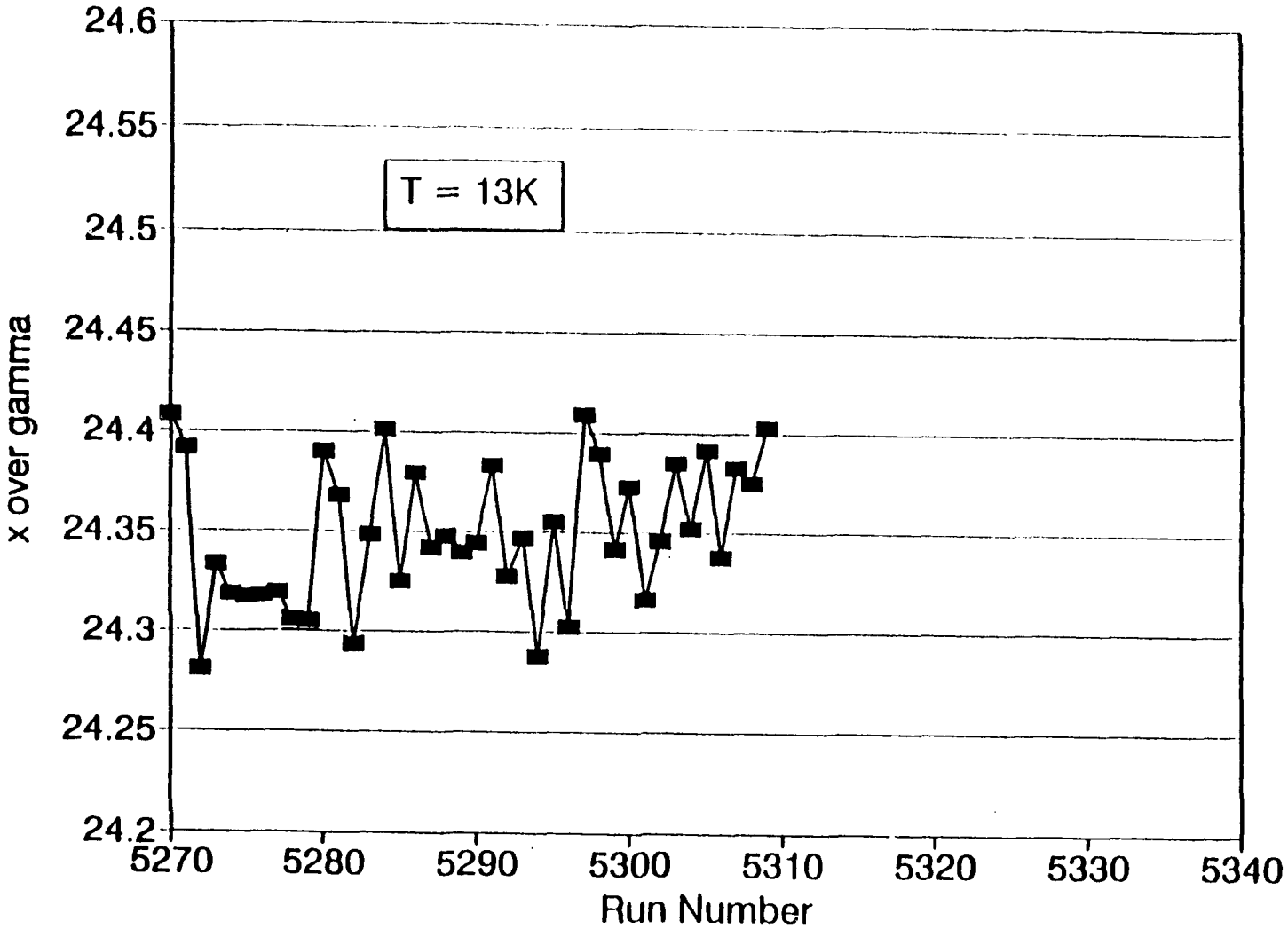

Fig. 4. X/γ ratio obtained as a function of run number for series 7. One run number corresponds to a 6 hour collection time. Identification of series appears in Table II. Series 7 corresponds to a measurement performed at T = 13K with the ^{109}Cd/Ag source immersed in a 30μ Gauss field.

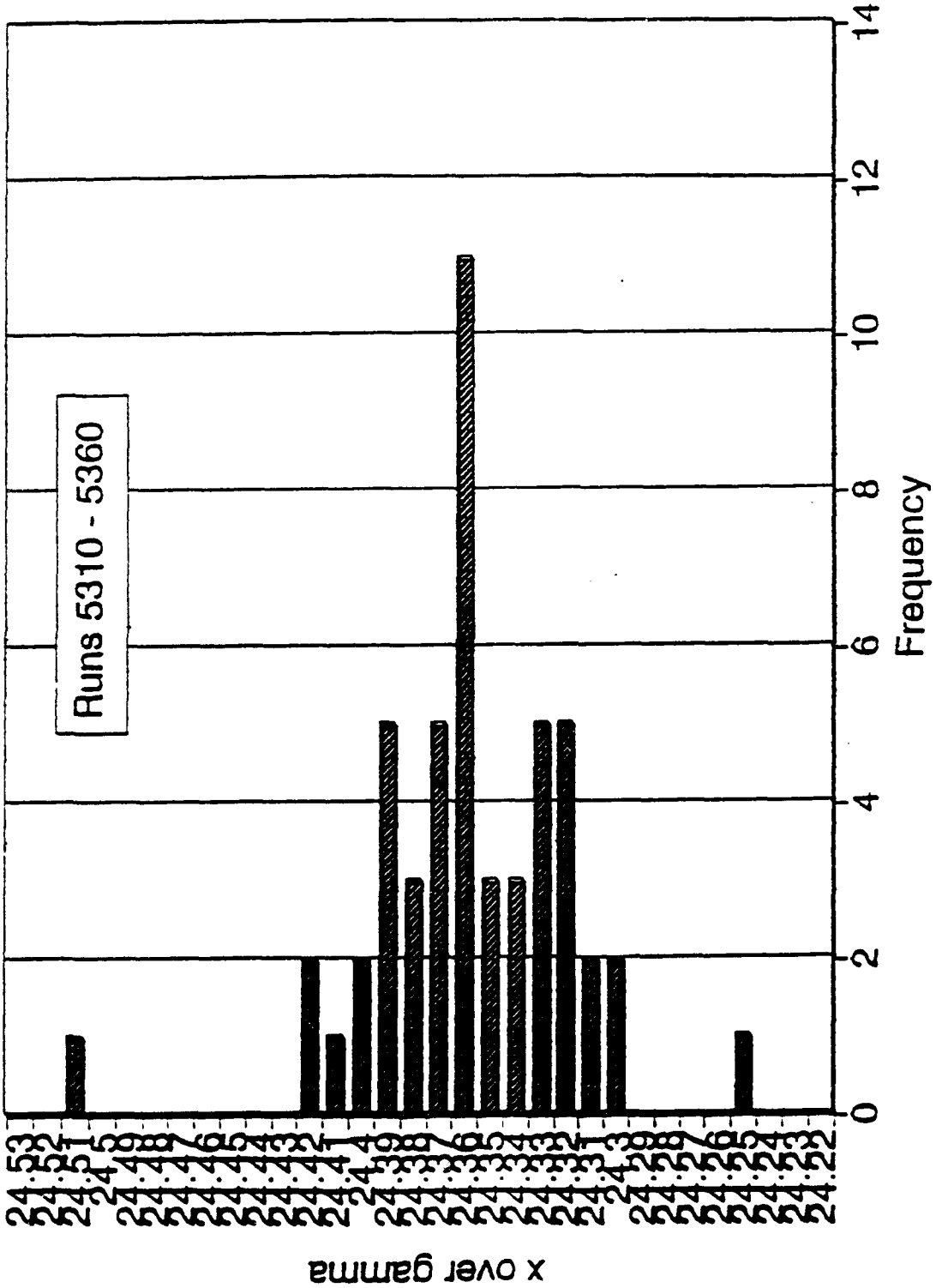

Fig. 4a. Displays X/γ ratio distribution for series 7 runs.

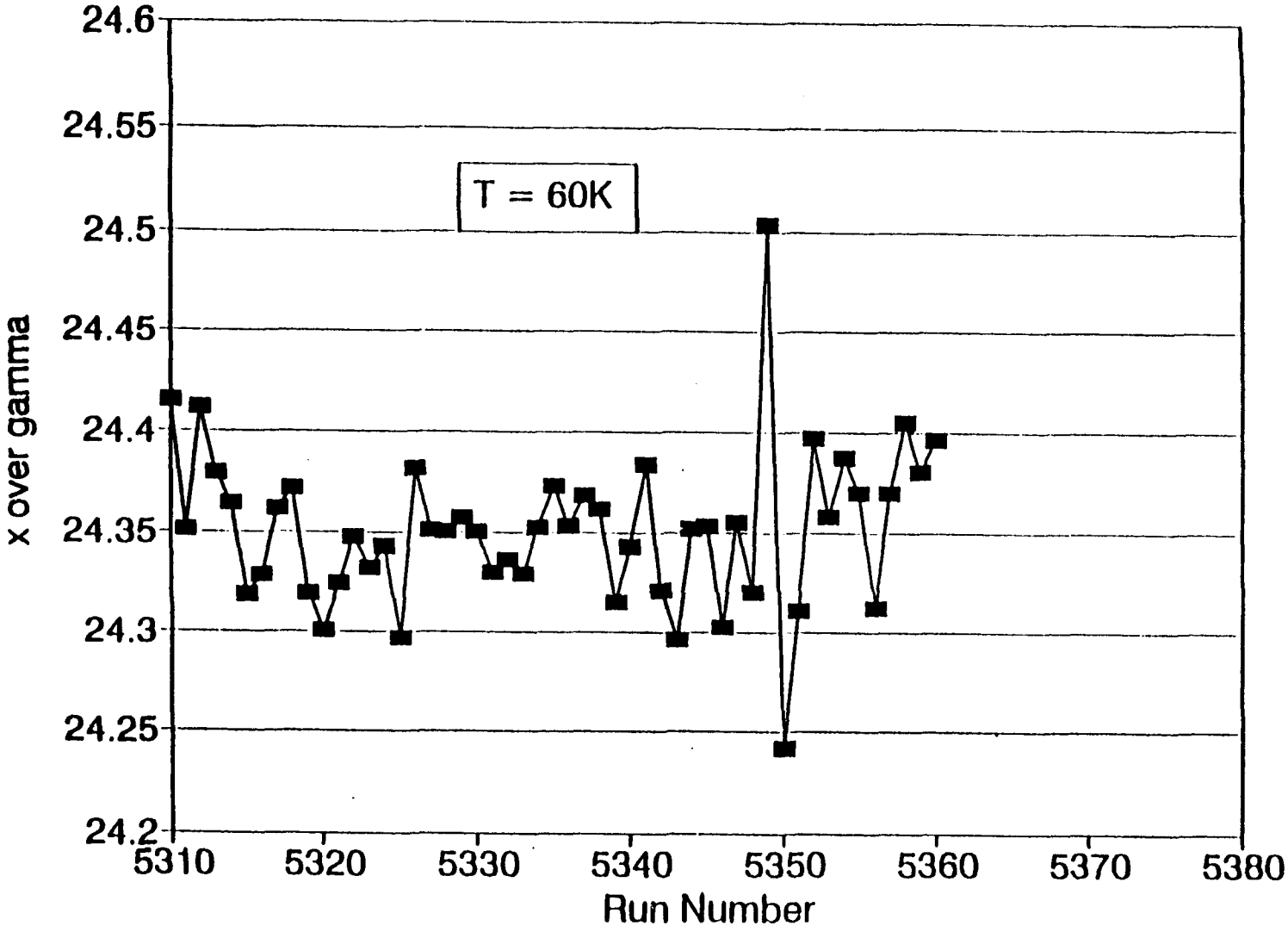

Fig. 5. X/γ ratio obtained as a function of run number for series 8. Series 8 corresponds to a measurement performed at T=60K with the $^{109}Cd/Ag$ source immersed in a 30μ Gauss field.

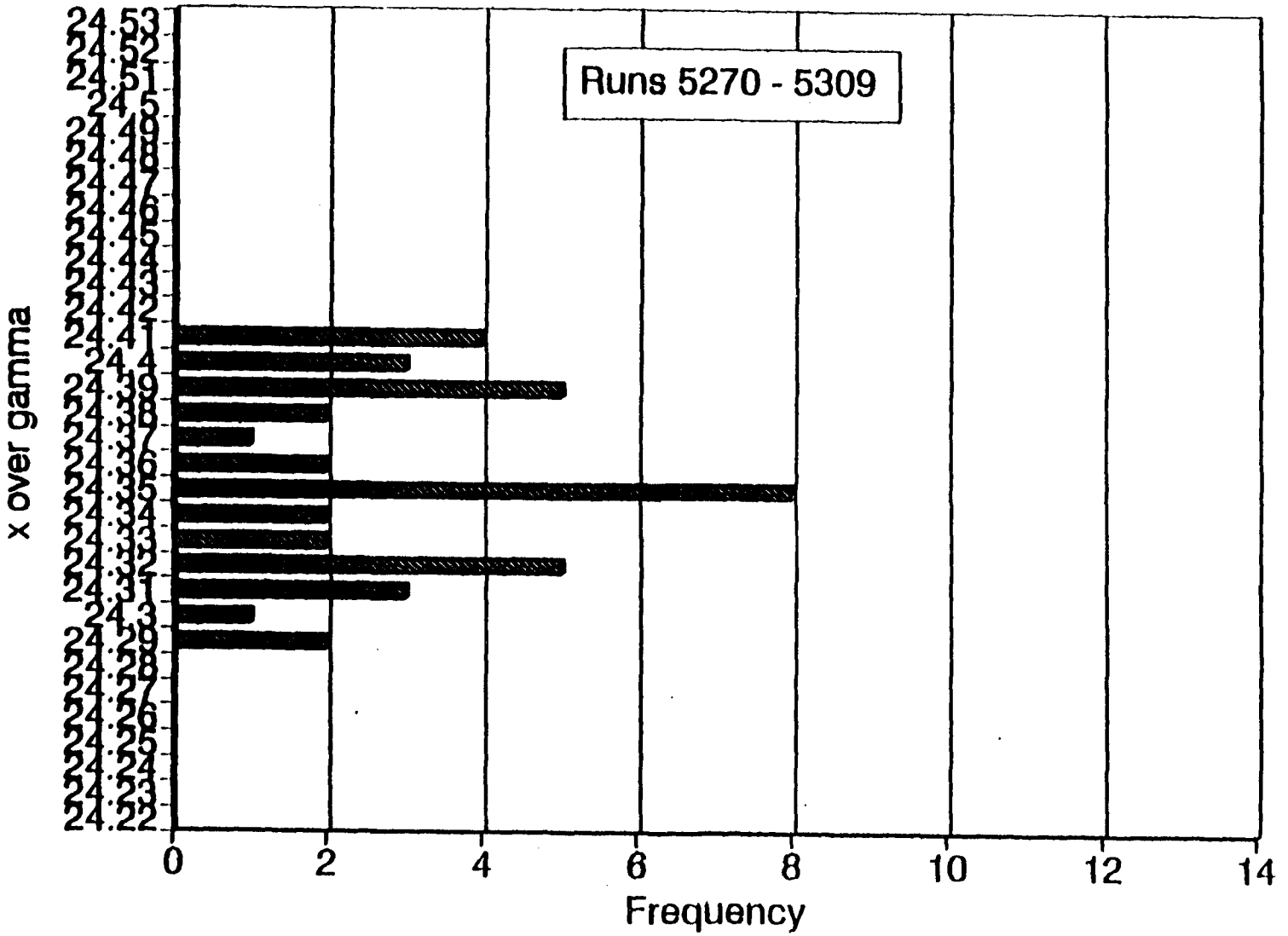

Fig. 5a. Displays X/γ ratio distribution for series 8 runs.

TABLE II

SERIES	RUNS*	TEMPERATURE	MAGNETIC FIELD	X/γ
1	5060 → 5085†	12.9K	3 milligauss	26.527 ± 0.010
2	5092 → 5118	60K	3 milligauss	26.495 ± 0.010
3	5119 → 5179	14K	3 milligauss	26.490 ± 0.007
4	5180 → 5242	60K	3 milligauss	26.482 ± 0.007
5	5243 → 5242	14K	3 milligauss	26.503 ± 0.015
Following runs with ^{109}Cd/Ag source between superconducting films				
6	5255 → 5269	300K	30 microgauss	24.389 ± 0.012
7	5270 → 5309	13K	30 microgauss	24.350 ± 0.007
8	5310 → 5360	60K	30 microgauss	24.352 ± 0.007

*A run implies 6 hour counting time on the pulse height spectrum with the Ge detector. The detector is rigidly attached to the source assembly. The attached slide shows the experimental arrangement.

†5050-5085 indicates a total of 26 runs, i.e. 26x6 = 156 hours of counting time on the first series for which the T = 12.9K and the magnetic field on the source of ~ 3m Gauss.

III. TUNABILITY OF HOMOGENEOUS LINEWIDTH AT NUCLEAR LEVEL CROSSINGS

In this section we include a manuscript which was recently presented at the Hyperfine Interaction Conference held in Osaka, Japan, August 17-21, 1992. The manuscript is scheduled for publication in Hyperfine Interactions. It provides a concise summary of our results on nuclear level crossings using the ^{12}B probe in Al.

IDENTIFICATION OF CROSS–RELAXATION RESONANCES OF ^{12}B IMPLANTED IN S.C. ALUMINUM.

G. S'heeren, M. Van Den Bergh and R. Coussement
Instituut voor Kern– en Stralingsfysika, K.U. Leuven,
Celestijnenlaan 200D, B–3001 Heverlee, BELGIUM

M. Cyamukungu, J. Lehmann, R. Pirlot and L. Grenacs
Université Catholique de Louvain, Louvain–la Neuve, BELGIUM

P. Boolchand, University of Cincinnati, Ohio 45221–0030, USA

Abstract : *Polarized ^{12}B nuclei were produced and recoil implanted in single crystals of f.c.c. aluminum. The boron decay asymmetry and relaxation times were measured as a function of external magnetic field values and at different orientation angles of the crystal. To identify the resonances at certain field values in the ^{12}B depolarization in Al, a consistent theory based on the principle of a multi–spin system and nuclear level–crossing has been developed. A unique identification of the resonances, based on the resonant interaction between boron and particular pairs of aluminum neighbours, is perfectly possible. The strong dissipative coupling of the Al nuclei with the electron bath of the lattice makes a straightforward interpretation of the resonance width and depth, based on the developed theory impossible.*

Cross relaxation measurements of ^{12}B nuclei recoil implanted in f.c.c. Al (S=5/2) single crystals have been performed at the Van de Graaff accelerator at Louvain–La–Neuve (Belgium). The ^{12}B (I=1, τ=29.4 ms) nuclei are produced in a spin polarized state by the interaction of a 1.5 MeV deuteron beam with a thin ^{11}B foil mounted on an inox backing. A maximal spin polarization perpendicular to the reaction plane can be achieved by selecting the ^{12}B nuclei recoiling at 49° with respect to the beam direction (fig. 1). An external magnetic field B_z is applied along the polarization axis and the ^{12}B spin polarization is established by measuring the up–down asymmetry of electrons emitted from the $^{12}B \rightarrow ^{12}C$ decay.

In these measurements, we focused our attention on two problems concerning resonant cross relaxation. First we identified the Al neighbours to which the ^{12}B is coupled resonantly, secondly we studied the processes involved in the loss of polarization. In order to allow the identification and the interpretation of the width and the depth, a consistent theory based on the principle of a two–spin system and nuclear level crossing and mixing[1,2] has been developed and the results compared to the experiment.

Since the ^{12}B impurity is known to occupy the octahedral interstitial position in Al[3,4], the Al neighbours feel a quadrupolar interaction due to the presence of the boron.

The electric field gradient induced by the ^{12}B on each Al pair is axial symmetric and directed along the axis that connects the B with the Al pair. First we consider the Hamiltonian of the two–spin system neglecting any coupling between ^{12}B and ^{27}Al nuclei assuming that the magnetic field is aligned with the polarization axis [5]:

$$H_0 = H_1(^{12}B) + H_2(^{27}Al) \qquad (1)$$

$$= A + B + C + D + E$$

with

$$A = -\underline{\omega}_1 I_z$$

$$B = -\underline{\omega}_2 S_z$$

$$C = \underline{\omega}_Q \frac{1}{2} (3 \cos^2\underline{\beta} - 1) (3 S_z^2 - S^2)$$

$$D = \underline{\omega}_Q 3 S_x^2 \sin^2\underline{\beta}$$

$$E = \underline{\omega}_Q \frac{3}{2}(S_z S_x + S_x S_z) \sin 2\underline{\beta}$$

where $\underline{\beta}$ represents the angle between the axial symmetric electric field gradient V_{zz} at the ^{27}Al nuclei and B_z.

$\underline{\omega}_{1(2)} = \underline{\gamma}_{1(2)} B_z/\hbar$

$\underline{\omega}_Q = e^2qQ/4S(2S-1)\hbar$

Special cases occur at $\underline{\beta}=0$ and $\underline{\beta}=\underline{\pi}/2$. Since for $\beta=0$ terms D and E of H_0 vanish, only diagonal elements will occur in the $|m_1,m_2>$ representation and the energy levels of the two–spin system can cross as function of B_z. A special case concerns $\underline{\beta}=\underline{\pi}/2$ where only term E vanishes so that H_0 is no longer diagonal in the $|m_1,m_2>$ representation. However, as term E (mixing levels with $|\Delta m_2|=1$) is missing, the Hamiltonian can be reduced to two sub – Hamiltonians and the eigenvalues of one Hamiltonian can cross, without repulsion with the eigenvalues of the other one. If however, $\underline{\beta}$ deviates from 0 or $\underline{\pi}/2$ so that term E becomes important, the level scheme will show only repulsing and no crossing levels anymore.

By considering also the perturbation interactions the Hamiltonian becomes :

$$H = H_0 + H_{B-Al} \qquad (2)$$

in which H_{B-Al} describes the interactions between boron and aluminum. This term which can normally be neglected becomes very important when the energy levels cross. At this field values the perturbation interaction couples the boron and aluminum resonantly so that the boron can transfer a part of its initial polarization to the Al neighbours so that their levels become equally occupied.

Having a look at figure 2 where boron is placed in the Al lattice, the six nearest neighbours (nns) can be divided into two groups. The Al pair along the [001] axis has $\underline{\beta}$ equal to zero. For the 4 Al nns in the basal plane residing along the [100] and [010] axis, $\underline{\beta}$ is equal to $\underline{\pi}/2$. This second group splits into two different pairs when the crystal is rotated about an angle $\underline{\phi}$ around the [010] axis with the Al pair along the rotation axis

remaining at $\beta=\pi/2$ so that the other one along the [100] axis having an angle $\beta=\pi/2\pm\phi$. For the Al nns pair along the [001] axis β is always equal to ϕ. For increasing values of β, energy levels will repulse what results in a broadening and finally a disappearing of some resonances, while new resonances will appear at fields where accidentally two levels approach close enough in order to be mixed by the coupling term H_{B-Al}.
A study of the next nearest Al neighbours (corners of the cube) is also possible when the [111] axis of the crystal is rotated in the magnetic field direction. Such resonances have been identified but will not be discussed here.

The field dependence of the polarization of the ^{12}B nuclei was studied at room temperature and for different orientation angles ϕ so that using the developed theory and concepts, a unique identification of the resonances is possible. The resonance at 682 Gauss (fig. 3, $\phi=0$) must be assigned to the Al pair along the [001] axis, while the resonance at 408 Gauss is caused by the 4 nns in the basal plane ($\phi=0,\beta=\pi/2$). This assertion becomes clear when looking at figure 3 where for $\phi=10°$, the 408 Gauss resonance splits into two resonances. The one remaining at 408 Gauss corresponds to the Al pair along the rotation axis ($\beta=\pi/2$) while the other dip can be assigned to the Al pair along the [100] axis. The two Al pairs for which β changes with ϕ, shift to other field values and broaden as a function of ϕ as explained before.
The Hamiltonian as described in equation (2) is not able to explain the large depth of the obtained resonances. This means that ^{12}B is not simply transferring a part of its polarization to one or more Al pairs and vice versa but the polarization is lost by the Al neighbours before it can be returned to the boron. Due to the fact that the density of electrons at the Fermi level in Al is much larger than for the boron atom, the Al atoms have a smaller T_1 relaxation time than the ^{12}B and so the polarization that is transferred from the ^{12}B nuclei will be quickly dissipated to the lattice as soon as the resonant coupling ^{12}B—^{27}Al is effective. This dissipative coupling is expected to disappear at low (He) temperatures where T_1 for Al becomes much larger[6] than the nuclear life–time.

The boron and its aluminum neighbours will be isolated from their surrounding. Experiments at this temperature are in preparation.

Finally, T_1 relaxation experiments versus external field clearly supports the strong dissipative character in aluminum (fig. 4) and this explains why the loss of polarization does not follow the level mixing theory.

Using this theory, the widths of the resonances can be calculated assuming the perturbation being strictly nuclear dipole–dipole. In that case the calculated value is much smaller than the experimental one. This fact enables to conclude that the indirect coupling in Al is much more important.

This work was sponsored by SDIO/IST and managed on ONR grant N00014–88–K–2035.

References

[1] R. Coussement, P. Put, G. Scheveneels and F. Hardeman, Hyp. Int. 23 (1985) 273–309.

[2] P. Put, R. Coussement, G. Scheveneels, F. Hardeman, I. Berkes, B. Hlimi, G. Marest, J. Sau and E.H. Sayouty, Phys. Lett. 103A (1984) 151–154.

[3] H.–J. Stöckmann, E. Jäger, G. Sulzer, B. Ittermann, H. Ackermann, e. Diehl, R. Dippel, B. Fischer, H.–P. Frank and W. Seelinger, Hyp. Int. 49 (1989) 235–252.

[4] E. Jäger, B. Itterman, G. Sulzer, K. Bürkmann, B. Fischer, H.–P. Frank, H.–J. Stöckmann and H. Ackermann, Z.Phys. B 80 (1990) 87–94.

[5] C.P. Slichter, in Principles of Magnetic Resonance, eds. M. Cardona, P. Fulde, H.–J. Queisser (Springer–Verlag, Berlin, Heidelberg, New–York, 1978) p. 289.

[6] C.P. Slichter, in Principles of Magnetic Resonance, eds. M. Cardona, P. Fulde, H.–J. Queisser (Springer–Verlag, Berlin, Heidelberg, New–York, 1978) p. 149.

Figure Captions

Fig. 1 ^{12}B are produced and polarized by $^{11}B(d,p)^{12}B$ reaction and recoil implanted in f.c.c. Al. The polarization is proportional to the measured asymmetry of the emitted β–rays, detected in the up and down telescope detector system.

Fig. 2 F.c.c. Al (open circle) with interstitial ^{12}B (filled circle) octahedrally coordinated to 3 pairs of Al nns. The boron possesses a cubic symmetric position, but for the Al neighbours the cubic symmetry is broken. The electric field gradient for the Al pair along the [001] axis (pair 1) makes an angle β=0 with the B_z–axis while for the 4 nns (pairs 2 and 2')along the [010] and [100] axis β equals $\pi/2$.

Fig. 3 ^{12}B spin polarization as function of B_z, measured at different crystal orientations ϕ. For ϕ=0, the resonance at 682 Gauss must be assigned to the Al pair along the [001] axis with β=0 while the resonance at 408 Gauss corresponds to the Al pairs in the basal plane with $\beta=\pi/2$.

Fig. 4 At the cross relaxation field, the polarization is transferred to the Al and from the Al neigbours further dissipated to the electron bath of the lattice.

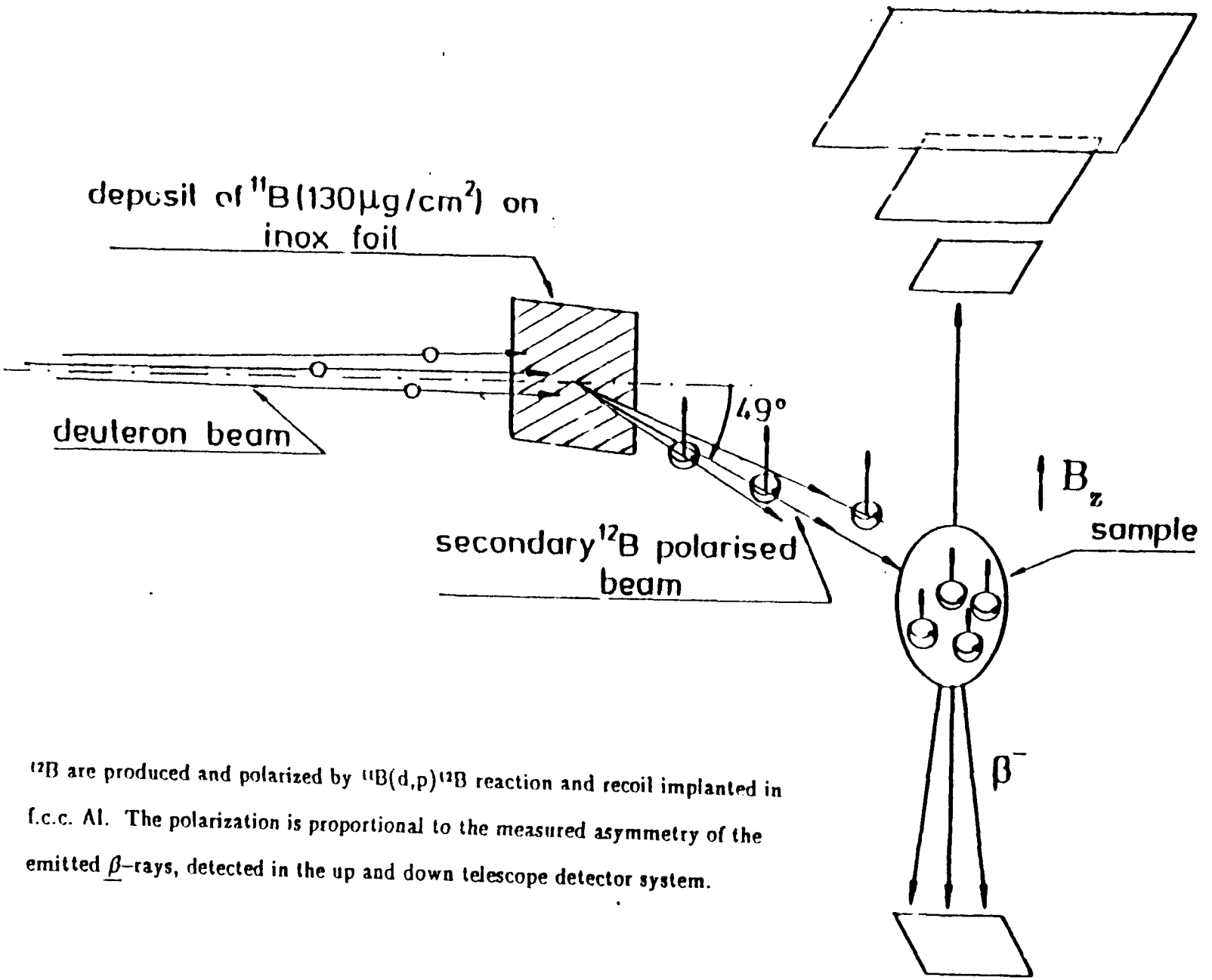

Fig. ^{12}B are produced and polarized by $^{11}B(d,p)^{12}B$ reaction and recoil implanted in f.c.c. Al. The polarization is proportional to the measured asymmetry of the emitted β–rays, detected in the up and down telescope detector system.

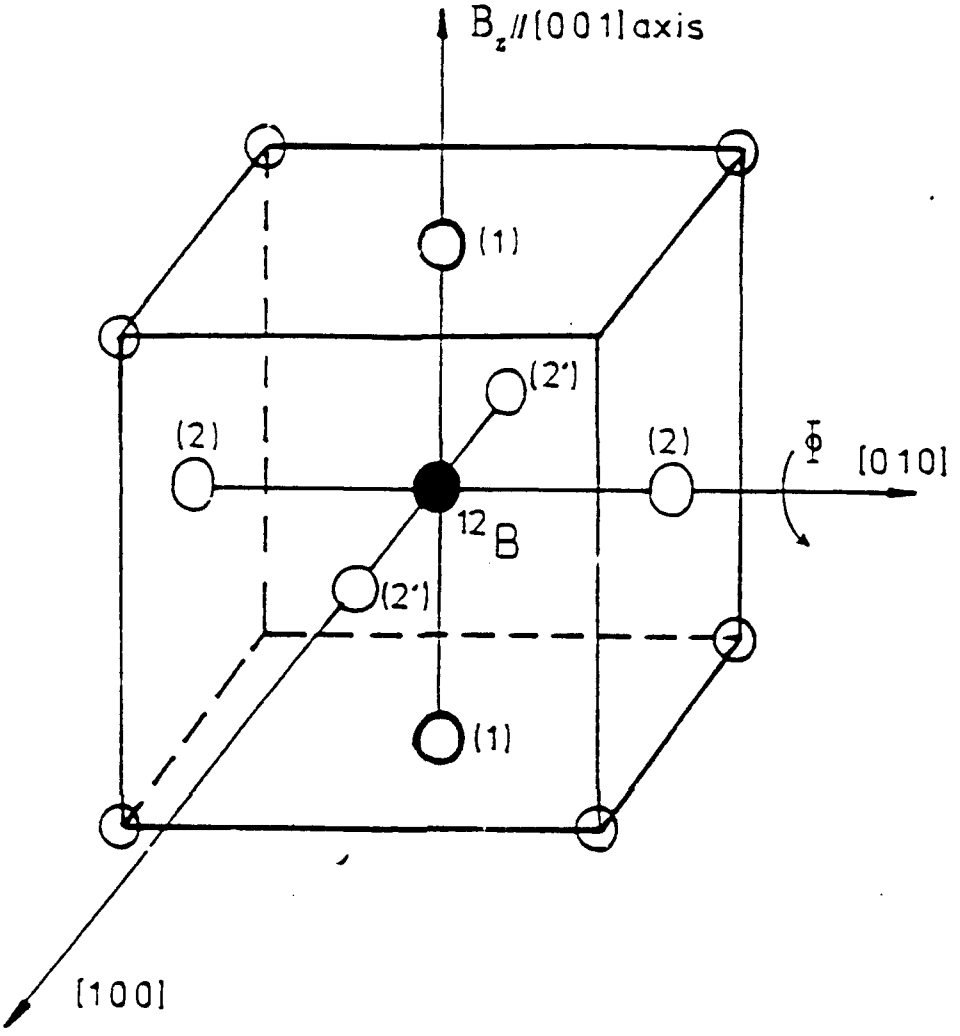

Fig. 2 F.c.c. Al (open circle) with interstitial ^{12}B (filled circle) octahedrally coordinated to 3 pairs of Al nns. The boron possesses a cubic symmetric position, but for the Al neighbours the cubic symmetry is broken. The electric field gradient for the Al pair along the [001] axis (pair 1) makes an angle $\underline{\beta}$=0 with the B_z–axis while for the 4 nns (pairs 2 and 2')along the [010] and [100] axis $\underline{\beta}$ equals $\underline{\pi}/2$.

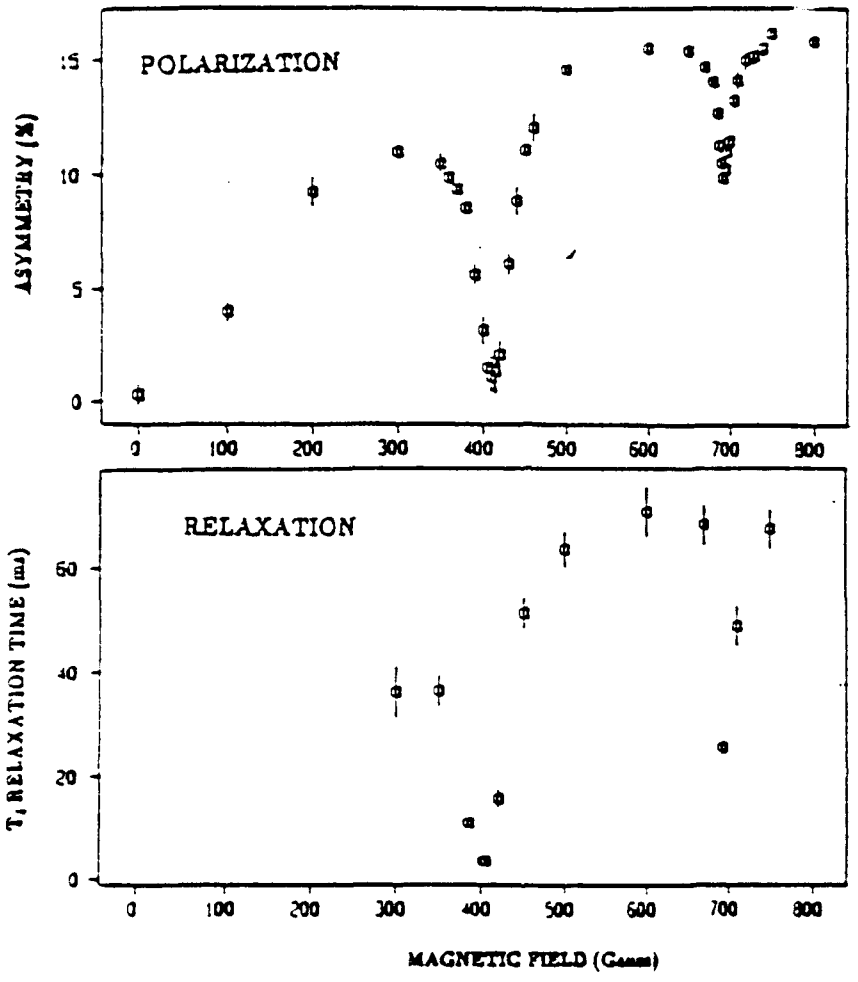

Fig. 3 ^{12}B spin polarization as function of B_z, measured at different crystal orientations ϕ. For ϕ=0, the resonance at 682 Gauss must be assigned to the Al pair along the [001] axis with β=0 while the resonance at 408 Gauss corresponds to the Al pairs in the basal plane with $\beta=\pi/2$.

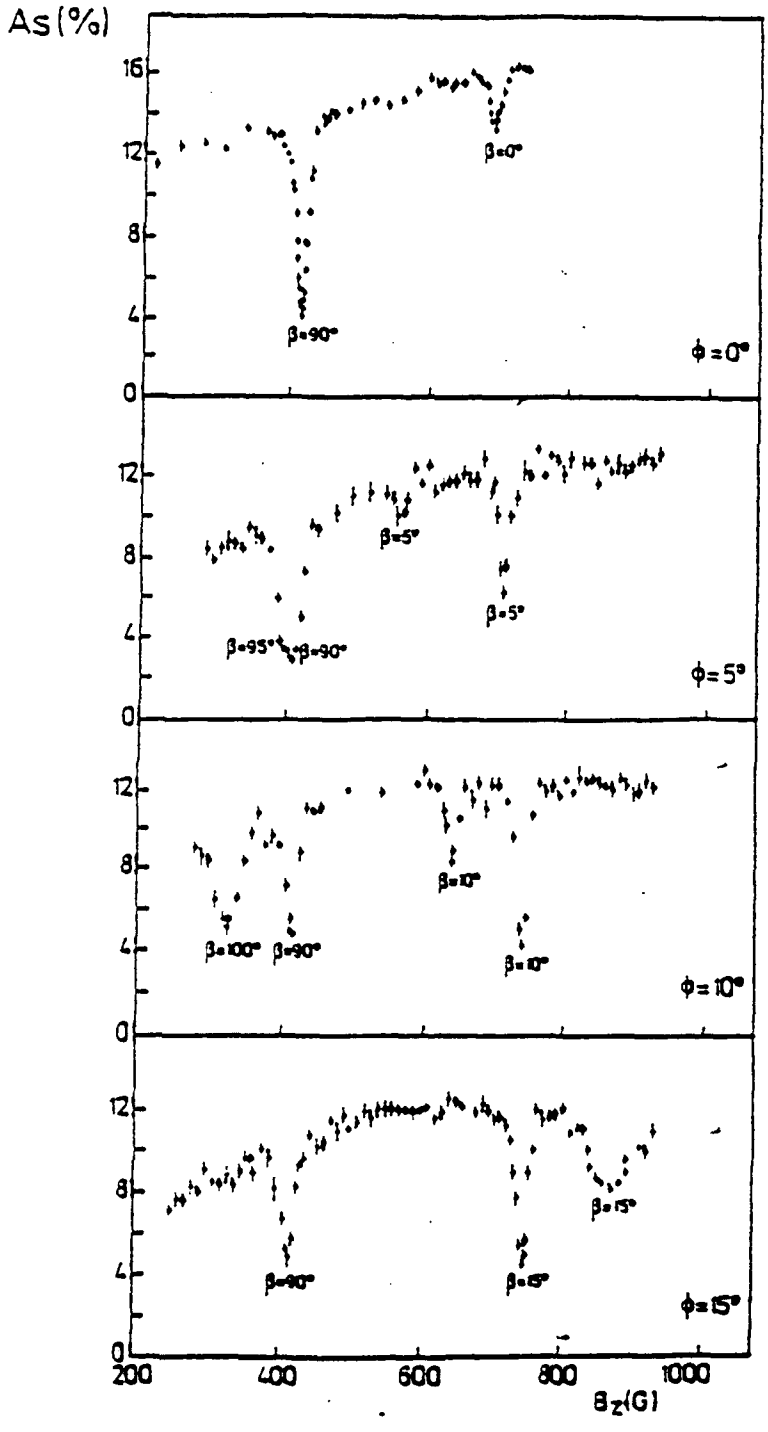

Fig. 4 At the cross relaxation field, the polarization is transferred to the Al and from the Al neigbours further dissipated to the electron bath of the lattice.

IV. Concluding Remarks and Future Plans

Absence of a Mössbauer effect in ^{109}Ag from the undertaken resonant self-absorption experiments, lead to the basic question: is the T-dependence of the resonant absorption for a long-lived state (τ > few msec) given by the usual expression of f(T) used for the case of short-lived (τ < few msec) nuclear-states? This we are in the process of examining theoretically. It is possible that absorption processes for the case of long-lived nuclear states may include, besides zero-phenon, one- and two-phonon events, thus altering the usual T-dependence of resonant absorption. In that case the emission lineshapes will consist of a narrow line (zero-phonon) superposed on an extremely broad line due to resonant processes involving phonons. The phonon assisted emission and absorption processes may have a significant role in the gamma resonant absorption measurements because of the long lifetime of the nuclear state. The linewidths of the phonon-assisted resonant processes are extremely large (10^{-2}eV) in relation to the zero phonon process (10^{-18}eV) linewidths. The resonant self-absorption probability or effect may become largely T-independent, since both emitting and absorbing nuclei are present in the same chemical environment.

If one observes the Mössbauer effect by separating the source and absorber and providing a relative motion, then it is possible to separate the zero-phonon from the phonon-assisted resonant processes largely because of the small scan velocities used. These permit only the zero-phonon part to be observed. Furthermore, since only the zero-phonon resonant process is T-dependent, one expects the velocity spectrum to display a T-dependence.

Experimentally, this requires providing a controlled relative motion between the source and absorber in the 1 nm/s range. Such a motion can be provided by a micropiezoelectric transducer. Such transducers are the basic components of the scanning device used in present day tunelling microscopes (STM) or atomic force microscopes (AFM). Plans to build such a transducer are under way to perform an on-off experiment on ^{109}Ag.

To achieve coherent emission of γ-rays in a solid, ideally one would like absorption processes both electronic and nuclear to be switched off at the γ-ray energy of interest as it traverses in a solid. During the course of the present work, we realized that in a Mössbauer experiment, it is possible to realize a condition of non-reciprocity of γ-emission and absorption due Quantum Coherence at level-crossings. This is a relatively new idea in the field. Theoretically, we have summarized the concept in a manuscript that is currently under review. Experimentally, plans are underway to test the concept. We believe once those basic concepts have been unambiguously tested, more realistic plans to choose suitable candidate isomers and crystalline host materials can be developed to build a γ-ray laser.

V. PUBLICATIONS

1. **Non-reciprocity of gamma emission and absorption due to quantum coherence at nuclear-level crossings**, by R. Coussement, M. Van Den Bergh, G. S'heeren, G. Neyens, R. Nouwen and P. Boolchand (manuscript submitted to Phys. Rev. Letters, Nov. 20, 1991 and currently under review.

2. **Nuclear resonant absorption in long-lived isomeric transition** by R. Coussement, G. S'heeren, M. Van Den Bergh and P. Boolchand, Phys. Rev. B45, 9755 (1992).

3. **Nuclear level mixing assisted relaxation, homogeneous broadening and gamma-ray lasers**, by R. Coussement, M. Van Den Bergh, G. S'heeren G. Neyens, R. Nouwen and P. Boolchand (to be published in Lasers '91 Conference Proc.)

4. **Gamma-ray laser based on storage level as the lasing level**, by G. S'heeren, M. Van Den Bergh, R. Coussement, R.N. Enzweiler, R. Harris, Y. Wu, P. Boolchand, R.D. Taylor, M. Cyamukungu, J. Lehman and L. Grenacs, (Lasers '90 Conf. Proc). p. 17.

5. **Mössbauer absorption on ^{109}Ag - Fake or Reality?** R. Coussement, M. Van Den Bergh, G. S'heeren, P. Boolchand, Hyperfine Interactions 68, 1487 (1992).

6. **"Nuclear Zeeman Splitting in ^{109}Ag"**, R. Harris et al., Bull. Am. Phys. Soc. 36, 626 (1991).

7. **"Mössbauer effect in ^{109}Ag"**, R. Enzweiler et al., Bull. Am. Phys. Soc. 36, 626 (1991).

8. **"Pico and Sub-pico electron volt hyperfine interaction"**, R. Coussement et al., Bull. Am. Phys. Soc. 36, 626 (1991).

9. **Quantum Interferences in Nuclear Decay**, R. Coussement, N. Van Den Bergh, G. S'heeren, G. Neyens, R. Nouwen, and P. Boolchand (to be published in Hyperfine Interactions).

10. **Identification of Cross-Relaxation Resonances of ^{12}B Implanted in Single Crystal Aluminum**, G. S'heeren, M. Van Den Bergh, R. Coussement, M. Cyamukungu, J. Lehmann, R. Pirlot, L. Grenacs and P. Boolchand (to be published in Hyperfine Interactions).

VI. PARTICIPANTS

University of Cincinnati

Punit Boolchand
(Professor)
Wayne Bresser
(Research Associate)
Ray Enzweiler†
(Visiting Faculty, Summer)
Yaoxiong Wu
(Ph.D. student)
Richard Harris
(M.S. student)

R. Dean Taylor
(Los Alamos National Laboratory)

Leuven University

Romain Coussement
(Professor)
Griet S'heeren
(Ph.D. student)
Marlene Van Den Bergh
(Ph.D. student)

Laslo Grenacs
(Prof., Louvain-la-Neuve)

†Professor of Physics
Northern Kentucky University
Covington, KY

VII. PREPRINTS AND REPRINTS

PHYSICAL REVIEW B VOLUME 45, NUMBER 17 1 MAY 1992-I

Nuclear resonant absorption in long-lived isomeric transitions

R. Coussement, G. S'heeren, and M. Van Den Bergh
Instituut voor Kern- en Stralingsfysika, Katholieke Universiteit, 3001 Leuven, Belgium

P. Boolchand*
Department of Electrical and Computer Engineering, University of Cincinnati, Cincinnati, Ohio 45221-0030
(Received 15 October 1991)

The temporal behavior of γ-ray emission and absorption from long-lived ($\tau > 1$ ms) nuclear states is modified qualitatively by interaction with the lattice, leading to homogeneous broadening. In contrast, for the usual short-lived ($\tau < 0.1$ ms) states, such nucleus-lattice interaction invariably leads to inhomogeneous broadening. It is shown that resonant emission and absorption with long-lived states can be observed provided the homogeneously broadened width, rather than the natural width, exceeds the solid-state-induced inhomogeneous width.

I. INTRODUCTION

There is general recognition in Mössbauer spectroscopy that when the lifetime τ of a nuclear state exceeds 10^{-3} s, the natural linewidth Γ_n of the corresponding Mössbauer transition becomes rather narrow ($\Gamma_n = \hbar/\tau = 10^{-12}$ eV) and the observation of the resonance absorption rather difficult on account of inhomogeneous broadening. A survey[1] of the literature indicates that typical values of inhomogeneous line broadening in the best crystals amounts to 10^{-12} eV or more. Consequently, if one attempts to observe the Mössbauer effect with a γ ray that has a natural linewidth of, for instance $\Gamma_n = 10^{-17}$ eV, crystalline inhomogeneities will broaden the line by six orders of magnitude, making the observation of the effect impossible. It was therefore a real surprise when two groups independently attempted to observe the Mössbauer effect with the 88-keV γ ray in ^{109}Ag ($\Gamma_n \approx 10^{-17}$ eV) diffused in Ag metal and claimed evidence for a small but positive effect.[2,3] This is indeed unexpected. In the present work we examine the issue at hand theoretically and identify the conditions under which resonant absorption from long-lived isomers can be possible.

II. DESCRIPTION OF LONG-LIVED NUCLEAR STATES IN A LATTICE

In considering the absorption or emission of γ rays, one must recognize that, when the lifetime is long, the interaction of the nuclei with the radiation field actually becomes weaker than the interaction of the nuclei with the crystalline lattice (consisting of electrons and nuclei). In the case of ^{109}Ag we can roughly estimate an upper limit to the interaction energy with the radiation field as the inverse of the lifetime (or the natural width) $\hbar/\tau_n$: 10^{-17} eV, while the interaction energy with the lattice is at least 10^{-13} eV. It is therefore not possible to handle the coupling of the nuclei with the radiation field as if the nuclei are free objects. In fact, we must consider the system of the nuclei plus lattice as a whole interacting with the radiation field. It is clear that this particular situation occurs only because of the extremely long lifetime or the extremely weak coupling to the radiation field. The most general procedure to treat the problem consists of solving the Hamiltonian of the total system, i.e., the observed quantum system plus its environment and the mutual interaction. When an observable on the selected or observed quantum system is needed, one must perform a partial trace over all reservoir observables. This procedure is, however, of purely theoretical interest, since it is difficult to take into account the nearly infinite number of reservoir degrees of freedom.

We assume the coupling between the surrounding and the nuclei to be weak enough so that the surrounding will induce small but frequent changes on the nuclei, which on average will have a small effect. When averaged over a time scale, long compared with a typical correlation time for the lattice, the effect of fluctuations on the nuclei can be smoothed out and described by a continuous function $f(t)$, with a mean fluctuation time T_R that is much longer than the correlation time of the lattice.

When we describe the interaction of the total system with the radiation field, the following approximation will be used. In calculating the emission and absorption amplitudes, we will replace the wave functions of the initial and/or final states by a nonstationary wave function of the type

$$\psi(\mathbf{x},t) = \psi(\mathbf{x},0) f(t) e^{-\Gamma_n t/2} e^{-i\omega_0 t}, \tag{1}$$

which includes the damping on account of nuclear decay and the function $f(t)$ displaying the effect of the surroundings on the nucleus. Here an analogy can be made. The function $f(t)$ describes the effect of fluctuations due to the surroundings, while the damping factor takes into account the effect of vacuum fluctuations on the nuclei. The damping factor leads to a transition of the nuclei from the excited to the ground state, while $f(t)$ does nothing of that kind. Even without a detailed knowledge of the function $f(t)$, reasonable assumptions lead to

 ©1992 The American Physical Society

From Conference Proceedings of Lasers 90

GAMMA–RAY LASER BASED ON STORAGE LEVEL AS THE LASING LEVEL.

G. S'heeren, M. Van Den Bergh, R. Coussement
Katholieke Universiteit Leuven,
3001 Heverlee, Belgium.

R.N. Enzweiler, R. Harris, Y. Wu, P. Boolchand
University of Cincinnati,
Cincinnati, Ohio 45221–0030.

R.D. Taylor
Los Alamos National Laboratory,
Albuquerque, New Mexico.

M. Cyamukungu, J. Lehmann, L. Grenacs
Université Catholique de Louvain–la–Neuve,
Ottignie, Belgium.

Abstract – In this proposal for a γ–ray laser, we investigate the possibility to use the isomeric level as storage and lasing level. Discussing the problem of inhomogeneities, we point out the essential role of relaxation. We give results of experiments intended to demonstrate the possibility to tune relaxation times.

Introduction

In achieving a γ–ray laser, two main problems will emerge. The first problem is the pumping, the second will be the occurrence of inhomogeneities in the solid in which the nuclei must be built–in in order to obtain a sufficient recoilless fraction. The schemes presented to date try to avoid at least one of these problems.
In every scheme, the main part of the energy is stored in an isomeric level, requiring production, separation and preparation of proper isomeric material. As it is mainly believed that inhomogeneities cannot be avoided to a certain limit, most of the schemes are intended to convert the population of the isomeric state to a short lived state. For this last one the natural line width is larger then the inhomogeneous one. However in that case the problem concentrates on the conversion or pumping. It is indeed necessary to pump with an intense radiation to a level very near in energy to the isomeric state. It is known in nuclear physics that the occurrence of such a doublet implies a special forbiddeness on the γ–transition from the isomeric state, which does not apply on the short lived one of the doublet. In most cases the isomeric levels are indeed spin isomers and this implies also a large spin difference between the isomeric and lasing level.

The conversion process then must have a multi photon character decreasing the transition probabilities in such a tremendous way that fabulous intensities of pumping power would be required. In order to avoid the large spin differences, attention was drawn to the possible occurrence of low spin but shape isomers. Such doublets have not been detected yet, despite the theoretical expectations. Furthermore it will not solve the problem as shape forbiddeness will also affect the conversion or pumping process to the short lived state. Another approach to the problem of pumping is investigated by the Dallas group. In this research it is found that photo–reactions through door–way states, using intense beams of brehmstrahlung, are much faster than previously expected and could provide a possible transfer mechanism from an isomeric level or ground level to the short lived lasing level.

In our approach we investigate the possibility to use the isomeric level as the storage and lasing level. In such a scheme, it is clear that the natural line width is at least many orders of magnitude

smaller than the width of the inhomogeneities which cannot be avoided anyway. For example the inhomogeneities from nuclear dipole–dipole interactions are of the order of 10^{-13} eV, while for the isomeric states, which we estimate long enough for the preparation, we can figure a natural width of $10^{-19} - 10^{-22}$ eV. It is reasonable to expect that in such a condition there can be no evolution to superradiance. Indeed the indirect coupling between nuclei through the radiation field is ineffective, since this is many orders of magnitude smaller than the energy difference due to inhomogeneities, between two nuclei. Therefore such an ensemble can be expected to radiate only in an incoherent way.

Theoretical approach

We have assumed that the nuclei, which interact with the radiation field are free and isolated. This assumption cannot hold for long lived states because the coupling with the radiation field is much lower than the coupling with the lattice ($10^{-12} - 10^{-13}$ eV). This is in contrast to the usual case of shorter lived states for which the coupling with the electromagnetic field is indeed much stronger than the one with the lattice. In the case of long lived states we must consider the coupling of the radiation field with the nucleus, which continuously interacts with its surrounding and not with an isolated nucleus. We must therefore consider nucleus plus surrounding as one single system which interacts weakly with the radiation field.

In this approach the energy degeneracy has to be considered on the total system. It means that a photon can induce not only a nuclear transition, but also some changes on the lattice part.
Because of the relative weakness of the interaction with the radiation field, the evolution induced by the latter on the nuclear system is much slower than the evolution induced by the lattice. We can define an observation time T for absorption, long compared to the characteristic evolution time induced by the lattice, but short compared to the nuclear lifetime.
On this time scale T, on which we observe the electromagnetic transition of the nuclei, the interaction with the lattice is taken into account by considering the nuclear wave functions as fluctuating rapidly. We have therefore assumed that the initial and the final wave functions can be expressed as the product of an unperturbed wave function and a fluctuation function f(t).
Then the transition amplitude can be written as :

$$a(T) = -\frac{i}{\hbar}\int_0^T \langle gr,n=1|\ V\ |exc,n=0\rangle_{t=0}\ f(t)\, e^{-\frac{i}{\hbar}\omega t}\, dt \qquad (1)$$

where $\hbar\omega = E_\beta - E_\alpha - \hbar\omega_\gamma$ is the detuning between the initial $(E_\alpha + \hbar\omega_\gamma)$ and final state (E_β).

Without the fluctuation f(t) the amplitude is of Lorentzian shape having a natural line width $\hbar/\tau_n$. The allowed detuning becomes extremely small as soon as the observation time T increases. In such a case, because of the detuning induced by inhomogeneities, each photon can interact with only a very small portion of the present nuclei.

However when fluctuations are taken into account, the situation is completely changed.
For the fluctuation function f(t) we can make a few simple assumptions, namely a fast modulation and a weak coupling regime, which means that the nuclear system is very frequently perturbed, but that the effect of each perturbation on the nuclear system is very small. Therefore we can assume that f(t) can be smoothed out to a continuous function when considered over a time scale T. We further assume that the fourier transform of the fluctuations is independent of the time interval considered (stationary process).

One obtains for the amplitude in fourier transform version

$$a(T) = -\frac{i}{\hbar} <||> \int_{-\infty}^{\infty} F^T(\omega)\, L(\omega + \frac{i}{\tau_n})\, d\omega \qquad (2)$$

in which $L(\omega + \frac{i}{\tau_n})$ is a Lorentzian amplitude of natural width γ_n and centered around $\omega = 0$.

As the natural width is assumed to be very small compared to the width of the distribution $f^T(\omega)$ one can approximate the Lorentzian by a delta – function, so that the amplitude reduces to

$$a(T) = -\frac{i}{\hbar} <||> F^T(\omega) = a^T(\omega) \qquad (3)$$

Such a simple expression tells us that the amplitude is distributed over a range of detuning that is related to the frequency distribution width of the fluctuations, instead of to the natural line width. In this case a photon of definite energy can interact with more nuclei of the inhomogeneous broadened ensemble; however the coupling strength to each nucleus, even if it is in perfect tuning, is weakened because of the fact that the distribution $f^T(\omega)$ must be properly normalized to

$$\frac{1}{T} |f^T(\omega)|^2 = 1 \qquad (4)$$

When emission is considered under the same conditions, also the emitted photon is described as a linear superposition of waves with frequency ω_γ each wave having the amplitude $a^T(\omega)$.

In order to test these ideas we have considered the case of absorption of such photons on a system of nuclei, subjected to fluctuations from the lattice (or homogeneous broadened by the interaction with the lattice). Two uncorrelated fluctuation functions f(t) and g(t) are introduced[1], f(t) describes the fluctuations on the absorbing nucleus and g(t) describes the fluctuations on the emitted photon and has a fourier transform called $g^T(\omega)$. Under such conditions, it is shown that the absorption probability is not weakened when the homogeneous width of the emitter matches the width of the absorber. This fact is in contrast to the previous case where only one side was homogeneously broadened. From that calculation we obtained for the absorption rate :

$$R^T(\omega_0 - \omega_0') = \frac{2\pi}{\hbar^2} |<||>|^2 \frac{1 - e^{-2\gamma_n T}}{2\gamma_n} \frac{1}{\Delta T} \int_0^{\infty} f^{\Delta T}(\omega_\gamma - \omega_0)^*\, g^{\Delta T}(\omega_\gamma - \omega_0')\, d\omega \qquad (5)$$

When both distributions are of the same type and width, as it is the case in a self–absorption experiment, one obtains for the last factor

$$\frac{1}{\Delta T} \frac{1}{2\pi} \int_0^{\infty} f^{\Delta T}(\omega_\gamma - \omega_0)^*\, g^{\Delta T}(\omega_\gamma - \omega_0')\, d\omega = \frac{1}{\Delta T} \frac{1}{2\pi} \int_0^{\infty} |f^{\Delta T}(\omega - \omega_0)|^2\, d\omega \qquad (6)$$

The last expression is the averaged power absorbed and is equal to unity for one photon and equal to the total flux of photons for a beam of photons.
It is clear that when the width is changed, this value does not change and consequently the weakening of the coupling does not occur. When inhomogeneities are now introduced the detuning is

different for each nucleus and therefore each emitted photon will find only a limited number of nuclei with which it can interact. Without fluctuations this width is equal to the natural width, however with fluctuations the width is much larger and given by the shape $f^{\Delta T}(\omega)$.

Experiments on ^{109}Ag

It is in the above context that the observation of the Mössbauer effect with the 88 keV γ–ray in ^{109}Ag (τ = 57.14 sec), attracted our interest. The natural line width $\hbar/\tau = 1.15\ 10^{-17}$ eV of this resonance is at least four orders of magnitude smaller than the crystalline inhomogeneities ($\sim 10^{-13}$ eV) that one expects due to nuclear dipole–dipole interaction in a solid[2]. Conventional wisdom thus indicates that for such a case, chances of observing the Mössbauer effect, if any, are virtually nil[3,4]. However if we consider that not the natural width, but the fluctuation width must be compared to the inhomogeneous one, then these widths could be comparable and one has a chance to observe Mössbauer absorption.

Cognizant to this background, we designed the ^{109}Ag experiment to look for the small Mössbauer effect reported previously[3,4]. A vibration–free closed–cycle refrigerator facility for continuous operation in the T–range 12K<T<300K was used to mount a surface diffused ^{109}Cd in a 0.50 mm thick (111) grown Ag–single crystal to detect γ–rays in the transverse geometry. An intrinsic Ge–detector with 0.6 keV resolution at 88 keV was used to record pulse–height spectra. The source temperature could be regulated in the T–range 15K<T<150K and stabilized on long term (week) to ± 0.2K. Typically at a given temperature, 100 million counts were accumulated over a 5–day period under each γ– and X–ray peaks, yielding a statistical error of about 0.02% for the X/γ ratio. Our use of the transverse geometry, i.e. the γ–ray detection axis (k) normal to the long–axis (z) of the cold–finger, significantly reduces (by two orders of magnitude) changes in solid–angle due to thermal contraction of the cold–finger, in relation to the longitudinal geometry (where k is parallel to z) employed by previous workers[3,4]. Hoy and Taylor[4] recognized that in these resonant self–absorption measurements the ratio R of X– to γ–ray integrated intensity, compensates for a change in the counting rate due to the parent ^{109}Cd source decay ($t_{1/2}$ = 462 days), as well as for a change in detector solid–angle due to thermal contraction of the cold–finger. The presence of the Mössbauer effect in Ag would then in principle result in an increased ratio R(T) a lower temperatures, because of a reduction in the transmission of the γ–rays due to resonant absorption.

To obtain the ratio R from the pulse height spectra, we developed a procedure to subtract the background under the γ–ray photo peak and the X–ray peaks which would be insensitive to small shifts (~ 150 eV) in the peak centroid. The result of this analysis gave the T–dependence of the ratio R(T) which is displayed in fig. 1. The smooth line through the data points is a guide to the eye. These results were obtained at ambient magnetic field, which was measured to be about 400 mGauss at the source location in our laboratory.

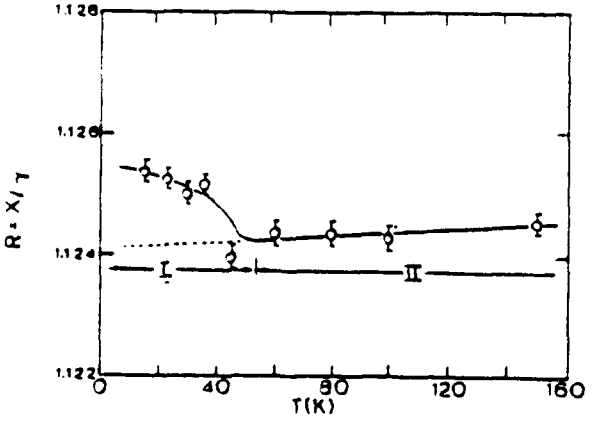

fig. 1

T–dependence of the ratio R, displaying evidence of a small Mössbauer effect at T ≤ 50K.

Two distinct regions in the R(T) variation can be discerned from the plot of fig. 1 : in region I (15K<T<50K) R(T) is found to decrease with increasing temperature and at T>60K, to more or less saturate in region II. The decrease in R(T) with T in region I mimics the T–dependence[4] of the Debye–Waller factor (f–factor) for the 88 keV γ–ray in Ag–metal (θ_D = 225K). The R(T) variation in region I thus has the right trend to suggest that it constitutes evidence for a rather small (0.09 ± 0.02%) but positive Mössbauer effect. At T > 60K the f–factor becomes minuscule (less than 0.01) and one does not expect any resonant self–absorption to contribute to the R(T) ratio in region II. In this region thermal expansion[4] of the Ag–metal source matrix is primarily responsible for the linear variation of R(T). The thermal expansion effect in region II for our case is determined by the effective depth to which the ^{109}Cd activity is diffused in Ag–crystal. In these experiments we chose to record pulse height spectra from that side of the Ag crystal, on which ^{109}Cd activity was surface diffused, merely to keep the thermal expansion effect as small as possible.

We conclude with two final comments. The smallness of the Mössbauer effect observed here 0.09(2)%, we believe, is in keeping with the conditions prevailing in our experiment. A careful examination of the ratio R(T) in region I reveals that its increase at T = 15K is the result largely of enhanced X–ray counting rate and not so much a decreased γ–ray counting rate. This is precisely what one would expect for a surface diffused source. The γ–counting rate did not decrease because for the γ–rays that are emitted towards the detector, the thickness of silver is extremely small. For the γ–rays emitted in the backwards hemisphere, there is large thickness of Mössbauer nuclei. A nucleus that has absorbed an 88 keV photon will decay for about 90% by electron conversion emitting an X–ray, producing the increase in X–ray intensity we have observed.

It is also clear that in an ambient field of 400 mGauss, the nuclear Zeeman splitting of the ^{109}Ag resonance is 2.22 10^{-11} eV, which is six–orders of magnitude larger than the natural width (γ_n = 1.15 10^{-17} eV). A consequence of this circumstance is that only 27.58% of the resonant cross–section is accessible for the present self–absorption experiments, which merely probes the v = 0 mm/s component of the split source, split absorber hyperfine structure[5]. It is abundantly clear that by a judicious choice of the design of this experiment, such as reduce the ambient magnetic field, detect conversion electrons rather than γ–rays, the size of the resonant self–absorption signal can be significantly enhanced, if the Mössbauer effect, that we claim to observe here, is real. This we are currently in the process of implementing.

Experiments on ^{12}B

We also want to test a concept of changing the relaxation time by adjusting a magnetic field. The general concept is that relaxation is induced by small interactions, H_p, that are non–diagonal in the eigenstate representation of the main hamiltonian H_o. As long as the energy gaps between all eigenvalues of H_o remain large compared to the non–diagonal matrix element $< H_p >$, the effect of the perturbation is very small. However from the study of level crossing and anti–crossing of a two level system, we know that the levels strongly mix, as soon as the two levels come closer than $< H_p >$. The effect of H_p then dominates the evolution of the two–level system.

We performed a series of experiments in which ^{12}B is produced, polarized and recoil implanted by a ^{11}B (d,p) ^{12}B reaction in an Al single crystal[6]. We measured the asymmetry of the β–decay as a function of external field. We know that ^{12}B implants interstitially[6] (fig. 2) in Al.
So ^{12}B sees a surrounding that has a perfect cubic symmetry, while for its neighbouring Al nuclei, the cubic symmetry is broken by the presence of the ^{12}B. Thus the Al nuclei feel an electric field gradient that decreases with the distance from the ^{12}B.
As a consequence the quadrupole interaction of the Al in the different neighbouring shells are different and the coupling between these Al nuclei, which in a normal crystal is resonant, is now no more resonant and thus these Al nuclei from different shells are more or less mutually decoupled.

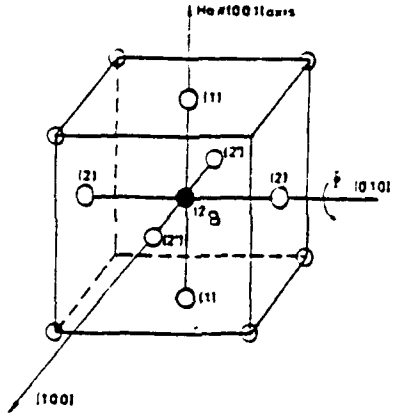

fig. 2

F.c.c. Al (open circle) with interstitial ^{12}B (filled circle) octahedrally coordinated to 3 pairs of Al nns.

The polarization direction is perpendicular to the reaction plane and a magnetic field can be applied in the same direction. In these experiments the Al s.c. is directed with a [001] axis in the polarization and magnetic field axis. As visualized in fig. 2, the first shell consists of 6 Al nuclei, which split in two groups under influence of the magnetic field. For the two Al nuclei along the [001] axis the magnetic field is parallel to the E.F.G.–axis, while for the four other ones the field is perpendicular to the E.F.G.–axis. At well defined magnetic fields some hyperfine splitting gap on ^{12}B can be equal to a gap in the neighbouring Al nucleus. Then the coupling is resonant and can be observed by a resonant change of the ^{12}B polarization. The resonant magnetic field will be different for the two groups. Indeed as shown in fig. 3 two distinct resonant depolarizations are observed as a function of the magnetic field.

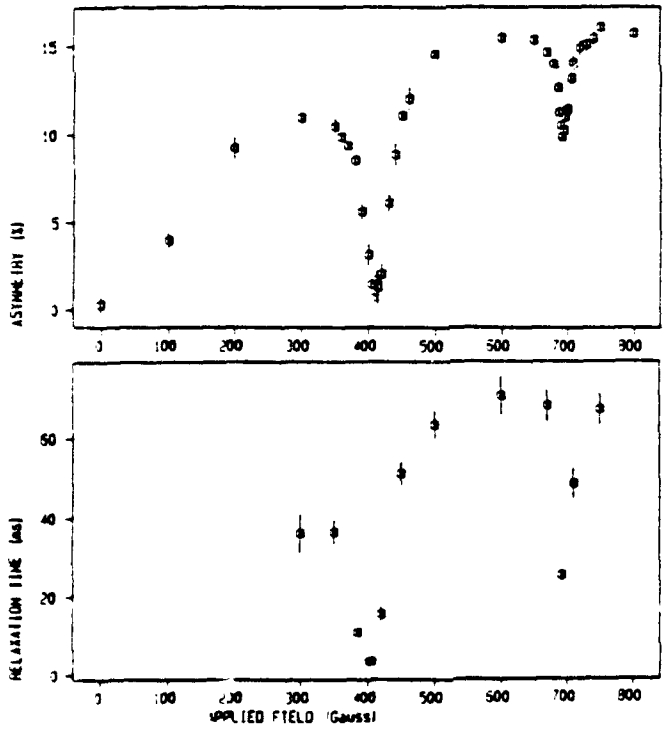

fig. 3

^{12}B spin polarization as a function of magnetic field.

fig. 4

Spin relaxation time as a function of magnetic field.

In order to start the study of the process of polarization exchange between ^{12}B and his Al nearest neighbours, we started to measure the polarization as a function of time, in and out of resonance. We observed an enhancement of the relaxation of ^{12}B as soon as it is resonantly coupled to its neighbouring Al nuclei (fig. 4). Further experiments are planned to fully understand these phenomena.

Conclusion

For the realization of a γ–ray laser in which the long lived isomer is both the storage and lasing level, two concepts need to be demonstrated; the effect of homogeneous broadening on the coupling to the radiation field and the enhancement of relaxation under the influence of a 'resonant' magnetic field. For both these concepts we have proof of feasibility from the present ^{109}Ag and ^{12}B experiments. In a parallel theoretical effort, the basic ideas, underlying these phenomena, have been refined. These studies are very closely connected to previous studies on nuclear–level–mixing.

References

1 Nuclear resonant absorption for long living isomeric transitions. R. Coussement, P. Boolchand, G. S'heeren, M. Van Den Bergh, in preparation.

2 P. Boolchand, J. Quant. Spec. Radiat. Transfer 40, 777 (1988).

3 W. Wildner and U. Gonser, J. Phys. (Paris) 40, C2 47 (1979).

4 G. R. Hoy and R. D. Taylor, J. Quant. Spec. Radiat. Transfer 40, 763 (1988).

5 R. Harris, Y. Wu, R. Enzweiler, P. Boolchand, M. Van Den Bergh and R. Coussement, Bull. Am. Soc. 36, 626 (1991).

6 H.–J. Stöckmann, E. Jäger, G. Sulzer, B. Ittermann, H. Ackermann, E. Diehl, R. Dippel, B. Fisher, H.–P. Frank and W. Seelinger, Hyp. Int. 49, 235 (1989).

*Research is sponsored by SDIO/IST and managed by ONR on grant N00014–88–K–2035.

Hyperfine Interactions 71 (1992) 1487-1490

MÖSSBAUER ABSORPTION ON ^{109m}Ag, FAKE OR REALITY?

R. COUSSEMENT, M. VAN DEN BERGH, G. S'HEEREN

Katholieke Universiteit Leuven, 3001 Heverlee, Belgium

and P. BOOLCHAND

University of Cincinnati, Cincinnati, Ohio 45221-0030, U.S.A.

1. Introduction

In ^{109m}Ag, the natural line width ($\tau_0 \cong 10^{-17}$eV) is about four orders of magnitude smaller than the inhomogeneous width, unavoidable in a solid state material ($\geq 10^{-12}$eV). Therefore one will expect that resonant absorption cannot be detected because each photon can interact resonantly with only a very few nuclei in the absorber. However, for long–lived isomers, the temporal behavior of an emission and absorption process must be considered and one must include the interaction of the nuclei with the lattice during that process.

2. Description of nucleus and photon

For long–lived states the interaction with the radiation is very weak and the interaction with the lattice dominates. During the emission or absorption process the lattice can induce frequent modifications in frequency and phase. Therefore a single photon which is emitted from such an interacting nucleus will be frequency– and phase–modulated and thus contains information about the interaction of the emitting nucleus with the lattice.

For shorter–lived nuclei however the interaction with the radiation field is stronger and the emission or absorption process is much shorter so that the lattice has no chance to induce any change during that process. The emitted photon will pick up a momentary value of frequency and phase and in this case the information about the fluctuations, induced by the lattice, can be obtained only from observables on a large ensemble. So for short–lived isomers, each photon is somewhat different in frequency and phase, leading to inhomogeneous broadening.

In contrast when long–lived isomers are considered, the wave functions of each nucleus and of each emitted photon of the ensemble are all identical. They are however not stationary states but coherent superpositions of them. We can therefore introduce a fluctuation function in the time domain, which is the Fourier transform of that superposition spectrum.

We can thus express the non–stationary wave function as

$$\Psi(\vec{x},t) = \psi(\vec{x},0)\, f(t)\, e^{-\Gamma_n t/2}\, e^{-i\omega_0 t} \tag{1}$$

in which ω_0 is the main energy of the fluctuating state. The damping factor $e^{-\Gamma_n t/2}$ reflects the interaction with the continuum of the radiation field, while f(t) reflects the interaction with the lattice.

We can describe the amplitude for a photon with detuning $(\omega - \omega_0)$ emitted at time T as

$$A^T(\omega-\omega_0) = -\frac{i}{\hbar} \langle f|V|i\rangle_{t=0} \int_0^T f(t)\, e^{-\Gamma_n t/2}\, e^{-i(\omega-\omega_0)t}\, dt \tag{2}$$

$$= -\frac{i}{\hbar} \langle f|V|i\rangle_{t=0} \frac{1}{\sqrt{2\pi}} \mathcal{F}^T(\omega-\omega_0)\,. \tag{3}$$

J.C. Baltzer A.G., Scientific Publishing Company

It means that at time T, the system has emitted a photon, which is a superposition of photon states with different frequencies ω. The width and shape of the frequency distribution is given by $\mathcal{F}^T(\omega-\omega_0)$, which is the Fourier transform of the fluctuation and the damping functions. So we can conclude that the photon is also modulated and damped in the same way as the nucleus from which it is emitted.

3. Absorption of photons in a self-absorption geometry

When absorption of such a photon is considered, the photon will carry the fluctuations from the emitting source and in the expression of the absorption amplitude we will have two fluctuation functions, one form the source and one from the absorber. These functions, called $g(t)$ and $f(t)$, can be exactly the same when source and absorber are in the same material at the same temperature and in the same other conditions. It is the case when self-absorption in ^{109}Ag is considered. However it is important to notice that the fluctuations $f(t)$ and $g(t)$ are not correlated.

We introduce it in the absorption amplitude

$$A^T(\omega_0-\omega'_0) = -\frac{i}{\hbar}\langle f|V|i\rangle \int_0^T f(t)g^*(t)\, e^{-\Gamma_a t}\, e^{-i(\omega_0-\omega'_0)t}\, dt \qquad (4)$$

and using Parcivals theorem we obtain

$$A^T(\omega_0-\omega'_0) = -\frac{i}{\hbar}\langle f|V|i\rangle \int_0^\infty \mathcal{F}^T(\omega-\omega_0)\, \mathcal{G}^T(\omega-\omega'_0)^*\, d\omega \qquad (5)$$

in which $\mathcal{F}^{\Delta T}(\omega-\omega_0)$ and $\mathcal{G}^{\Delta T}(\omega-\omega_0')$ are the Fourier amplitudes of the fluctuations at the absorber resp. the emitter.

Thus the amplitude is a convolution of the source and the absorber frequency spectra. Such a convolution depends on the shapes and positions of the two spectra. However if we can assume that they have the same shape, then at zero detuning ($\omega_0=\omega_0'$), the convolution will no more depend on the shapes at least if the Fourier spectra are properly normalized as

$$\frac{1}{T}\int_0^T |f(t)|^2\, dt = 1 \qquad \text{or} \qquad \frac{1}{T}\frac{1}{2\pi}\int_{\omega=0}^{\infty} |\mathcal{F}^T(\omega-\omega_0)|^2\, d\omega = 1\,. \qquad (6)$$

Until now we didn't specify the shape of the Fourier spectrum, neither the time dependence of $f(t)$. We assume that the coupling of the lattice to the nucleus is a weak coupling in this sense that the lattice changes very frequently, inducing at each event only a very tiny change on the nucleus. In the obervation time scale, the function $f(t)$ can be regarded as a continuous and smooth function. We also assume that the nuclear system is in equilibrium with the lattice so that the function $f(t)$ is assumed to fluctuate around unity and that the Fourier spectrum is independent on the choice of time interval. Under these assumptions the transition rate can be written simply as a function of the detuning between emitter and absorber :

$$R^T(\omega_0-\omega'_0) = \frac{2\pi}{\hbar^2}|\langle f|V|i\rangle|^2\, \frac{1-e^{-2\Gamma_a T}}{2\Gamma_a}\, \frac{1}{\Delta T}\int_0^\infty \mathcal{F}^{\Delta T}(\omega-\omega_0)\, \mathcal{G}^{\Delta T}(\omega-\omega'_0)^*\, d\omega\,. \qquad (7)$$

In the case of self–absorption absorber and emitter display the same Fourier spectrum and the detuning is zero. Under these conditions for optimal convolution, the absorption rate is not only optimal, but this optimal value is independent of the shape of the Fourier spectrum.

However in such a self–absorption experiment inhomogeneities /1/ can introduce serious detuning for which the convolution integral and consequently the absorption is smaller. When the detuning distribution corresponding to the inhomogeneous distribution would be large compared to the homogeneous width, then the total absorption probability would decrease. However, if the inhomogeneous width is much smaller than the width of the Fourier spectrum, then the inhomogeneities will almost not affect the total absorption rate.

For ^{109}Ag, we estimate the homogeneous width to be associated with the T_1 relaxation and not with the nuclear decay. Therefore in order to observe Mössbauer absorption it will be sufficient that the inhomogeneous broadening is smaller than 10^{-12}eV, which is a much less stringent condition than to be less than the natural width (10^{-17}eV).

4. Experiments

We found therefore that the positive results, reported in /2/ and /3/, could be real. We designed a self–absorption experiment in which we avoid geometry changes which occur when the sample is cooled to He–temperature. We used a cold finger, cooled by a closed cycle refrigerator and we detected the gamma rays in a detector perpendicular to the cold finger or the direction of shrinking (fig. 1). Because of that geometry and because of the short length of the cold finger, our experiment is about hundred times less sensitive to geometry changes induced by the cooling, than previous experiments. Furthermore we have the advantage that we can measure in the full temperature range from 10 K up to room temperature, without touching the system.

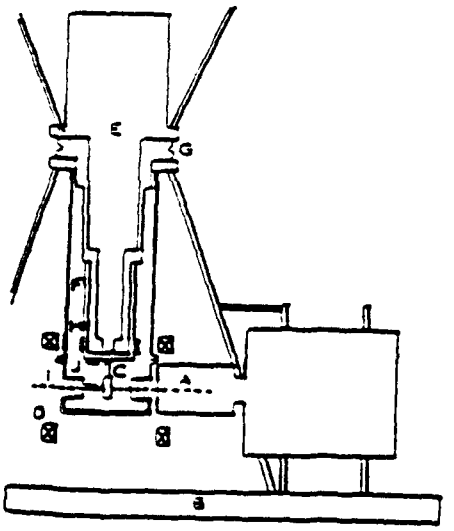

A: Ge detector
B: Vibration–free platform
C: ^{109}Cd/Ag source
D: Helmholtz coils
E: Closed cycle refrigerator
F: Cold finger
G: Rubber bellows
H: Heater
I: Hall probe insert
J: Si–diode thermometer

fig. 1 Experimental set–up

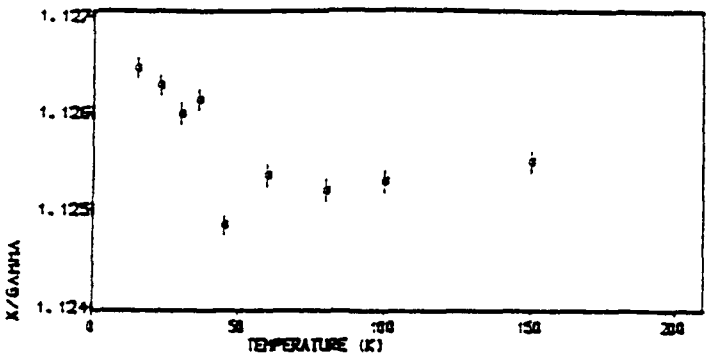

fig. 2 X/gamma measurement as function of temperature.

Our preliminary results, indicate a small effect, which shows up at the right temperatures (fig. 2). However before concluding, we want to make some supplementary experiments, in order to exclude every systematic error. One of the most critical will be to reduce the ambient magnetic field to such a level that the Zeeman splitting is smaller than the homogeneous width. In that case the Mössbauer effect must increase by a factor of about four. However we don't have precise data on the homogeneous width, but we estimate from relaxation in Ag that the width could be of the order of magnitude of 10^{-12}eV. In order to achieve the above condition we must reduce the ambient field to a level below 1 mGauss, which is not trivial.

5. Conclusions

For long-lived isomers, the condition for Mössbauer effect is not that the natural line width, but that the homogeneous line width must overwhelm the inhomogeneities. This homogeneous line broadening can be due to the action of the lattice and is much larger than the natural one. Experiments are not conclusive yet, but improvements are expected.

Acknowledgements

This work was sponsored by SDIO/IST and managed by ONR grant N00014-88-K-2035.

References

/1/ P. Boolchand, J. Quant. Spectrosc. Radiat. Transfer 40, 777 (1988).
/2/ W. Wildner and U. Gonser, J. Phys. 40, C2 47 (1979).
/3/ G. Hoy and R. Taylor, J. Quant. Spectrosc. Radiat. Transfer 40, 783 (1988).

Manuscript submitted to Physical Review Letters

Non–reciprocity of Gamma Emission and Absorption due to Quantum Coherence at Nuclear Level–Crossings

R. Coussement, M. Van Den Bergh, G. S'heeren, G. Neyens, R. Nouwen
Katholieke Universiteit Leuven,
3001 Heverlee, Belgium.

P. Boolchand
University of Cincinnati,
Cincinnati, Ohio 45221–0030, U.S.A.

We show that presence of destructive interference due to quantum coherence at nuclear Zeeman level–crossings precludes absorption but not emission of γ–rays. The underlying principle can be demonstrated in a Mössbauer effect experiment and has broad consequences in the domain of gamma–optics.

The presence of quantum coherence effects at level–crossings either in an atomic, nuclear or muon–spin related system offers possibilities of exploring new physical effects. In the atomic case, for example, the non–reciprocity between emission and absorption of optical radiation at such crossings has led to the concept of lasing without inversion[1-3], dark–line resonances[4] and more recently to the recognition of an enhancement of the index of refraction[5]. The corresponding nuclear case has remained largely unexplored in this regard. In this Letter, we show for the first time that the reciprocity between gamma emission and absorption, so well documented in Mössbauer spectroscopy experiments will cease to occur at Zeeman–level crossings due to quantum coherence effects. In particular, for an excited nuclear state, the destructive interference between a pair of Zeeman levels in a crossing condition will preclude absorption of γ–rays although not their emission . The underlying principle appears to be generic and has important consequences for gamma optics and in particular for stimulated emission of γ–rays, as we shall comment later.

Each level–crossing experiment in practice entails a specific experimental scheme to produce a coherent superposition of a pair of levels. In the atomic case, this is usually achieved for instance by interaction of an atomic system with an electromagnetic field[6,7]. In the nuclear case, an elegant and controlled way[8] to achieve level–crossing of Zeeman levels can be achieved by a combined Electric Field Gradient (EFG) from a non–cubic crystalline host and and external magnetic field producing a field B at the nucleus. The arrangement is schematically illustrated in figure 1.

Let us consider a nucleus of spin I ($I > 1/2$) subject to a predominant electric quadrupole interaction $eQV_{zz}/4I(2I-1) = \hbar\omega_Q$ due to a static EFG from a crystal and a magnetic–dipole interaction $g\mu_n B = \hbar\omega_B$ due to a magnetic field $\vec{B}$ applied at a small angle β ($< 10°$) wrt the symmetry axis of the EFG (V_{zz}). For simplicity we assume the EFG tensor to be axially symmetric, i.e. $V_{xx} = V_{yy}$. The lack of collinearity of the V_{zz} component and the direction of B is critical and is a point we shall return to later.

The hamiltonian describing the hyperfine interaction of the nuclear spin I with the EFG and external magnetic field B, applied at an angle β wrt V_{zz} consists of three terms as follows :

$$\mathcal{H} = \frac{\omega_Q}{\hbar}(3I_z^2 - I^2) - \omega_B \cos\beta\, I_z + \frac{\omega_B}{2}\sin\beta\,(I_+ + I_-) \qquad (1)$$

The first two terms describe the axial symmetry preserving interaction ($\mathcal{H}_\parallel$) and lead to a crossing of the Zeeman levels at specific magnetic field values B as illustrated in fig. 2. The third term describes the axial symmetry breaking interaction $\mathcal{H}_\perp$, and leads to a mixing of the crossed Zeeman levels which is controlled by the tilt angle β. For small values of B, we can neglect the third term in expression (1) to first order and obtain the level–crossings by requiring the eigenvalues of the symmetric part of the hamiltonian to become degenerate for a pair of Zeeman levels (m,m') :

$$E_m - E_{m'} = \hbar\,\omega_Q\,[3(m^2 - m'^2)] - \hbar\,\omega_B\cos\beta\,(m - m') = 0 \qquad (2)$$

leading to the level–crossing condition :

$$\omega_B = 3\,(m + m')\,\omega_Q\,/\,\cos\beta. \qquad (3)$$

as illustrated in the Breit–Rabi diagram of fig.2, drawn for the first excited state (I=3/2) of ^{57}Fe as an example.

At and near level–crossing fields, the symmetry breaking term in the hamiltonian although small cannot be neglected because of the degeneracy of the two crossing levels (m,m'). This term then strongly admixes the pure states $|m>$ and $|m'>$ and results in eigenfunctions and eigenvalues that are easily calculated analytically.
The eigenfunctions, $|1>$ and $|2>$ are a coherent superposition of the pure $|m>$ and $|m'>$ states,

$$|1> = \frac{1}{\sqrt{1+R^2}}\{|m> - R\,|m'>\} \qquad (4)$$

$$|2> = \frac{1}{\sqrt{1+R^2}}\{R\,|m> + |m'>\} \qquad (5)$$

in which the mixing factor R is a function of the ratio between the splitting of the unperturbed levels $E_m - E_{m'}$ and the perturbation coupling between the crossing levels $W_{mm'}$.
For a crossing of first order, $\Delta m = |m - m'| = 1$, this perturbation coupling is the non–diagonal element of the perturbation hamiltonian :

$$W_{mm'} = <m|\,\mathcal{H}_\perp\,|m'> = \frac{\omega_B}{2}\sin\beta <m|(I_+ + I_-)|m'>. \qquad (6)$$

For crossings with $\Delta m > 1$ one finds the perturbation coupling by Δm–th order perturbation theory as given in ref.9.
It is these matrix elements which are responsible for the mixing of the eigenstates and for the repulsion between the energy levels because of the reduction in symmetry, due to the misalignment β between the EFG–axis and B. The energy difference between the mixed states $|1>$ and $|2>$ is now

$$|E_1 - E_2| = \sqrt{(E_m - E_{m'})^2 + (2\,W_{mm'})^2}. \qquad (7)$$

As long as the energy difference between a pair of levels is much larger than the perturbation coupling, $|E_m - E_{m'}| >> |2\,W_{mm'}|$, the mixing is negligible and pure states are found. The mixing is total at the crossing points, $E_m = E_{m'}$ and R =1, independently of the strength of the perturbation

and the order of the crossing. In these points the energy difference reaches a minimum value $|E_1 - E_2|_{min} = |2\ W_{mm'}|$. This energy difference can be thought of as a Rabi splitting. It is analogous to the frequency difference between two normal modes of a system of two coupled identical oscillators.

Let us now consider a gamma absorption process between a ground state $|\mu>$ and two excited states $|m>$ and $|m'>$, for which the selection rules allow the transition between the ground state and the pure state $|m'>$ but forbid the transition to the pure state $|m>$ (fig.3). Near the level–crossing field, the pure states are admixed to form the eigenstates $|1>$ and $|2>$ as described by equations (4) and (5). A photon of frequency ω (fig.3) can be absorbed in two modes A_1 and A_2, corresponding to the absorption amplitude to state $|1>$, respectively state $|2>$. This is possible because both the admixed states $|1>$ and $|2>$ contain the pure state $|m'>$, to which the selection rules allow a transition provided the detunings (energy differences) are not too large. If δ_1 and δ_2 represent the detunings between the initial state and the two final states $|1>$ and $|2>$, the absorption amplitudes are given by :

$$A_1 = \frac{-i}{\hbar} < 1|V|\mu> \int_0^{+\infty} e^{i\delta_1 t}\, dt \tag{8a}$$

$$A_2 = \frac{-i}{\hbar} < 2|V|\mu> \int_0^{+\infty} e^{i\delta_2 t}\, dt \tag{8b}$$

where V is the transition operator. In a Mössbauer absorption experiment, the γ–ray energy of the emitter ($\hbar\omega$) relative to a stationary absorber, can be modulated by Doppler shift :

$$\omega = \omega_0 \left(1 + \frac{v}{c}\right), \text{ so} \qquad \delta_1 = \left|\omega_0 \left(1 + \frac{v}{c}\right) - \omega_1\right|$$
$$\delta_2 = \left|\omega_0 \left(1 + \frac{v}{c}\right) - \omega_2\right|. \tag{9}$$

Let us assume that the states $|1>$ and $|2>$ are radiatively broadened due to the interaction with the vacuum fluctuations of the radiation field. Absorption to a decaying system can be seen as a process in which not only the transition from the groundstate to the excited state takes place, but where also the excited state decays in a continuum of final states. In the case of decay by re–emission of a γ–ray, the continuum is due to all possible frequencies, directions and polarisations of the re–emitted radiation. The fact that one deals with an open system is usually taken into account by adding a damping factor $e^{-\Gamma_n t/2}$ to the wave function [10].

One then obtains :

$$A_1 = \frac{-i}{\hbar} <1|V|\mu> \int_0^{+\infty} e^{-\Gamma_n t/2}\, e^{i\delta_1 t}\, dt = \frac{-i\sqrt{2\pi}}{\hbar} <1|V|\mu>\, \mathcal{F}(\delta_1) \tag{10a}$$

$$A_2 = \frac{-i}{\hbar} <2|V|\mu> \int_0^{+\infty} e^{-\Gamma_n t/2}\, e^{i\delta_2 t}\, dt = \frac{-i\sqrt{2\pi}}{\hbar} <2|V|\mu>\, \mathcal{F}(\delta_2) \tag{10b}$$

This situation is very similar to what is described in ref.1, ref.2 and ref.3, for atomic systems.

The two transition amplitudes are coherent because we consider a proces with two quantum paths both starting from an initial state $|\mu>$, one passing through state $|1>$, the other through state $|2>$ and both ending at the same levels $|K>$ of the previous described continuum. Therefore, we must add the amplitudes A_1 and A_2 as they are phase–locked to the same initial state (ground state plus one photon) :

$$A = A_1 + A_2 \tag{11}$$

Adding the amplitudes leads to interference terms in the transition probability. In most cases this interference disappears, e.g. when states $|1>$ and $|2>$ are stationary states without finite line width or when the energy difference between the levels is so large that the overlap can be neglected.
However in the case of mixed and repulsing levels, the separation can be tuned by choosing the misalignment angle β in such a way that overlap of the line shapes is achieved. In this case interferences play a critical role.

Taking into account the mixed structure of the eigenfunctions and the selection rules, we obtain for the partial amplitudes :

$$A_1(\delta_1) = \frac{-i\sqrt{2\pi}}{\hbar} <m'|V|\mu> \frac{-R}{\sqrt{1+R^2}}\, \mathcal{F}(\delta_1) \tag{12}$$

$$A_2(\delta_2) = \frac{-i\sqrt{2\pi}}{\hbar} <m'|V|\mu> \frac{1}{\sqrt{1+R^2}}\, \mathcal{F}(\delta_2). \tag{13}$$

The total amplitude, as a function of the photon frequency ω, can now be written as :

$$A(\omega) = \frac{-i\sqrt{2\pi}}{\hbar} <m'|V|\mu> \frac{\mathcal{F}(\delta_2) - R\,\mathcal{F}(\delta_1)}{\sqrt{1+R^2}} \tag{14}$$

leading to the absorption probability :

$$|A(\omega)|^2 = \frac{2\pi}{\hbar^2} |<m'|V|\mu>|^2 \frac{|\mathcal{F}(\delta_2) - R\,\mathcal{F}(\delta_1)|^2}{1 + R^2} \tag{15}$$

In equation (15) we see that near the level crossing field we have destructive interference and the probability $|A(\omega)|^2$ begins to vanish. Specifically, at the level–crossing, the mixing factor R = 1

and then we get a complete destructive interference of the amplitudes A_1 and A_2 when $\mathcal{F}(\delta_1) = \mathcal{F}(\delta_2)$, which occurs for the frequency $\omega = (\omega_1 + \omega_2)/2$. Away from the level–crossing field, one expects the interference effect due to level–crossing to disappear. Thus, in effect, quantum coherence at Zeeman level–crossings leads to a hole–burning in the absorption spectrum only around the crossing field.

In a Mössbauer emission experiment utilizing the same two levels $|1>$ and $|2>$ a totally different situation prevails. Emission can occur from state $|1>$ or from state $|2>$ and there is no coherent superposition since these states are fed from a parent state independently. So one can write the total probability for emission as made up of the individual probabilities for each decay :

$$P(\omega) = p_1 \, |A_1(\omega)|^2 + p_2 \, |A_2(\omega)|^2 \tag{16}$$

where p_1 and p_2 represent the initial populations of states $|1>$ and $|2>$. Assuming $p_1 = p_2 = p$ we obtain for the emission :

$$P(\omega) = \frac{2\pi}{\hbar^2} p \; | <m'|V|\mu> |^2 \frac{|\mathcal{F}(\delta_2)|^2 + R^2 \, |\mathcal{F}(\delta_1)|^2}{1 + R^2}. \tag{17}$$

Equation (17) shows that no destructive interference can occur in the emission processes. We thus conclude that gamma–emission will take place, even at those frequencies for which the absorption vanishes.

We want to emphasize that this effect can only be observed if one can select the sublevel of the ground state for which destructive interference takes place. Otherwise the constructive interference term corresponding to the other sublevel will cancel the effect.
In this particular case of level mixing however, the upper levels are nearly degenerate while the ground levels are fully split. This allows the destructive and constructive interferences to occur at different γ–energies or different modulation velocities in the Mössbauer spectrum.

In summary, we have shown that a non–reciprocity between γ–ray absorption and emission processes can occur at the nuclear level–crossing condition. The absence of absorption is intrinsically due to a destructive interference between two absorption amplitudes. A specific design of a controlled nuclear level–crossing experiment using combined EFG and external magnetic field is proposed, which is amenable to a test using a Mössbauer effect experiment. Indeed, demonstration of such an effect will open several exciting possibilities, one of which includes the feasibility of switching on and off γ–absorption attenuation by merely applying an appropriate external magnetic field.
An application of this concept resides in γ–ray lasers[11] where the attenuation of absorption will significantly ease the pumping and gain requirements for lasing to occur. One could pump the γ–ray laser in a normal mode and then move to a level–crossing condition to initiate lasing, thus providing a trigger for the device.

We are particularly grateful to Professor Bernard Goodman for many helpful suggestions.
This work was supported by Strategic Defense Initiative Organization / Innovative Science and Technology and managed by U.S. Office of Naval Research grant N00014–88–K–2035.

References

1 S.E. Harris, Phys.Rev.Lett. 62, 1033 (1989).
2 A. Imamoglu and S.E. Harris, Opt. Lett. 14, 1344 (1989).
3 A. Imamoglu, Phys. Rev. A 40, 2835 (1989).
4 G. Alzetta, A. Gozzini, L. Moi and G. Orriols, Nuovo Cimento **36B**, 5 (1976) ibid **52b**, 209 (1979); also see H. Gray, R. Whitley and C. Stroud, Opt. Lett. 3, 218 (1979).
5 M.O. Scully, Phys. Rev. Lett. 67, 1955 (1991).
6 K.–J. Boller, A. Imamoglu and S.E. Harris, Phys. Rev. Lett. 66, 2593 (1991).
7 J.E. Field, K.H. Hahn and S.E. Harris, Phys. Rev. Lett. 67, 3062 (1991).
8 R. Coussement, P. Put, G. Scheveneels and F. Hardeman, Hyp. Int. **23**, 273 (1985).
9 P. Put, R. Coussement, G. Scheveneels, F. Hardeman, I. Berkes, B. Hlimi, G. Marest, J. Sau and E.H. Sayoutry, Phys. Lett. **103A**, 151 (1984).
10 C. Cohen–Tannoudji, J. Dupont–Roc, G. Grynberg in "Processus d'interaction entre photons et atomes" (Interedition et Edition du CNRS, 1988), p. 328
11 See for example, J. Quant. Spect. Radiative Transfer 40, (1988) edited by B. Balko, L. Cohen and D.A. Sparrow for a recent view of developments in the field of γ–ray lasers.

Fig.1 *Magnetic field B applied at an angle β wrt the symmetry axis of the EFG provides a convenient way to produce nuclear level–mixings.*

Fig.2 *Breit – Rabi diagram for the excited state in ^{57}Fe subject to a quadrupole splitting of 1 mm/s and a collinear magnetic field B.*
Note the $\Delta m = 2$ and $\Delta m = 1$ Zeeman level crossing at 7.45 T and 14.9 T.

Fig.3 *Mixing of the pure Zeeman–levels $|m>$ and $|m'>$ leads to the mixed states $|1>$ and $|2>$ which are repulsed by an energy $\hbar(\delta_1 + \delta_2)$ at the crossing field where $\beta \neq 0$.*

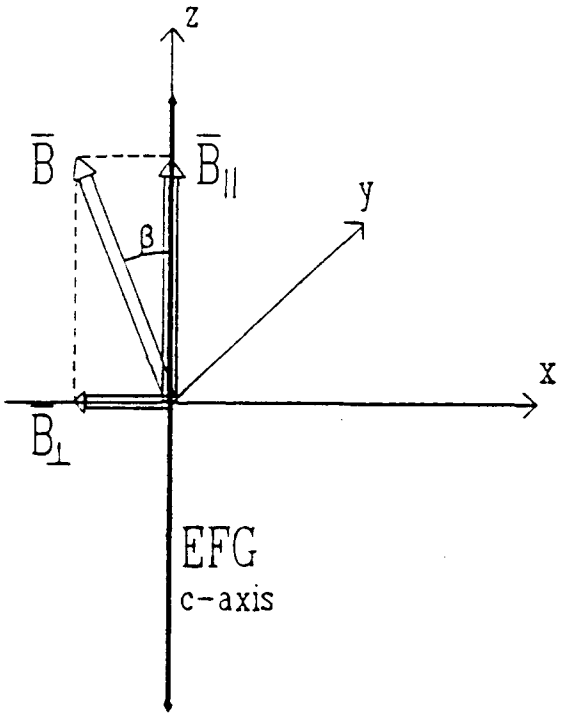

Figure 1.

Figure 2.

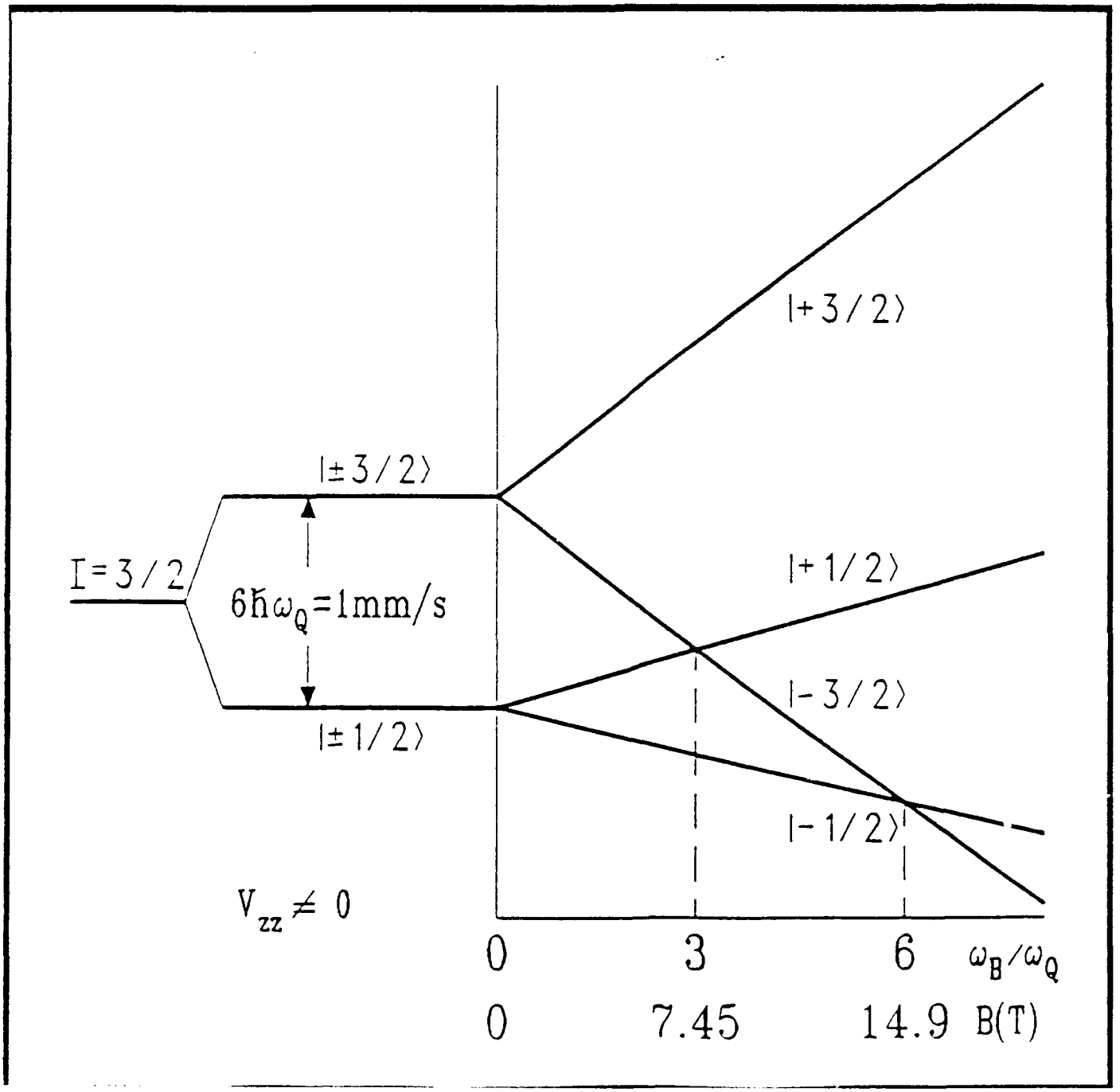

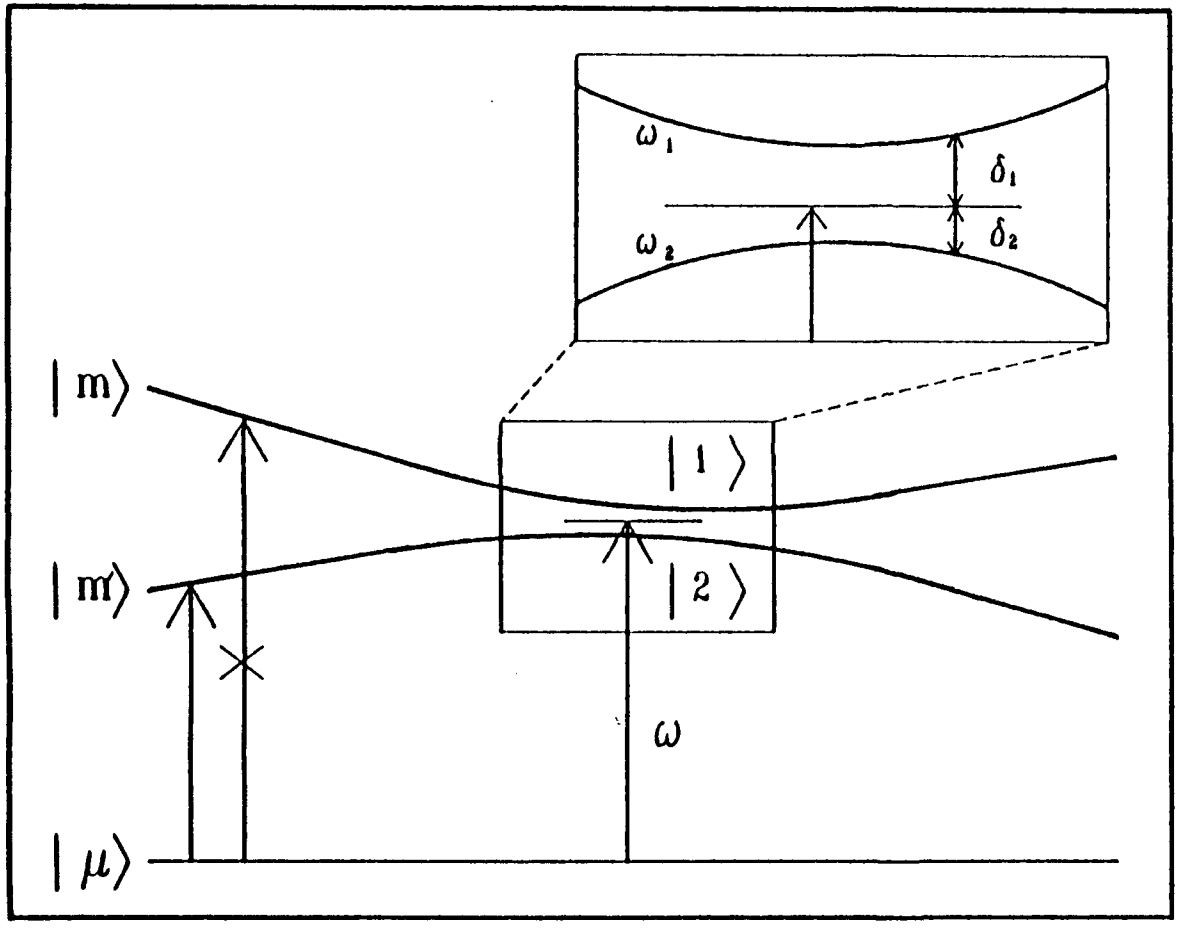
ω_1
δ_1
ω_2
δ_2
$|m\rangle$
$|1\rangle$
$|m'\rangle$
$|2\rangle$
ω
$|\mu\rangle$

Figure 3.

To be published in Hyperfine Interactions, presented at Hyperfine Interactions Conference, Osaka, Japan, August, 1992

QUANTUM INTERFERENCES IN NUCLEAR DECAY

R. Coussement, M. Van Den Bergh, G. S'heeren, G. Neyens, R. Nouwen

Instituut voor Kern – en Stralingsfysica, K.U. Leuven,

Celestijnenlaan 200D, B–3001 Leuven, BELGIUM

P. Boolchand,

University of Cincinnati, Cincinnati, Ohio 45221–0030, U.S.A.

Abstract : *At nuclear level mixing condition, interferences between different transition amplitudes can occur. In a narrow frequency range, absorption can be hindered while not the emission. This feature offers interesting applications on the design of a graser and of a resonant scatterer for γ – rays.*

Radiation physics using atomic systems is actually in rapid growth and continues to offer new surprising results. As most of the new effects explore the coherence of a laser beam, it is generally not applicable to nuclear systems. However a few of the ideas can be translated to nuclear radiation. We will show that nuclear systems offer some advantages compared to the atomic ones [1–7] because of the possibility of controlled nuclear level mixing phenomena.

Nuclear level mixing has been studied extensively in earlier papers [8–9]. Applying a magnetic field directed along the EFG axis of a quadrupole splitted nuclear system, will lift the $\pm$m degeneracy and some pairs of levels will cross for ω_B/ω_Q = 3, 6, 9 .. (fig. 1). When the magnetic field is slightly misaligned with respect to the EFG – axis the axial symmetry is slightly broken and the $|m\rangle$ states are no longer eigenstates of the system. The hamiltonian can be written as :

$$H = \frac{\omega_Q}{\hbar}(3I_z^2 - I^2) - \omega_B \cos\beta\, I_z + \omega_B \sin\beta\, (\frac{I_+ + I_-}{2}),$$

with the first term the quadrupole interaction hamiltonian, the second the Zeeman interaction due to the large component of the magnetic field along the EFG axis and the third term the Zeeman interaction due to the component perpendicular to it. The last term is the symmetry breaking one and its effect is to mix the $|m>$ – states. As the misalignment β is small, this mixing can be neglected except for two m – levels at and near the crossing fields. Near this crossing fields, the eigenfunctions can be calculated in a two–level approximation; they are coherent superpositions of the wave functions of the two crossing levels m and m' :

$$|1> = \frac{1}{\sqrt{1+R^2}}[\,|m> - R\,|m'>\,] \quad \text{and} \quad |2> = \frac{1}{\sqrt{1+R^2}}[\,R\,|m> + |m'>\,].$$

R is the mixing factor and at crossing fields one has always R = 1. Thus at the crossing field we obtain two wave functions, one being called the anti–phase, the other the in–phase superposition, similar to the system of coupled oscillators :

$$|1> = \frac{1}{\sqrt{2}}[\,|m> - |m'>\,] \quad \text{and} \quad |2> = \frac{1}{\sqrt{2}}[\,|m> + |m'>\,].$$

The levels $|1>$ and $|2>$ repel and the distance between them is given as :

$$|E_1 - E_2| = \sqrt{(E_m - E_{m'})^2 + 2\,W_{mm'}},$$

in which E_m and $E_{m'}$ are the eigenenergies of the Hamiltonian without the third term and $W_{mm'}$ is the matrix element of the third term. So we see that the minimum distance between level $|1>$ and level $|2>$ is obtained at the crossing field where $E_m = E_{m'}$ and equals $2\,W_{mm'}$. As that matrix element is dependent on β by the factor $\sin\beta$, one can easily control the level distance by adjusting the misalignment angle. Thus in a nuclear system it is rather easy to produce two close – lying levels of the in–phase and anti–phase type and to adjust their level spacing so that the two levels overlap by the radiative or lifetime broadening.

Let us now consider a gamma absorption between a ground state $|\mu>$ and the

system of two mixed levels $|1>$ and $|2>$ (fig. 2). In a Mössbauer set–up, the frequency of the gamma–ray can be doppler tuned : $\omega = \omega_0 \, (1 + \frac{v}{c})$. There is a frequency range, for which both the transition amplitude to state $|1>$ and the transition amplitude to state $|2>$ are contributing to the absorption. As both transitions are locked in phase to the same initial state (ground state + one photon), they can interfere. The total absorption amplitude is then given by :

$$A(\omega) = A_1(\omega) + A_2(\omega) \qquad \text{and} \qquad P(\omega) = |A(\omega)|^2.$$

The transition amplitudes to level $|1>$ and $|2>$ are given as :

$$A_i(\omega) = \frac{-i}{\hbar} <i|V|\mu> \int_0^\infty e^{-\Gamma t/2} \, e^{i\delta_i t} \, dt,$$

in which δ_i is the detuning to the first, respectively second level :

$$\delta_1 = |\omega_0 \, (1 + \tfrac{v}{c}) - \omega_1| = |\omega - \omega_1| \qquad \text{and} \qquad \delta_2 = |\omega_0 \, (1 + \tfrac{v}{c}) - \omega_2| = |\omega - \omega_2|.$$

The amplitudes are thus proportional to the Lorentzian amplitudes :

$$F(\delta_1) = \frac{1}{\delta_1 + i\Gamma/2} \qquad \text{and} \qquad F(\delta_2) = \frac{1}{\delta_2 + i\Gamma/2}.$$

The interference $A_1 A_2^* + cc$ will contribute only if the distance between level $|1>$ and level $|2>$ is of the order of the line width Γ. We can calculate the amplitudes $A_1(\omega)$ and $A_2(\omega)$ as :

$$A_1(\omega) = \frac{i\sqrt{2\pi}}{\hbar} \left[<m'|V|\mu> \frac{R}{\sqrt{1+R^2}} F(\delta_1) - <m|V|\mu> \frac{1}{\sqrt{1+R^2}} F(\delta_1) \right]$$

$$A_2(\omega) = \frac{i\sqrt{2\pi}}{\hbar} \left[-<m'|V|\mu> \frac{1}{\sqrt{1+R^2}} F(\delta_2) - <m|V|\mu> \frac{R}{\sqrt{1+R^2}} F(\delta_2) \right].$$

The transition matrix element contains a pure nuclear matrix element and a radiation-amplitude. This last one depends on the polarization σ of the photon and its direction θ with respect to the EFG – axis, chosen as the Z–axis. Furthermore we can apply the Wigner–Eckart theorem to the nuclear matrix element :

$$<m|V|\mu> = \sum_\sigma d^1_{m-\mu,\sigma}(\theta) \, C_{m\mu} \, <I_f\|V\|I_i>,$$

with $C_{m\mu}$ the Clebsch–Gordon coefficient $<I_i \, \mu, \, 1 \, m-\mu| \, I_f \, m>$. The resultant amplitude is

now given as :

$$A(\omega) = \frac{i\sqrt{2\pi}}{\hbar} \langle I_f \| V \| I_i \rangle \left[C_{m'\mu}\, d_{m'-\mu,\sigma}(\theta) \frac{1}{\sqrt{1+R^2}} \{ R\, F(\delta_1) - F(\delta_2) \} \right.$$
$$\left. - C_{m,\mu}\, d_{m-\mu,\sigma}(\theta) \frac{1}{\sqrt{1+R^2}} \{ F(\delta_1) + R\, F(\delta_2) \} \right].$$

We see clearly that when the selection rules allow the absorption from $|\mu\rangle$ to $|m'\rangle$ but not from $|\mu\rangle$ to $|m\rangle$, one obtains destructive interference while in the opposite case constructive interference occurs. One can easily deduce that at the level crossing field, where $R = 1$, the amplitude from $|\mu\rangle$ to $|m'\rangle$ can be completely hindered for the frequency $\omega = \frac{\omega_1 + \omega_2}{2}$ at which $F(\delta_1) = F(\delta_2)$. If furthermore the transition to $|m\rangle$ is forbidden by the selection rules, the absorption is completely hindered at that frequency. On the other hand, the emission from such a pair of incoherently populated levels $|1\rangle$ and $|2\rangle$ will not show interference, because of the random relative phase between the levels $|1\rangle$ and $|2\rangle$.

There are two methods to demonstrate these interferences. The most direct one is to observe the decrease or increase of a Mössbauer absorption line when the magnetic field is turned on to a crossing field. In fig 1 we display the Rabi diagram of the spin 3/2 case in ^{57}Fe. At the first crossing field the transition $\mu = +1/2$ to $m = -3/2$ is Δm–forbidden, while the $\mu = +1/2$ to $m' = +1/2$ is allowed. In this situation, complete destruction of the $\mu = +1/2 \rightarrow m = +1/2$ transition amplitude can be observed at the crossing field.

A second, but less direct test follows from the fact that it is possible to repeat the same argumentation for γ – ray emission from a sublevel $|\mu\rangle$ to a pair of mixed levels. The emission amplitudes are both phase locked to the same initial state and therefore coherent emission is achieved. As a consequence the transition probability to the pair of mixed levels can be enhanced or hindered. Considering the partial transition probability from the sublevel $|\mu\rangle$ to all final levels $|m_f\rangle$, $|m\rangle$ and $|m'\rangle$, the result is a decrease or increase in the partial lifetime. In order to formalize it, the partial transition probability from sublevel $|\mu\rangle$ is separated in a part containing the transition probabilities to

non–mixed $|m_f>$ levels and another part to expressing the transition probability to the pair of mixed levels $|1>$ and $|2>$:

$$P_\mu(\omega,\theta) = |<I_f\|V\|I_i>|^2 \sum_{m_f}{}' |C_{m_f,\mu}|^2 |\sum_\sigma d^1_{m_f-\mu,\sigma}(\theta)|^2 |F(\delta_{m_f})|^2 + |C_{m,\mu}|^2 |\sum_\sigma d^1_{m-\mu,\sigma}(\theta)|^2 \frac{1}{1+R^2} |F(\delta_1) - R\,F(\delta_2)|^2 + |C_{m',\mu}|^2 |\sum_\sigma d^1_{m'-\mu,\sigma}(\theta)|^2 \frac{1}{1+R^2} |R\,F(\delta_1) + F(\delta_2)|^2 + C_{m,\mu}\,C_{m',\mu} \sum_{\sigma,\sigma'} d^1_{m-\mu,\sigma}(\theta)\, d^{1\,*}_{m'-\mu,\sigma'}(\theta) \frac{1}{1+R^2} [F(\delta_1) - R\,F(\delta_2)]\,[R\,F(\delta_1) + F(\delta_2)]^*.$$

The helicity $\sigma(\sigma')$ is $+1$ or -1 for γ–rays. When considering the partial lifetime, the direction of propagation is random and we must integrate over the angle θ. Consequently the last term will disappear because of the orthogonality relation :

$$\int d^1_{m-\mu,\sigma}(\theta)\, d^{1\,*}_{m'-\mu,\sigma'}(\theta) \sin\theta\, d\theta \simeq \delta_{mm'}\,\delta_{\sigma\sigma'}.$$

We must also integrate over all frequencies ω, which results in an integration over the detunings δ_{m_f}, δ_1 and δ_2. As the line shapes are normalized such that $\int |F(\delta_1)|^2\, d\omega = 1$, we get for the partial probability :

$$P_\mu = |<I_f\|V\|I_i>|^2 \left[1 + \left(|C_{m,\mu}|^2 - |C_{m',\mu}|^2\right) \frac{2R}{1+R^2} \int_\omega F(\delta_1)\,F(\delta_2)^*\, d\omega\right].$$

We can conclude that the partial lifetime of a single initial substate μ can be increased or decreased according to the relative norm of the Clebsch–Gordon coefficients. When transition $|\mu> \rightarrow |m>$ is forbidden, the lifetime is increased, while it is decreased if the other transition is forbidden. We can thus conclude that there are two ways to show interference in nuclear decay.

There are a few important applications. As has been shown, it is possible that the absorption amplitude is completely hindered, while the emission is not. As a consequence, the condition for population inversion is not required for lasing at these particular

frequencies where overlap of shapes can be achieved and at particular magnetic field values where level mixing occurs. These features are extremely interesting for the proposal of the following scenario for a graser. At a first time, the system can be pumped when the magnetic field is out of the critical condition. After pumping, when lasing must be achieved, the field can be changed to its critical level–crossing value. The bandwidth of the graser will be limited to the frequency zone for which overlapping of shapes is achieved and this width will thus be nearly the natural line width.

Another important application is the use of resonant scattering on a material that has no absorption in the previously described frequency range, so that the reflectivity is high. Indeed under previous conditions for a completely hindered absorption, the resonant scattering is not affected. It can be shown in the following way. The scattering amplitude $S(\omega)$ is due to a contribution to level $|1>$ and to level $|2>$:

$$S(\omega) = \frac{<m_i|V|1><1|V^+|m_i>}{\delta_1 - i\Gamma/2} + \frac{<m_i|V|2><2|V^+|m_i>}{\delta_2 - i\Gamma/2}.$$

At the conditions for a hindered absorption rate, one gets

$$S(\omega) = \frac{2\pi}{\hbar^2} |<m'|V|m_i>_{t=0}|^2 \left[\frac{R^2}{1+R^2}\frac{|F(\delta_1)|^2}{\delta_1^2 + (\Gamma/2)^2} + \frac{1}{1+R^2}\frac{|F(\delta_2)|^2}{\delta_2^2 + (\Gamma/2)^2}\right].$$

At the crossing fields it gives

$$S(\omega) = \frac{2\pi}{\hbar^2} |<m'|V|m_i>_{t=0}|^2 \, 2\,\frac{|F(\delta_1)|^2}{\delta_1^2 + (\Gamma/2)^2}.$$

Introducing Mössbauer cross–sections for ^{57}Fe one can estimate that total reflection is possible for angles smaller than 0.3 degrees. For such small angle scattering good reflectivity requires low absorption. This requirement is only achieved for the narrow frequency band as described above.

This work was supported by Strategic Defense Initiative Organization / Innovative Science and Technology and managed by U.S. Office of Naval Research grant N00014–88–K–2035.

References

[1] S.E. Harris, Phys.Rev.Lett. 62, (1989) 1033.

[2] A. Imamoglu and S.E. Harris, Opt. Lett. 14, (1989) 1344.

[3] A. Imamoglu, Phys. Rev. A 40, (1989) 2835.

[4] G. Alzetta, A. Gozzini, L. Moi and G. Orriols, Nuovo Cimento 36B, 5 (1976) ibid 52b, (1979) 209;
see also H. Gray, R. Whitley and C. Stroud, Opt. Lett. 3, (1979) 218.

[5] M.O. Scully, Phys. Rev. Lett. 67, (1991) 1955.

[6] K.–J. Boller, A. Imamoglu and S.E. Harris, Phys. Rev. Lett. 66, (1991) 2593.

[7] J.E. Field, K.H. Hahn and S.E. Harris, Phys. Rev. Lett. 67, (1991) 3062.

[8] R. Coussement, P. Put, G. Scheveneels and F. Hardeman, Hyp. Int. 23, (1985) 273.

[9] P. Put, R. Coussement, G. Scheveneels, F. Hardeman, I. Berkes, B. Hlimi, G. Marest, J. Sau and E.H. Sayouty, Phys. Lett. 103A, (1984) 151.

Figure captions

Fig. 1 : Breit – Rabi diagram for the excited state in ^{57}Fe subject to a quadrupole splitting of 1 mm/s and a collinear magnetic field B.
Note the $\Delta m = 2$ and $\Delta m = 1$ Zeeman level crossing at 7.45 T and 14.9 T.

Fig. 2 : For $\beta \neq 0$, mixing of the pure Zeeman–levels $|m>$ and $|m'>$ leads to the mixed states $|1>$ and $|2>$ which are repulsed by an energy $\hbar(\delta_1 + \delta_2)$ at the crossing field.

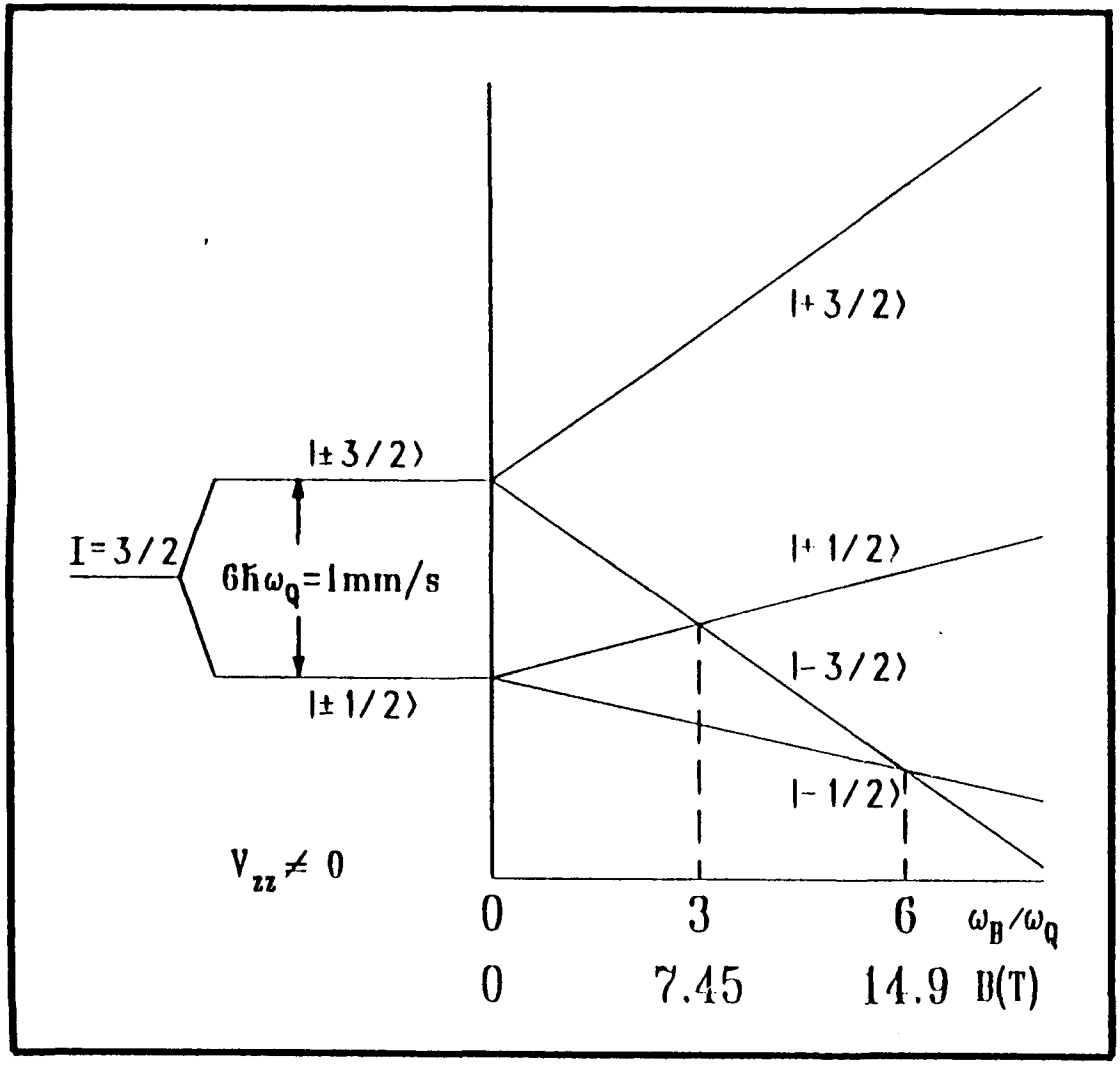
|+3/2⟩
|±3/2⟩
I=3/2
6ħω_Q=1mm/s
|+1/2⟩
|-3/2⟩
|±1/2⟩
|-1/2⟩
V_zz ≠ 0
0
3
6
ω_B/ω_Q
0
7.45
14.9
B(T)

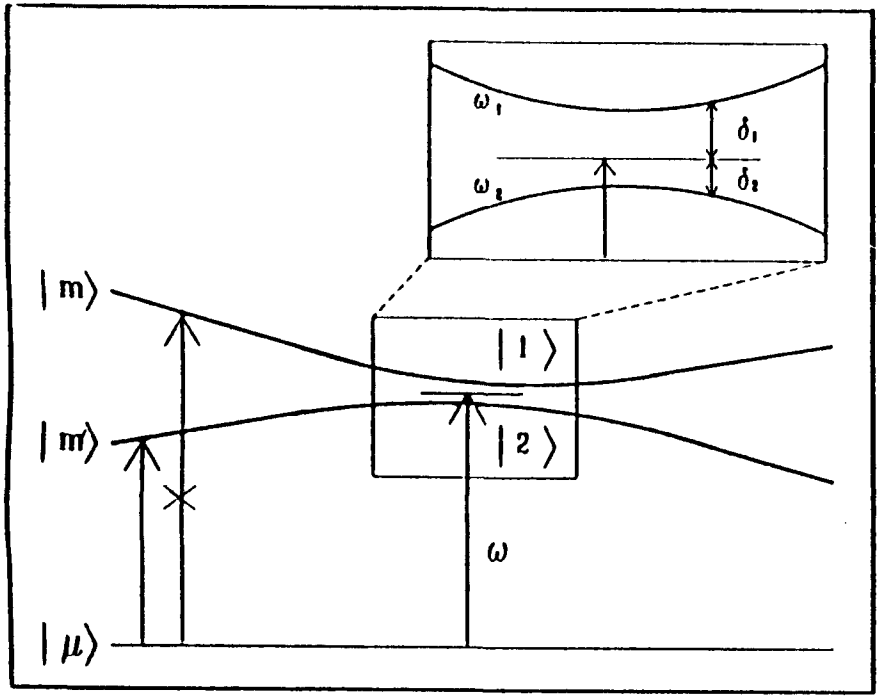
ω_1
δ_1
ω_2
δ_2
$|m\rangle$
$|1\rangle$
$|m'\rangle$
$|2\rangle$
ω
$|\mu\rangle$

Manuscript to appear in Lasers 91 Conference Proceedings

NUCLEAR LEVEL MIXING ASSISTED RELAXATION HOMOGENEOUS BROADENING AND GAMMA RAY LASERS.

R. Coussement, M. Van Den Bergh, G. S'heeren, G. Neyens, R. Nouwen
Katholieke Universiteit Leuven,
3001 Heverlee, Belgium.

P. Boolchand
University of Cincinnati,
Cincinnati, Ohio 45221–0030.

Abstract – In this paper we show that, taking into account the temporal behavior of the emission and absorption process, resonant absorption must be possible, even for very long lived isomeric states. Secondly we claim that, due to special quantum effects, it is possible to create such conditions that absorption of γ–rays can be strongly attenuated and even forbidden, while emission remains unchanged. These two features both relax the severe problems of pumping and gain requirements for γ–rays lasing to occur.

Introduction

In order to achieve a realistic concept of a gamma ray laser different fundamental problems must be solved. The problem of the pumping and level inversion is certainly a severe one for nuclear levels. In this paper we will consider two particular features that can be of critical importance for γ–ray lasing. We first point out that Mössbauer absorption must be possible even for very long lived isomeric states, allowing the use of these levels as storage and lasing levels, provided a triggering mechanism is built–in. Secondly we report on a study in which it is shown that under very particular magnetic field conditions, we can strongly attenuate and even annihilate the absorption while the emission probability remains unchanged. Such phenomena allow us to relax the pumping conditions as inversion is no more required. Moreover as the magnetic field conditions are very strict but easily changed, we have achieved a triggering system, as one can alternate pumping and lasing periods by simply adjusting the magnetic field.

1. Resonant absorption of γ–photons into a long lived isomeric state

For long lived isomeric states, one must consider the temporal behavior of the emission and absorption process and include the interaction of the nuclei with the lattice during that process, which is a much stronger interaction than the interaction with the radiation field. During the emission or absorption process the lattice can induce frequent modifications in frequency and phase. Therefore a photon, emitted from such an interacting nucleus will be frequency– and phase–modulated and thus contains information about the interaction of the emitting nucleus with the lattice. We assume thus that the nuclear wave functions can be expressed as the product of an unperturbed wave function and a fluctuation function $f(t)$, which reflects the interaction with the lattice :

$$\psi(\vec{x},t) = \psi(\vec{x},0)\, f(t)\, e^{-\Gamma_n t/2}\, e^{i\omega_0 t} \qquad (1)$$

We include a damping factor $e^{-\Gamma_n t/2}$ for the the interaction with the continuum of the radiation field, while ω_0 is the main energy of the fluctuating state.
The amplitude for transition between initial state $|i\rangle$ and final state $|f\rangle$ (with V the transition operator) for an emitted photon with detuning $(\omega - \omega_0)$, becomes :

$$A(\omega-\omega_0) = -\frac{i}{\hbar}\langle f|V|i\rangle_{t=0}\int_{-T}^{+T} f(t)\, e^{-\Gamma_n t/2}\, e^{i(\omega-\omega_0)t}\, dt \qquad (2)$$

or using the Fourier transform

$$\mathcal{F}^T(\omega-\omega_0) = \frac{1}{\sqrt{2\pi}}\int_{-T}^{+T} f(t)\, e^{-\Gamma_n t/2}\, e^{i(\omega-\omega_0)t}\, dt \qquad (3)$$

we see that the amplitude is given by the Fourier spectrum of the damping and the fluctuation function :

$$A(\omega-\omega_0) = \frac{-i\sqrt{2\pi}}{\hbar}\langle f|V|i\rangle_{t=0}\,\mathcal{F}^T(\omega-\omega_0)\,. \qquad (4)$$

We conclude that the amplitude is distributed over a range of detuning that is related to the frequency distribution width of the fluctuations, given by $\mathcal{F}(\omega-\omega_0)$, instead of to the natural width ; one says that the system is homogeneously broadened by the interaction with the lattice.

We consider now the absorption of a photon on a system of nuclei subjected to fluctuations from the lattice. The photon will carry the fluctuations from the emitting source and will be modulated and damped in the same way as the nucleus from which it is emitted, so in the expression of the absorption amplitude we will have two uncorrelated fluctuation functions $g(t)$ and $f(t)$, one from the source and one from the absorber :

$$A(\omega_0-\omega_0') = -\frac{i}{\hbar}\langle f|V|i\rangle\int_{-T}^{+T} f(t)g(t)^*\, e^{-\Gamma_n t}\, e^{i(\omega_0-\omega_0')t}\, dt \qquad (5)$$

and using Parcivals theorem we obtain

$$A(\omega_0-\omega_0') = \frac{-i\ 2\pi}{\hbar}\langle f|V|i\rangle\int_0^{\infty} \mathcal{F}^T(\omega-\omega_0)\,\mathcal{G}^T(\omega-\omega_0')^*\, d\omega\,. \qquad (6)$$

The amplitude is a convolution of the source and the absorber frequency spectra. Such a convolution depends on the shapes and positions of the two spectra. If the nuclear system is in equilibrium with the lattice, the function $f(t)$ and $g(t)$ can be assumed to fluctuate around unity and the Fourier spectra to be independent on the choice of time interval T. We further assume that the fluctuation functions can be regarded as continuous and smooth functions during the observation time. Under these assumptions the transition rate can be written as a function of the detuning between emitter and absorber :

$$R^T(\omega_0-\omega_0') = \frac{2\pi}{\hbar^2}\,|\langle f|V|i\rangle|^2\,\frac{1-e^{-2\Gamma_n T}}{2\,\Gamma_n}\,\frac{1}{T}\int_0^{\infty}\mathcal{F}^T(\omega-\omega_0)\,\mathcal{G}^T(\omega-\omega_0')^*\, d\omega. \qquad (7)$$

When source and absorber are in the same material, at the same temperature and in the same other conditions, $\mathcal{F}(\omega)$ and $\mathcal{G}(\omega)$ will have the same shape and homogeneous width. In that case if the detuning is zero ($\omega_0=\omega_0'$), the convolution and also the absorption rate will reach their optimal value which is independent of the shapes, at least if the Fourier spectra are properly normalized as

$$\frac{1}{T}\int_0^T |f(t)|^2\, dt = 1 \qquad \text{or} \qquad \frac{1}{T}\frac{1}{2\pi}\int_0^{\infty}|\mathcal{F}^T(\omega-\omega_0)|^2\, d\omega = 1\,. \qquad (8)$$

However one still has to deal with the problem of the inhomogeneous detuning, what leads to a spreading out of the resonant absorption at the expense of the size of the effect at the central frequency. The occurrence of inhomogeneities in a solid cannot be avoided to a certain limit ; typical values of inhomogeneous line broadening in the best crystals amount to 10^{-12}eV or more. For long lived states the natural line width is at least several orders of magnitude smaller than the inhomogeneous one, so one could believe that in this case observation of resonant absorption is impossible. But in the presence of homogeneous line broadening, as described above, one is able to overwhelm these solid state effects (which contribute to inhomogeneous broadening) and restore the resonant absorption if the homogeneous line width, and not the natural line width, is larger than the inhomogeneous detuning.

For example in the long lived isomer ^{109}Ag ($\Gamma_n = 10^{-17}$eV), we estimate the homogeneous width to be associated with the T_2 relaxation (10^{-12}eV) and not with the nuclear decay, so in order to observe Mössbauer self-absorption it will be sufficient that the inhomogeneous broadening is smaller than the homogeneous width, which is a much less stringent condition than to be less than the natural width. So Mössbauer absorption can occur even for very long lived isomeric states, opening the possibility to use the isomeric level as the storage and lasing level, by influencing the relaxation time[1].

Another problem in the concept of a γ-rays laser, namely the requirement of population inversion, can be strongly relaxed by the feasibility of switching off the γ-absorption, while the emission remains unchanged, due to a quantum interference effect, that can be achieved by nuclear level mixing of hyperfine levels.

2.Non-reciprocity of γ- emission and absorption

The presence of quantum coherence effects at level mixings offers possibilities of exploring new physical effects. In atomic physics level mixing or anti-crossing is known since the beginning of quantum mechanics and, for example, the non-reciprocity between emission and absorption of optical radiation at such mixings has led to lasing without inversion[2], dark-line resonances[3] and more recently to the recognition of an enhancement of the index of refraction[4]. Also in muon spin physics the level mixing phenomena are introduced.

Consider a gamma absorption process between a ground state $|\mu>$ and two excited states $|m>$ and $|m'>$, for which the selection rules allow the transition between the ground state and the level $|m'>$ but forbid the transition to $|m>$ (fig.1). Let us now assume that we are in a specific level mixing condition so the eigenstates are the mixed states $|1>$ and $|2>$, which are a coherent superposition of the pure $|m>$ and $|m'>$ states, with mixing factor R

$$|1> = \frac{1}{\sqrt{1+R^2}}\{|m> - R\,|m'>\} \quad \text{and} \quad |2> = \frac{1}{\sqrt{1+R^2}}\{R\,|m> + |m'>\}. \tag{9}$$

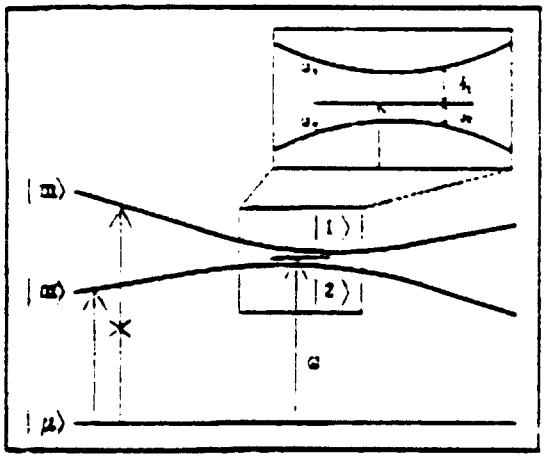

Fig.1 *Mixing of the pure levels $|m>$ and $|m'>$ leads to the mixed states $|1>$ and $|2>$ which are repulsed by an energy $\hbar(\delta_1 + \delta_2)$.*

A photon of frequency ω (fig.1) can be absorbed in two modes A_1 and A_2. These modes correspond to the absorption amplitude to the state $|1>$, respectively to the state $|2>$. This is perfectly possible because both the states $|1>$ as well as $|2>$ contain a component $|m'>$ to which the selection rules allow a transition provided the detunings (energy differences) are not too large. The two amplitudes are coherent as their phases are locked to the same initial state (ground state plus single photon), so one must add the two partial amplitudes in order to find the total one :

$$A = A_1 + A_2 \tag{10}$$

Let us further assume that the two nuclear isomeric wave functions are equally homogeneously broadened, either from the nuclear decay or from fluctuations induced by the lattice. We must then include a damping factor for the decay $e^{-\Gamma_n/2}$ and for very long lived states a fluctuation function $f(t)$ that will simulate the interventions from the lattice as in equations (2–4). One then becomes :

$$A_1 = \frac{-i}{\hbar} < \tfrac{1}{2}|V|\mu> \int_{-\infty}^{+\infty} f(t) e^{-\Gamma_n t/2}\, e^{i\delta_1 t}\, dt \tag{11}$$

$$= \frac{-i\sqrt{2\pi}}{\hbar} < \tfrac{1}{2}|V|\mu> \mathcal{F}(\delta_1) . \tag{12}$$

in which δ_1 and δ_2 are the detuning between the initial state and the two stationary states $|1>$ and $|2>$. These detunings can be changed if the frequency of the photon is variable. In the case of a Mössbauer absorption experiment, the γ–ray frequency ω can be modulated by the relative velocity between the source and the absorber :

$$\omega = \omega_0 (1 + \tfrac{v}{c}), \text{ so } \quad \delta_1 = |\omega_0 (1 + \tfrac{v}{c}) - \omega_1| \quad \text{and} \quad \delta_2 = |\omega_0 (1 + \tfrac{v}{c}) - \omega_2| . \tag{13}$$

in which ω_1, ω_2 are $E_1/\hbar$, resp. $E_2/\hbar$.
Taking into account the mixed structure of the eigenfunctions and the selection rules, we obtain for the partial amplitudes :

$$A_1(\delta_1) = \frac{-i\sqrt{2\pi}}{\hbar} <m'|V|\mu> \frac{-R}{\sqrt{1+R^2}} \mathcal{F}(\delta_1) \tag{14a}$$

$$A_2(\delta_2) = \frac{-i\sqrt{2\pi}}{\hbar} <m'|V|\mu> \frac{1}{\sqrt{1+R^2}} \mathcal{F}(\delta_2). \tag{14b}$$

The total amplitude, as function of the frequency of the photon ω as single parameter can now be written as :

$$A(\omega) = \frac{-i\sqrt{2\pi}}{\hbar} <m'|V|\mu> \frac{\mathcal{F}(\delta_1) - R\,\mathcal{F}(\delta_2)}{\sqrt{1+R^2}} \tag{15}$$

and the probability becomes

$$|A(\omega)|^2 = \frac{2\pi}{\hbar^2} |<m'|V|\mu>|^2 \frac{|\mathcal{F}(\delta_1) - R\,\mathcal{F}(\delta_2)|^2}{1 + R^2} \tag{16}$$

Looking to equation (16) we see that near the level crossing we have a destructive interference of the two amplitudes and at certain frequencies ω the amplitude can even vanish as

$$\frac{\mathcal{F}(\delta_1) - \mathcal{F}(\delta_2)}{\sqrt{1 + R^2}} = 0. \tag{17}$$

At exact crossing, the mixing factor R = 1 and then we get a complete destructive interference of the amplitudes A_1 and A_2 when $\mathcal{F}(\delta_1) = \mathcal{F}(\delta_2)$, which occurs for the frequency $\omega = (\omega_1 + \omega_2)/2$. This is simulated in fig.2.

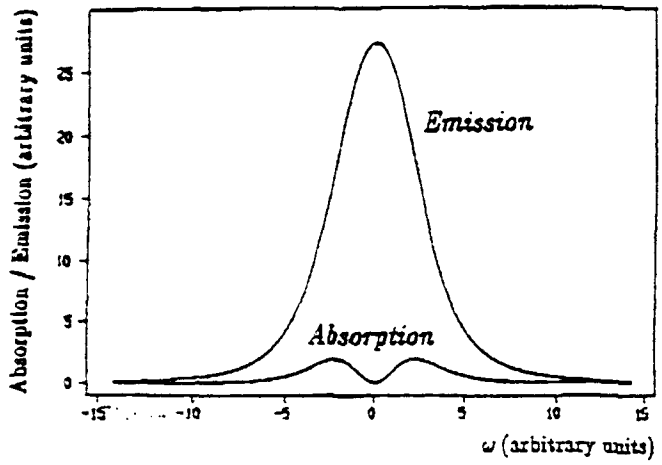

Fig.2 *Qualitative simulation of absorption resp. emission probability at exact crossing (R=1), as a function of γ-ray frequency.*

In a Mössbauer emission experiment a totally different situation prevails. Emission can occur from state |1> or from state |2> and there is no coherent superposition since these states are fed from a parent state independently. So one can write the total probability for emission as made up of the individual probabilities for each decay

$$P(\omega) = p_1 \, |A_1(\omega)|^2 + p_2 \, |A_2(\omega)|^2 \tag{18}$$

in which p_1 and p_2 are the initial populations of states |1> and |2>. Assuming them equal we obtain for the emission

$$P(\omega) = \frac{2\pi}{\hbar^2} \, | \langle m' | V | \mu \rangle |^2 \, \frac{|\mathcal{F}(\delta_1)|^2 + R^2 \, |\mathcal{F}(\delta_2)|^2}{1 + R^2} \tag{19}$$

In this expression there is no destructive interference and thus gamma–emission will take place, even at those frequencies for which the absorption vanishes (fig.2).

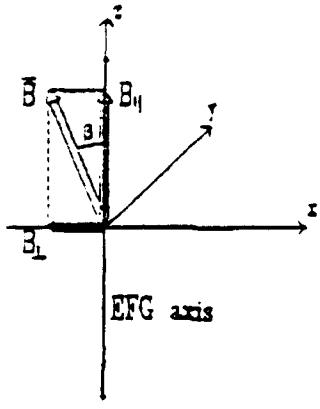

Fig.3 *Magnetic field B applied at an angle β wrt the symmetry axis of the EFG.*

The level mixing or coherent superposition of pure states in nuclear systems can be achieved in an elegant and controlled way by using a combination of an Electric Field Gradient and an external magnetic field, with a small misalignment. This arrangement is schematically illustrated in fig.3. We assume the EFG tensor to be axially symmetric ($V_{xx} = V_{yy}$). The misalignment of the magnetic field B with respect to the symmetry axis of the EFG (V_{zz}) is a critical point as will become clear later.

The hamiltonian describing the hyperfine interaction of the nuclear spin I (I>1/2) with a static EFG from a crystal and an external magnetic field B, applied at a small angle β (β<10°) wrt the EFG–symmetry axis consists of an electric quadrupole and a magnetic dipole interaction term :

$$\mathcal{H} = \frac{\omega_Q}{\hbar}\,(3I_z^2 - I^2) - \omega_B \cos\beta\, I_z + \frac{\omega_B}{2}\sin\beta\,(I_+ + I_-) \qquad (20)$$

in which $\omega_Q = \dfrac{e\,Q\,V_{zz}}{\hbar\,4I(2I-1)}$ is the fundamental quadrupole frequency (21)

and $\omega_B = \dfrac{g\,\mu_N\,B}{\hbar}$ is the Zeeman frequency. (22)

The first two terms of the hamiltonian, namely the quadrupole and the "parallel Zeeman" hamiltonian, have axial symmetry. The third term, the "perpendicular Zeeman" hamiltonian is the symmetry breaking part. For small misalignment we can, at least in first order, neglect the last term in expression (20) and find the eigenenergies of the axially symmetric part :

$$E_m = \hbar\,\omega_Q\,[3m^2 - I(I+1)] - \hbar\,\omega_B \cos\beta\, m. \qquad (23)$$

One can see that for certain values of the magnetic field some pairs of levels get the same energy, as illustrated in the Breit–Rabi diagram of fig.4, drawn for the first excited state (I=3/2) of ^{57}Fe as an example. We obtain these level crossings when the eigenvalues for a pair of Zeeman levels (m,m') become degenerate, i.e.,

$$E_m - E_{m'} = \hbar\,\omega_Q\,[3(m^2 - m'^2)] - \hbar\,\omega_B \cos\beta\,(m - m') = 0 \qquad (24)$$

leading to the level crossing condition

$$\omega_B = 3\,(m + m')\,\omega_Q / \cos\beta. \qquad (25)$$

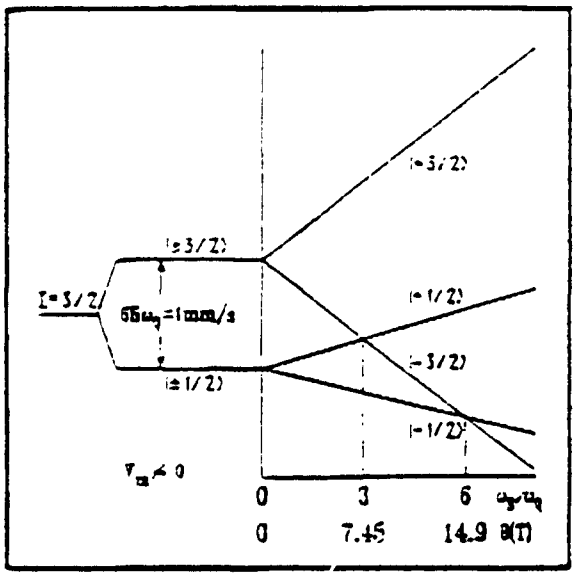

Fig.4 *Breit – Rabi diagram for the excited state in ^{57}Fe subject to a quadrupole splitting of 1 mm/s and a collinear magnetic field B.*
Note the $\Delta m = 2$ and $\Delta m = 1$ Zeeman level crossing at 7.45 T and 14.9 T.

In practice, as we can change the applied magnetic field, we can adjust ω_B to a value where the two levels cross. These values of the magnetic field, called level crossing points, are equidistant and the distance between two neighbouring points is equal to the value of the first level crossing point. At and near such crossing fields, the symmetry breaking term in the hamiltonian cannot be neglected and plays a most important role ; its effect will be to lift the degeneracy and mix each pair (m,m') of crossing levels. The coinciding energy levels repel each other and the corresponding eigenfunctions are strongly mixed. Eigenenergies and eigenfunctions can be calculated analytically for each pair by perturbation theory, using a two level approximation. One becomes eigenfunctions as in eq.(9) in which the mixing factor R is a function of the ratio between the splitting of the unperturbed levels $E_m - E_{m'}$ and the perturbation coupling between the crossing levels $W_{mm'}$:

$$R = \frac{E_m - E_{m'}}{2W_{mm'}} + \left[\left[\frac{E_m - E_{m'}}{2W_{mm'}} \right]^2 + 1 \right]^{1/2} \tag{26}$$

For a crossing of first order, $\Delta m = |m - m'| = 1$, this perturbation coupling is the non–diagonal element of the perturbation hamiltonian :

$$W_{mm'} = \langle m | \mathcal{H}_1 | m' \rangle = \frac{\omega_B}{2} \sin\beta \langle m | I_+ + I_- | m' \rangle. \tag{27}$$

For crossings with $\Delta m > 1$ one finds the perturbation coupling by Δm–th order perturbation theory as :

$$W_{mm'} = \frac{\langle m | (H_1)^{\Delta m} | m' \rangle}{\prod_{i=1}^{\Delta m - 1} (E_m - E_{m-i})}. \tag{28}$$

It is these matrix elements which are responsible for the repulsion between the energy levels and for the mixing of the eigenstates because of the reduction in symmetry, due to the misalignment β between the EFG–axis and B. The energy difference between the mixed states $|1\rangle$ and $|2\rangle$ is now

$$|E_1 - E_2| = \sqrt{(E_m - E_{m'})^2 + (2\ W_{mm'})^2}. \tag{29}$$

As long as the energy difference between a pair of levels is much larger than the perturbation coupling, $|E_m - E_{m'}| >> |2\ W_{mm'}|$, the mixing is negligible and pure states are found. The mixing is total at the crossing points, $E_m = E_{m'}$ and R =1, independently of the strength of the perturbation and the order of the crossing. In these points the energy difference reaches a minimum value $|E_1 - E_2|_{min} = |2\ W_{mm'}|$. This energy difference can be thought of as a Rabi splitting. It is analogous to the frequency difference between two normal modes of a system of two coupled and identical oscillators. In the scheme for ^{57}Fe in fig.4 there are two crossings; one corresponding to $\Delta m = 1$ and one to $\Delta m = 2$. In general the minimum repulsion energy difference is proportional to $(\sin\beta)^{\Delta m}$. So the misalignment angle β can be changed until the energy separation is comparable with the homogeneous width. For higher order mixings the energy differences between mixed levels are always smaller than for lower order mixings, but much more sensitive to β.

So by tuning a magnetic field, in presence of an EFG with a small misalignment, one can achieve a condition where the mixing of two levels is total. At this level crossing field we have complete absence of absorption for the γ–frequency $\omega = (\omega_1 + \omega_2)/2$. Away from the level crossing field one expects the interference effect due to level crossing to disappear. Thus quantum coherence at Zeeman level crossings leads to destructive interference in the absorption process, while there is no destructive interference in emission process.

Conclusion

For long lived isomers the condition for Mössbauer effect is not that the natural line width, but the homogeneous line width must be larger than the inhomogeneous detuning distribution. This opens the possibility to use these levels as storage and as lasing levels.

In well controlled conditions of level mixing one can achieve non–reciprocity between absorption and emission. Such conditions are easily kept under control in the described nuclear level mixing and therefore such system offers a unique opportunity to test such ideas of interference attenuation of absorption. Furthermore as we can create or destroy the required conditions only by adjusting the applied magnetic field, we have realized a magnetic trigger for the interference attenuation. Such a triggering effect could be attractive to include in the design of a gamma ray laser. One could indeed perform the pumping when not being in the level mixing condition and move in the proper condition when lasing is required.

References

1 G.S'heeren, M. Van Den Bergh, R. Coussement et al, Proceedings of the Int. Conf. on lasers '90, (San Diego, California, 1990)

2 S. Harris, Phys.Rev.Letter 62, 1022 (1989); A. Imamoglu and S. Harris, Opt. Lett. 14, 1344 (1989).

3 G. Alzetta, A. Gozzini, L. Moi and G. Orriols, Nuovo Cimanto 36B, 5 (1976) ibid 52b, 209 (1979); also see H. Gray, R. Whitley and C. Stroud, Opt. Lett. 3, 218 (1979).

4 Marlan O. Scully, Phys. Rev. Lett. 67, 1955 (1991).

5 R. Coussement, P. Put, G. Scheveneels and F. Hardeman, Hyp. Int. 23, 273 (1985).

Research sponsored by SDIO/IST and managed by ONR grant N00014–88–K–2035.

The following two reprints bear on preparation and characterization of high-T_c superconducting thin-films used in ^{109}Ag experiments.

Comparison of transport and magnetization critical currents in *c*-axis-oriented $Y_1Ba_2Cu_3O_{7-\delta}$ thin films

C. T. Blue, C. A. Blue,[a] and P. Boolchand
Department of Electrical and Computer Engineering, University of Cincinnati, Cincinnati, Ohio 45221

(Received 13 January 1992; accepted for publication 7 April 1992)

Transport, structural, and magnetic properties of *c*-axis-oriented $Y_1Ba_2Cu_3O_{7-\delta}$ thin films grown by off-axis *in situ* rf sputtering on MgO substrates have been investigated. By varying the substrate surface preparation prior to deposition, films could be grown with systematic improvements in their dc transport and structural properties. At the same time, these films display a systematic decrease in the irreversible magnetization $\Delta M(H)$ at all temperatures. Transport and inductive critical current densities in all cases displayed a temperature dependence that could be ascribed to flux creep and/or intragrain Josephson junctions. The irreversible magnetization for the films showed sample size dependence consistent with that of the Bean critical-state model. An anticorrelation between the transport and the magnetization critical current densities in the films was observed, which can be understood in terms of changes in the density of pinning sites as a function of substrate preparation.

I. INTRODUCTION

In the last few years, critical current densities (J_c's) in high-T_c superconductors have evoked both basic and technological interest. Many studies have focused on the role of microstructure in controlling flux pinning and thus the critical current densities of high-T_c superconducting samples. Numerous methods have been used to change the microstructure of the material and study the resulting changes in J_c. Some of these methods include grain texturing,[1-3] noble-metal addition,[4] shock compaction,[5] atomic substitution,[6-8] and neutron,[9] proton,[10] and heavy-ion irradiation.[11] Such studies have addressed the issue of pinning mechanisms in the cuprate superconductors. However, high-quality samples are needed to investigate the intrinsic properties of these materials. Single crystals[12] and, more recently, oriented thin films[13-16] have served as ideal materials for studying the intrinsic properties of the oxide superconductors. In the case of thin-film and single-crystal samples, it has been widely reported that defects either intrinsic (such as twin boundaries[17-19]) or induced (by irradiation[9-11]) can act as active pinning centers, thus enhancing the J_c's in the samples. However, most of these studies on thin films or single crystals report J_c enhancements exclusively from magnetization measurements (henceforth labeled $J_{c,m}$) without comparing these to transport critical current densities (henceforth labelled $J_{c,t}$) on the same samples. Recently, Moeckley *et al.*[20] reported on the effect of substrate preparation prior to deposition of laser-ablated $Y_1Ba_2Cu_3O_{7-\delta}$ thin films. They found that the defect density in the resulting film can be significantly reduced by thermal annealing of the substrate prior to deposition. The resulting films display superior transport and structural properties to those grown on unannealed substrates. However, no magnetization results were reported for these films.

In this work, we have investigated both magnetization and transport properties of sputter-deposited $Y_1Ba_2Cu_3O_{7-\delta}$ thin films as a function of substrate preparation. We observe for the first time an anticorrelation between the magnetization $J_{c,m}$ and transport $J_{c,t}$ critical current density as a function of substrate preparation. We explain this result in terms of a systematic reduction in the defect density of the films.

II. EXPERIMENT

A. Sputtering system and thin-film preparation conditions

The $Y_1Ba_2Cu_3O_{7-\delta}$ (YBCO) thin films used in this study were deposited by an off-axis magnetron sputtering technique similar to that of Eom *et al.*[21] The stoichiometric $Y_1Ba_2Cu_3O_{7-\delta}$ targets used were either fabricated in house or supplied by Superconductive Components. The RF magnetron sputtering gun (US Gun) housed in a stainless-steel bell jar was typically evacuated to a base pressure of $\sim 1 \times 10^{-7}$ Torr using a cryopump. All films were deposited onto (100) MgO single-crystal substrates which were heated during deposition using a Conductus high-temperature substrate heater.

The typical sputtering conditions used for growth of these films included a RF power of 60 W, a substrate block temperature of $\sim$730 °C, a substrate-to-target distance of 4.5 cm, a dc bias of ~ -80 V on the target with a total sputtering pressure (argon plus oxygen) of 200 mTorr with a molecular oxygen pressure of 20 mTorr. The argon and oxygen gases were introduce separately and localized at the target and substrate, respectively, using stainless-steel injection rings. Since the measured pressure is that inside the bell jar as a whole, the local argon pressure at the target and oxygen pressure at the substrate can be higher than the values quoted. It has been demonstrated that the use of injection rings to localize oxygen near the substrate can result in the growth of higher-quality films due to the reduction of negative-ion resputtering.[22]

[a]Department of Materials Science and Engineering, University of Cincinnati, Cincinnati, Ohio 45221.

 0021-8979/92/151021-09$04.00 © 1992 American Institute of Physics

These growth conditions gave us a deposition rate of $\sim 330 \pm 30$ Å/h as measured with a surface profilometer over 50-μm-wide patterned lines. After each deposition, the sputtering chamber was evacuated and oxygen introduced. The substrate temperature was then reduced to room temperature over a period of ~ 3 h. The samples were then removed from the chamber and analyzed without any postannealing.

B. Substrate preparation

All substrates used were (100) MgO single crystals chemically polished to a smooth surface. However, in order to grow films with varying superconducting properties, different groups of substrates received different preparations prior to thin-film deposition. The first group of MgO substrates were simply degreased and clamped directly to the Hastalloy heater block. We will henceforth label films grown on these substrates as case a films. The second group of MgO substrates were degreased and clamped to the Hastalloy heater block with a 10 μm silver film backing to enhance thermal contact. Films grown on these substrates will be henceforth labelled as case b films. A third group of substrates were annealed in air at ~ 1100 °C for 12–24 h prior to degreasing and clamping to the heater block with a 10 μm silver film backing for thermal contact. Films grown on these substrates will henceforth be labelled as case c films. The high-temperature annealing of the MgO substrate has been shown by Norton, Summerfelt, and Carter[23] to produce a high density of atomic steps on the surface of the substrate that helps to better nucleate growth of the YBCO film.

In each of the three cases of substrate preparation described above, the YBCO thin films were grown using identical growth conditions to a thickness of 3600–4600 Å. Therefore, the principal variable in processing is the substrate preparation prior to the growth of the YBCO thin film.

C. Measurements and thin-film patterning

X-ray-diffraction (XRD), magnetization, and resistivity measurements were systematically performed for each of the three groups of films to establish their structural and superconducting properties. Scanning electron microscopy (SEM) was also used to investigate the surface morphology and granularity of the films. Temperature-dependent magnetization $M(T)$ measurements in the range 14 K $< T < T_c$ were performed on thin films typically 5×10 mm^2 in size in an applied field (0–1 T) perpendicular to the film plane using an EG&G PAR model 4500 vibrating sample magnetometer (VSM) coupled to a He closed-cycle refrigerator system from APD Cryogenics. These thin-film samples were then patterned into 50-μm-wide lines (Hall bars) for dc transport measurements so that a direct comparison of the magnetization and transport properties could be made on the same film.

The Hall bars were patterned using a positive S-1400-31 photoresist with dilute phosphoric acid as the etchant. Due to the adverse reaction of solvents and especially water with the YBCO material, a dry etch process using an oxygen plasma was employed to remove the entire resist from the patterned film. The use of an oxygen plasma also helps to restore superconductivity to the surface layers of the YBCO film. Such patterned Hall bars were then loaded into a thermal evaporation system where 2-μm-thick Ag pads were deposited through a mechanical mask. The pads were then annealed at 550 °C in 1 atm of oxygen for ~ 30 min and slow cooled to room temperature. Such a thermal treatment helps to lower the contact resistance of the Ag pads. The patterned samples were then mounted on an oxygen-free high-purity (OFHP) copper chuck via silver paint where ultrasonic gold bonds were then made to the pads. Four-point dc resistivity and $J_{c,t}$ measurements were then made as a function of temperature in an exchange-gas liquid-helium dewar system. A dc test current in the range 1–10 μA was used for the resistivity measurements and $T_c(0)$ was defined as the temperature at which the film resistivity dropped to 1×10^{-3} of its normal-state resistivity at 100 K. $J_{c,t}$ was determined from the current necessary to produce a voltage less than 2 μV, or an electric field of 20 μV/cm. These transport critical current measurements were done in the absence of an applied magnetic field.

III. RESULTS

A. X-ray diffraction

X-ray diffractograms of typical films grown for cases a, b, and c are shown in Figs. 1(a), 1(b), and 1(c), respectively. In each case, the XRD scans indicate that the films grow largely with their c axis normal to the plane of the film. Only for the case a film could any presence of a-axis orientation normal to the plane be observed. This shows up as a weak trace of the (200) reflection in the XRD scan of Fig. 1(a). Case a films did not have a Ag backing for thermal contact and this apparently results in a somewhat lower temperature in certain areas of the substrate (i.e., those areas not in intimate contact with the heater block). The c-cell length of the films in all cases varied from 11.64(1) to 11.68(1) Å without any systematic difference between the different cases. However, a systematic trend was observed in the width of the diffraction peaks. Specifically, the full width at half-maximum (FWHM) of the (005) peak was found to vary from 0.245° for the case a film, to 0.222° for the case b film, to 0.190° for the case c film. This systematic decrease of the FWHM of the (005) peak with substrate preparation agrees well with the work of Moekley *et al.*[20] In their work, they also find a systematic decrease in the FWHM of the (005) peak of their laser-ablated 123 films as they vary the substrate preparation from a chemically polished substrate, to a mechanically polished substrate, to an annealed substrate. It should be mentioned that Moeckley *et al.* also performed ion channeling measurements, x-ray pole analysis, and high-energy oxygen resonance Rutherford backscattering spectroscopy on their films. These measurements correlated well with the FWHM x-ray-diffraction results in that they (Moekley *et al.*) observed a systematic increase in the crys-

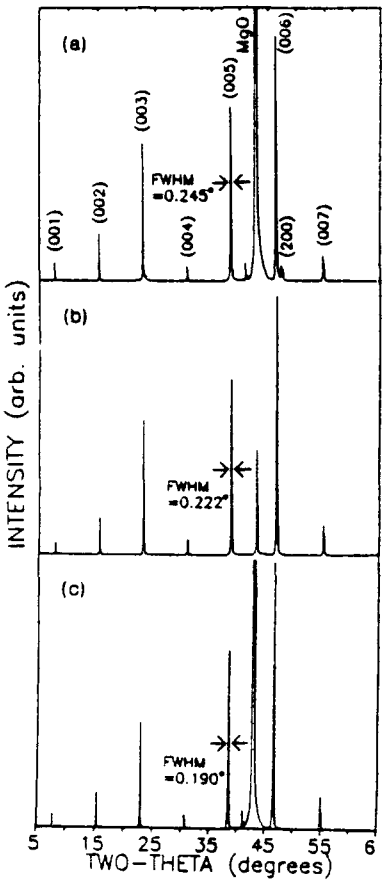

FIG. 1. Typical x-ray diffractograms of (a) film grown on MgO for case a, (b) film grown on MgO for case b, and (c) film grown on MgO for case c.

tallinity χ_{min} and in-plane epitaxy (x-ray pole) while observing a systematic decrease in oxygen disorder in going from a film grown on a chemically polished substrate, to one grown on a mechanically polished substrate, to one grown on a thermally annealed substrate. While we have not made direct measurements of the in-plane epitaxy or oxygen disorder, their work strongly suggests that the decrease in the FWHM of the diffraction peaks that we observe is evidence of a systematic improvement of the in-plane epitaxy, overall crystallinity, and decreased oxygen disorder in our films.

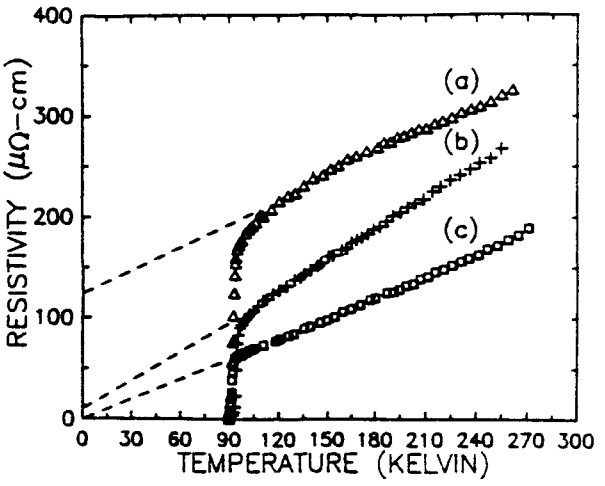

FIG. 2. Resistivity vs temperature behavior of typical films grown on MgO for (a) case a, (b) case b, and (c) case c. Dashed line shows extrapolated $\rho(T=0\ \mathrm{K})$.

B. Resistivity

The T dependence of resistivity of films grown for cases a, b, and c are shown in Figs. 2(a), 2(b), and 2(c), respectively. These measurements were made on 50-μm-wide lines patterned from the same thin-film samples used for the XRD measurements discussed above and the magnetization results to be presented in Sec. III C. No systematic difference in the zero-resistance T_c was observed for the films. In all cases, $T_c(0)$ ranged from 89.1 to 91.0 K and transition widths $\Delta T_c(90\%–10\%)$ were in the range of 1.8–2.5 K. The case a films generally showed the broadest transitions (typically 2.5 K) of the three types of films investigated and no significant differences in the transition widths were observed between films grown in cases b and c (typically 1.8 K). It is clear from Fig. 2 that the films display in general substantial differences in their normal-state resistivity, temperature coefficient of resistivity, and $T=0$ K intercept of resistivity. Table I summarizes the results of the $\rho(T)$ measurements along with the XRD results for films grown in the three different cases. Case a films display the highest normal-state resistivities, positive $\rho(T=0\ \mathrm{K})$ intercepts, and the lowest residual resistivity ratios $\rho(\mathrm{RT})/\rho(100\ \mathrm{K})$. This is expected since these films were not thermally anchored with any medium to the

TABLE I. Summary of resistivity versus temperature and x-ray-diffraction results for films grown in each of the three cases of substrate preparation.

Case	Substrate preparation	Orientation	FWHM (005) peak	ρ(100 K) ($\mu\Omega$ cm)	ρ(RT)/ρ(100 K)	ρ(T=0 K) extrapolated ($\mu\Omega$ cm)	$T_c(0)$ (K)	ΔT_c(90%–10%) (K)
a	unannealed not Ag attached	$c>a$	0.245°	184	2.0	125	89.7	2.5
b	unannealed Ag attached	c	0.222°	99	3.0	10	91.0	1.8
c	annealed Ag attached	c	0.190°	66	3.1	0	89.1	1.8

heater block and could well have grown at lower substrate temperatures (only the block temperature was fixed) than those films that were thermally anchored via a Ag backing. The lower substrate temperature results in a small fraction of *a*-axis-oriented grains [presence of (200) peak in x-ray diffractogram] forming in the predominately *c*-axis-oriented film. It is well known[24] that such a film growth pattern is characteristic when substrate temperatures $T<670$ °C, and further such films exhibit transport properties inferior to the purely *c*-axis-oriented films grown at higher substrate temperatures. Case c films invariably display the best dc transport properties as can be seen from Fig. 2 and Table I. These results agree well with the work of both Moeckley *et al.*[20] and Norton *et al.*[25] who have examined the effect of substrate topography on the microstructure of the resulting YBCO thin films. It is known that high-temperature annealing introduces step edges on the substrate surface which act as preferential sites for island nucleation growth.[23,25] The resulting YBCO film microstructure is improved (better in-plane epitaxy with fewer high-angle tilt boundaries) and the dc transport properties are generally superior to those films grown on chemically polished smooth substrates.

C. Magnetization

Magnetization measurements on the thin films grown for each case were used to determine the magnetization critical currents $J_{c,m}(T,H)$ as a function of temperature and applied magnetic field using the Bean Formula,[26,27]

$$J_{c,m}=[30M(H)]/r, \qquad (1)$$

where $J_{c,m}$ is in A/cm^2, $M(H)=\Delta M(H)/2$ is in emu/cm^3, and r is one-half the average sample dimension perpendicular to the applied field.[28]

Figure 3 displays magnetization hysteresis loops taken at $T=14$ K for $H_{appl}\perp$ film plane for thin films grown in each case. From this figure, one can clearly observe striking differences in the overall shape of the magnetization hysteresis as well as a dramatic and systematic reduction in the magnitude of the irreversible magnetization $\Delta M(H)$ in going from a case a to a case c film. Specifically, for the case a film, which displayed the worst transport and structural properties (Table I), the hysteresis curve indicates evidence of substantial pinning similar to that displayed by heavily twinned single crystals.[29,30] These case a films display a weak field dependence (drops by less than a factor of 2 from 0 to 1 T) and a large value of the irreversible magnetization $\Delta M(H_{appl}=5\text{ kG})=1.4\times10^4$ emu/cm^3 giving a magnetization critical current density $J_{c,m}(H_{appl}=5\text{ kG})=5.6\times10^5$ A/cm^2. Case b films, which displayed better transport and structural properties (Table I) than a case a film, display a hysteresis curve with a stronger field dependence and an overall lower value of the irreversible magnetization $\Delta M(H_{appl}=5\text{ kG})=6.0\times10^3$ emu/cm^3 giving a magnetization critical current density $J_{c,m}(H_{appl}=5\text{ kG})=2.3\times10^5$ A/cm^2. For the case c films, which invariably display the best transport properties (Table I), the irreversible magnetization is by far the most field dependent of the three cases investigated. Such films, we find, display the lowest value of the irreversible magnetization $\Delta M(H_{appl}=5\text{ kG})=1.0\times10^3$ emu/cm^3 resulting in the lowest magnetization critical current density $J_{c,m}(H_{appl}=5\text{ kG})=3.6\times10^4$ A/cm^2.

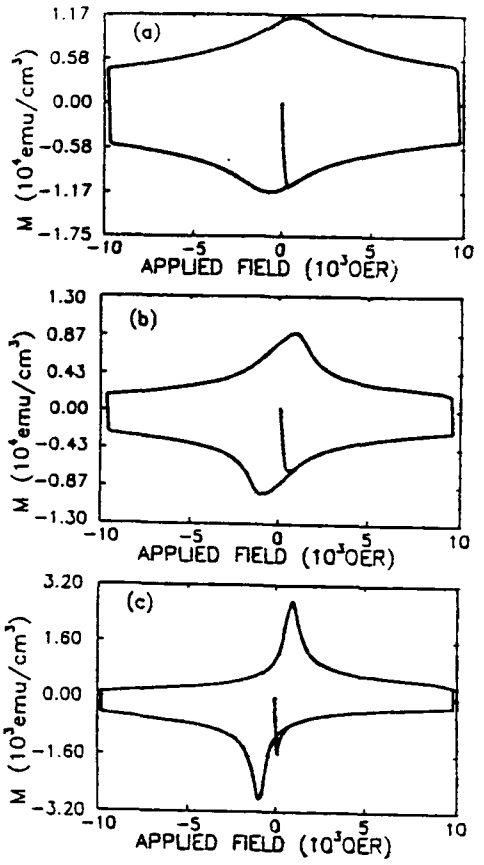

FIG. 3. Magnetization hysteresis loops taken at $T=14$ K with the applied field perpendicular to the film plane ($H_{appl}\parallel c$ axis) of (a) typical film grown on MgO for case a, (b) typical film grown on MgO for case b, and (c) typical film grown on MgO for case c.

Also, one can see from Fig. 3 that films grown in all cases display a non-zero-field flux peak in their hysteresis loop that progressively becomes more pronounced in going from a case a to a case b to a case c film. These peaks resemble large coupling peaks associated with losses characteristic of proximity-effect coupling.[31,32] Such peaks are generally characteristic of granular samples where at low magnetic fields the supercurrents flow around the entire sample and as the field is increased regions of the crystal become decoupled as the field breaks the weak links between the grains. In order to check these films for subgranularity[33] and to check the validity of the Bean formula we performed scaling experiments[18,34] with the films. In the scaling experiment, a thin-film samples' hysteresis is first measured on the whole sample and then measured on the same sample with an average dimension one-half the original dimension of the whole sample. This film is then scribed further to one quarter of the original dimension

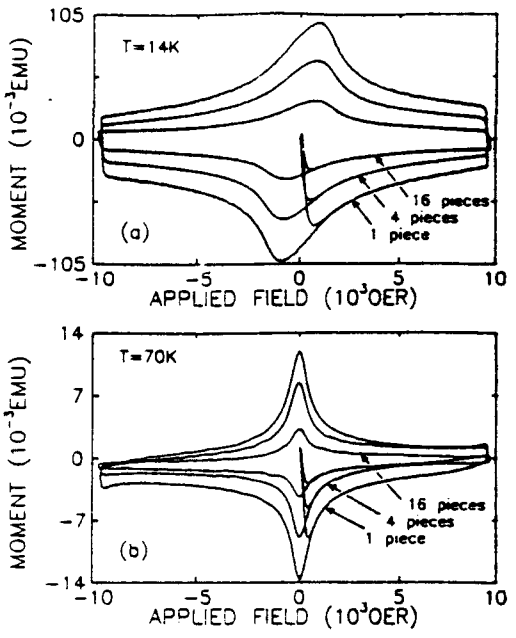

FIG. 4. Magnetization hysteresis loops of case b film measured as a function of sample dimension at (a) $T=14$ K and (b) $T=70$ K. The total volume of the sample was kept approximately constant with each scribing.

and measured again. One expects the irreversible magnetization to scale by one-half with each scribing if the currents flow throughout the entire sample. Figure 4 shows the result of this scaling experiment at two temperatures on a case b sample. At both temperatures we find the magnetization to scale with sample dimension indicating that the samples do not show subgranularity and that the Bean formula is valid in estimating $J_{c,m}$ at high fields. It should be mentioned that films in all three cases showed this scaling. Therefore, we conclude that the flux peak observed in Fig. 3 is not the coupling peak generally ascribed to subgranularity.

D. $J_{c,m}(T)$

Figure 5 displays the temperature dependence of the magnetization critical current density for films grown in each case. It can be seen from Fig. 5 that the magnitude of the magnetization critical current at all temperatures systematically decreases as we go from a case a to case b to case c film. The case a film grown on an unannealed unattached substrate displays by far the largest magnetization (Fig. 3) and therefore the highest $J_{c,m}$ at all temperatures. It should be noted that this is the same film that displayed the worst transport and structural data (Table I). The case c film, grown on an annealed substrate with Ag backing, clearly displays the worst magnetization (Fig. 3) and therefore the lowest $J_{c,m}$ at all temperatures (Fig. 5); however, this film displayed the best transport and structural properties. Thus, the films that display the best transport and structural properties generally display the worst mag-

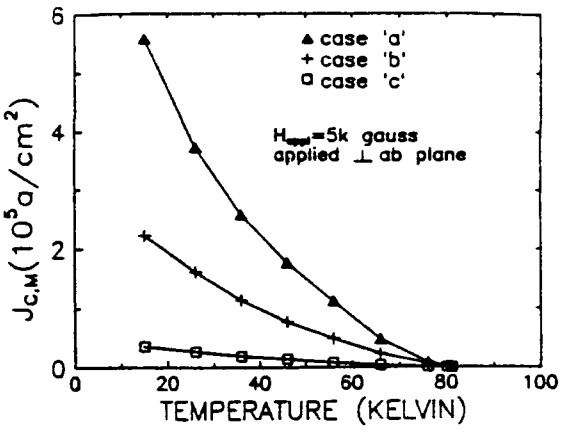

FIG. 5. Temperature dependence of the magnetization critical current density of films grown on MgO for cases a, b, and c.

netization properties and vice versa. In order to further investigate this result we measured the transport critical currents on these same thin films patterned to 50-μm-wide lines as described earlier. Also, this would allow for a direct comparison of the magnetization and transport critical current densities.

E. $J_{c,t}(T)$

Figure 6 displays the results of the measured transport critical current density $J_{c,t}(T)$ as a function of temperature for the case b and case c films. As stated earlier, these measurements were made in the absence of an applied field. Assuming that the current flows uniformally throughout the microbridge, the self-field due to the measuring transport current was calculated to be a maximum of 10 G at the surface of the film microbridge. This small field should not significantly affect the transport critical current. Thus, while the $J_{c,t}$ measurements represent essentially zero-field measurements, the $J_{c,m}$ values just reported were measured

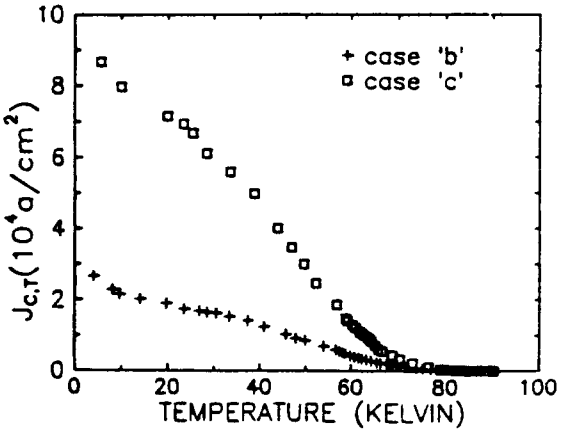

FIG. 6. Temperature dependence of the transport critical current density of films grown on MgO for cases b and c.

at an applied field of 5 kG in order to make the Bean model applicable. The different applied field used for the two measurements is not emphasized, however, since it is the trend of $J_{c,t}$ and $J_{c,m}$ with film microstructure that we are investigating. While the applied field may change the absolute value of the critical current slightly, it would not alter the systematic trend observed. $J_{c,t}(T)$ results of case a films are excluded from Fig. 6 since these films showed some degradation of T_c due to water exposure just prior to the $J_{c,t}(T)$ measurements. While these case a films generally did display the lowest transport $J_{c,t}$ at all temperatures, we could not count out the effects of the water exposure in determining the $J_{c,t}$. We would expect these films to display the lowest $J_{c,t}$'s since such films did display the worst transport and structural characteristics (Table I) prior to degradation. Also, case a films contained some a-axis-oriented grains which invariably will lead to lower in-plane $J_{c,t}$'s.[34] However, the results on case b and case c films are unambiguous and Figs. 5 and 6 clearly demonstrate that for these films $J_{c,t}(T)$ and $J_{c,m}(T)$ follow the opposite trends with substrate preparation. In other words, we observe an anticorrelation between the transport and magnetization critical current densities for such films.

IV. DISCUSSION

Many of the experimental phenomena observed in the high-T_c superconductors have been understood in terms of models developed for conventional low-T_c type-II superconductors. However, in comparing the physical characteristics of the two materials, two obvious differences emerge. The coherence length ξ of the low-T_c superconductors (typically 0.1–1 μm) is orders of magnitude larger than that of the high-T_c superconductors ($\xi \sim 3$–30 Å). Therefore atomic scale defects that do not play a role in determining critical currents in the low-T_c materials can act as both flux-pinning sites and weak links in controlling critical currents in the high-T_c materials. Furthermore, since T_c's in the high-T_c materials are elevated by almost an order of magnitude for the same flux-pinning energies, the decay of magnetization dM/dt ascribed to flux creep while absent in the low-T_c materials is a significant effect in the high-T_c materials. Therefore, transport ($J_{c,t}$) and magnetic ($J_{c,m}$) critical currents in the low-T_c superconductors represent static measurements and have been shown to scale with each other. However, this is not the case in the high-T_c superconductors as we discuss next.

In this section we begin by first addressing the issue of film microstructure as inferred from the observed temperature dependence of the critical currents. Next, we move on to discuss the central issue of the present work, namely, the observed anticorrelation between $J_{c,t}$ and $J_{c,m}$ as a function of substrate preparation. At the outset, it would be pertinent to mention that each of the critical currents measured ($J_{c,t}$ and $J_{c,m}$) in the c-axis-aligned films geometrically refer to currents flowing parallel to the CuO_2 planes.

A. Film microstructure from $J_{c,t}(T)$ and $J_{c,m}(T)$

Figure 7 displays the transport critical current density versus temperature for case b and case c films. These results taken from Fig. 6 are now normalized to $J_{c,t}(T=4$ K) and plotted as a function of reduced temperature, $t = T/T_c$. As illustrated in Fig. 7, the $J_{c,t}(t = T/T_c)$ result for the case c film is well described at low temperatures ($t < 0.8$) to a flux-creep-controlled transport current expression,[35]

$$J_c(0,t) = J_c(0)[1 - \alpha(0)t - \beta t^2], \tag{2}$$

where $\alpha(0)$ is related to the pinning energy $U(0,0)$ by the expression

$$\alpha(0) = [k_B T_c / U(0,0)] \ln(E_0/E). \tag{3}$$

In this expression E_0 represents the characteristic electric field and E is the electric-field criterion used for the $J_{c,t}$ measurement.[36] We could fit $J_{c,t}(t = T/T_c)$ results for the case c film using $\alpha \sim 0.9$ and $\beta \sim 0.4$ yielding a pinning energy of $U(0,0) \sim 60$ meV, taking E_0/E to be $\sim 10^3$. $J_{c,t}(t = T/T_c)$ for the case b film could not be fit as well using Eq. (3). However, attempts to fit $J_{c,t}(t = T/T_c)$ for the case b film to *SNS* or *SIS* models[37] yielded even poorer fits.

Figure 8 displays the temperature dependence of the magnetic critical currents $J_{c,m}(t = T/T_c)$ deduced from the VSM measurements in an applied field of 5 kG for the films grown in the three cases. In making this plot we have normalized the $J_{c,m}(T)$ results of Fig. 5 to $J_{c,m}(T = 15$ K) and have plotted the results as a function of reduced temperature $t = T/T_c$. Although films in the three cases display somewhat depressed critical current densities and a weak exponential temperature dependence of $J_{c,m}(t = T/T_c)$, the observed temperature dependence of $J_{c,m}(t = T/T_c)$ is inconsistent with superconducting grains separated by normal regions as expected for *SNS*-type granular films.[37] Following the de Gennes–Wethamer–Clarke[38–40] theory of proximity effect junctions, *SNS*-type materials should display a temperature dependence of the critical current given by

$$I_0 \propto (1 - t^2) \exp[-a_{s,t} t^{1/2} / \xi_{s,t}(T_c)], \tag{4}$$

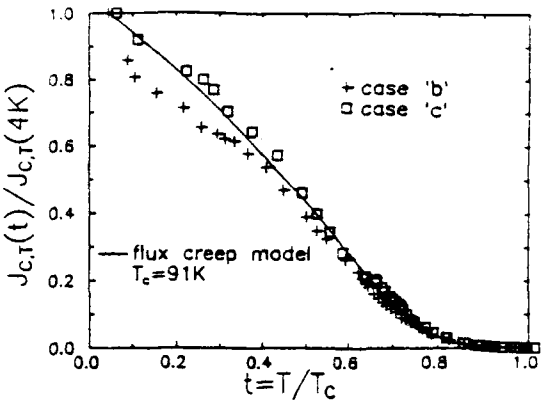

FIG. 7. Normalized transport critical current density vs reduced temperature for films grown in cases b and c. The solid line is theoretical plot of Eq. (2).

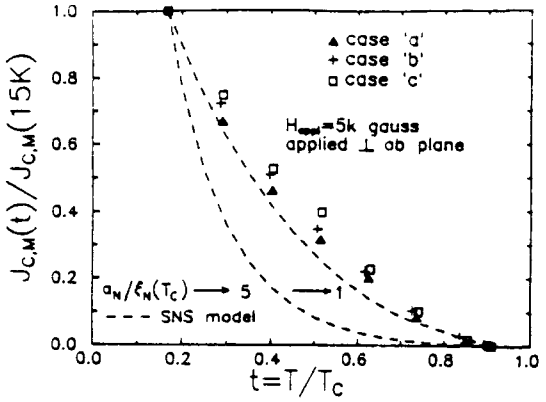

FIG. 8. Normalized magnetization critical current density vs reduced temperature for films grown in the three cases. The dashed lines are theoretical plots of Eq. (4).

where a_N is the thickness of the normal metal barrier and $\xi_N(T_c)$ is the normal metal coherence length, i.e., the distance the Cooper pairs penetrate the barrier.[37] At H_{appl} = 5 kG (the field at which the $J_{c,m}$ was taken), one expects the field to completely decouple the superconducting grains of a *SNS* superconductor and therefore require that $a_N/\xi_N(T_c) > 1$. The dashed lines in Fig. 7 are theoretical plots of Eq. (4) for the case of $a_N/\xi_N(T_c) = 1$ and the more probable case of $a_N/\xi_N(T_c) = 5$. Neither theoretical plot is a good fit to the $J_{c,m}(t = T/T_c)$ results. This indicates that the present films are not *SNS*-type granular films. This result is consistent with the magnetization scaling results of Fig. 4, since one would not observe sample size scaling of the magnetization in macroscopically granular superconducting material. We therefore conclude that our films are not granular in a "macroscopic" sense and that the T dependence of $J_{c,m}$ can be understood as due to a flux-creep phenomenon.[41] While the full T dependence at a finite magnetic field is not easily accounted for, it is known that the slope $d(J_{c,m})/d(T)$ at a given temperature increases with increasing magnetic field in the flux-creep model.[36] This is consistent with our $J_{c,m}(T)$ results.

We cannot, however, exclude the presence of internal Josephson junctions within the superconducting grains controlling J_c in our films. In this glassy picture, J_c is controlled by Josephson tunneling across microstructural defects which act as "micro" weak links within the superconducting grain.[42] Deutscher and Muller recognized that the smallness of the coherence length ($\xi \sim$ atomic spacing) in the high-T_c superconductors leads to an anomalous temperature dependence of J_c, $J_c \propto (T - T_c)^2$, near T_c, while at low temperatures, J_c has the usual dependence $J_c \propto (T - T_c)$.[42] These predictions are consistent with our $J_{c,i}$ results and may also explain the somewhat depressed $J_{c,i}$ and $J_{c,m}$ values reported here.[43] Thus, while we can exclude the presence of granularity on macroscopic scale for our films, both a flux-creep model and a model based on internal Josephson junctions can account for the T dependence of the critical currents in our films.

B. Observed anticorrelation of $J_{c,i}$ and $J_{c,m}$

Often $J_{c,m}$ and $J_{c,i}$ measurements on high-T_c superconductors are reported[44] as a function of applied magnetic field or temperature on one particular sample, but not as a function of sample processing as we have done presently for the first time to our knowledge. Film processing permits one to alter the film microstructure, and this has allowed us to examine how $J_{c,i}$ and $J_{c,m}$ change as a function of the nature of defects present in the films.

The systematic improvement in the normal-state electrical transport and structural properties (Table I) observed in going from a case a to a case c film is no doubt a consequence of a reduced defect density in the films. This reduction in defect density with substrate preparation has been observed by other groups and has been shown to invariably result in thin films with improved transport and structural properties. Moekley *et al.*[20] have shown that the primary defects suppressed in films grown on annealed substrates consist of high-angle and low-angle tilt boundaries. The authors also report a substantial reduction in the oxygen disorder in such films. Clearly, the reduction in the irreversible magnetization (and therefore $J_{c,m}$), in the case c films is a direct consequence of the reduced defect density since these tilt-boundary defects act as active flux pinning centers in the magnetization measurement. In the conventional flux-creep theory,

$$J_{c,m} \sim U_0/(Nbl) \tag{5}$$

where N is the number of vortices in a flux bundle, b is the average width of the potential, U_0 is the unperturbed pinning potential, and l is the average hoping distance between pinning centers.[41] Therefore, a reduction in the defect density (i.e., number of pinning sites) would also result in a substantial increase in l and therefore a decrease in $J_{c,m}$ from Eq. (5). This is consistent with our results in going from a high defect density film (case a film displaying large $J_{c,m}$ and poor transport properties) to a lower defect density film (case c film displaying small $J_{c,m}$ and superior transport properties). One might also have expected a reduction in the transport critical current with reduced defect density since $J_{c,i}$ is also determined by flux-line movement. However, our results show otherwise, and this may be understood as follows: Those defects that act as flux-pinning centers in the magnetization measurement also act as internal "micro" weak links within the superconducting grains in the transport measurements. Since the coherence length in the cuprates ($\xi \sim 3$–30 Å) is of the order of the underlying defect dimension, it is reasonable to expect that $J_{c,i}$ would in fact increase somewhat independent of pinning considerations as the film in-plane epitaxy is improved. Promotion of structural order in the CuO_2 planes on an atomic scale enhances $J_{c,i}$ largely because the superconducting order parameter becomes spatially more homogeneous in the *a-b* plane in the absence of these microscopic weak links. This glassy picture interpretation has been used to explain many of the experimental phenomena observed in the YBCO-type superconductors and appears to be consistent with the present results as well.[42]

Another manifestation of the observed anticorrelation between $J_{c,m}$ and $J_{c,t}$ that bears on the conventional flux-creep model is related to the effective pinning potential $U_{\rm eff}$. It has recently been shown from neutron[45] and proton[46]-irradiated $Y_1Ba_2Cu_3O_7$ single crystals that one can increase $U_{\rm eff}$ independently of $J_{c,m}$. This indicates that $J_{c,m}$ may be determined by the total number of pinning centers or possibly by specific defect structures that may not uniquely determine $U_{\rm eff}$. We have made preliminary measurements of the time-dependence decay of magnetization (flux creep) on films grown in each of the three cases in order to determine $U_{\rm eff}$ for each. While the detailed results of these measurements will be presented in a separate publication,[47] here we briefly summarize the main result as it relates to the observed anticorrelation of $J_{c,t}$ and $J_{c,m}$. For each film, $M(t)$ is found to be logarithmic in time in the range 10 s$\leq t \leq$1200 s and can be described by the simple relation[41,48]

$$M(t) = M(0)\left[1 - \frac{k_B T}{U_{\rm eff}(T)} \ln\left(\frac{t}{\tau_0}\right)\right]. \qquad (6)$$

In these flux-creep measurements, we find that the decay rate $dM(T=50\ \text{K})/d\ln(t)$ at 0.5 T decreases systematically in going from a case a to a case b to a case c film. This indicates that the effective pinning potential $U_{\rm eff}$ increases as the films become structurally better ordered. We thus find that the films with the highest $J_{c,t}$ values also display the highest $U_{\rm eff}$. On the other hand, $J_{c,m}$ may be controlled by the total number of pinning centers or possibly by shallow pinning centers that do not significantly affect $U_{\rm eff}$. The decrease in $J_{c,m}$ with increasing $U_{\rm eff}$ is not inconsistent with recent reports on $Y_1Ba_2Cu_3O_7$ single crystals that show substantial increases in the irreversible magnetization without changes in the effective pinning potential.[45,46,49] It appears that the origin of the differences in $U_{\rm eff}$ between the three types of films studied here is most likely the consequence of a systematic change in the distribution of pinning sites in our films.[50] For example, possibly the number of a specific shallow (low $U_{\rm eff}$) defect center is systematically reduced in going from a case a to a case c film, while the number of deep (high $U_{\rm eff}$) centers remains unchanged or even increases slightly. In such a way one can understand the systematic reduction in the irreversible magnetization with an increase in the effective pinning potential.[47]

V. SUMMARY

In summary we have studied the transport, structural and magnetic properties of *c*-axis-oriented $Y_1Ba_2Cu_3O_{7-\delta}$ thin films grown by an off-axis *in situ* sputtering technique on MgO substrates. We show that by varying the substrate surface preparation prior to deposition, films can be grown that display systematic improvements in their dc transport and structural properties. At the same time, the irreversible magnetization at all temperatures is systematically reduced, thus displaying for the first time an anticorrelation between the transport ($J_{c,t}$) and magnetization ($J_{c,m}$) critical current densities as a function of film microstructure. The anticorrelation can be understood in terms of a systematic reduction of the low-angle and high-angle tilt-boundary defects in the films. It is apparent that the defects play a dual role in determining J_c in the two measurements. While these defects act as flux-pinning sites and increase the irreversible magnetization, these same defects also act as "micro" weak links in the transport measurement thus limiting $J_{c,t}$.

Note added in proof. Since the submission of this manuscript, we have made similar measurements on $Y_1Ba_2Cu_3O_{7-\delta}$ thin films displaying higher transport and magnetic critical current densities ($J_{c,m} \sim 10^7$ A/cm^2 at 14 K) than those reported here. These films also display the same trends in $J_{c,t}$ and $J_{c,m}$ with substrate preparation illustrated in this manuscript.

ACKNOWLEDGMENTS

The authors would like to thank Dr. Ronald Goldfarb for helpful suggestions. We also acknowledge the assistance of Yaoxiong Wu, Rich Burrows, and Sun Warrier during the course of the experiments. This work was supported by NSF Grant No. DMR-89-02836.

[1] S. Jin, T. H. Tiefel, R. C. Sherwood, R. B. van Dover, M. E. Davis, G. W. Kamelott, and R. A. Fastnacht, Phys. Rev. B 37, 7850 (1988).
[2] S. Jin, R. C. Sherwood, E. M. Gyorgy, T. H. Tiefel, R. B. van Dover, I. S. Nakahara, L. F. Scheemeyer, R. A. Fastnacht, and M. E. Davis, Appl. Phys. Lett. 54, 584 (1989).
[3] K. Chen, B. Maheswaren, Y. P. Lie, B. C. Giessen, C. Chen, and R. S. Markiewicz, Appl. Phys. Lett. 55, 289 (1989).
[4] B. Dwir, M. Affronte, and D. Pavuna, Appl. Phys. Lett. 55, 399 (1989).
[5] S. T. Weir, W. J. Nellis, E. A. Early, C. L. Seaman, and M. B. Maple, Physica C 162, 1263 (1989).
[6] X. Z. Zhou, M. Raudsepp, Q. A. Pankhurst, A. H. Morrish, Y. L. Lou, and I. Maartense, Phys. Rev. B 36, 7230 (1987).
[7] M. Affronte, D. Pavuna, O. Martin, F. Licci, T. Besagni, and S. Cattani, Solid State Commun. 70, 951 (1989).
[8] S. Jin, T. H. Tiefel, G. W. Kammlott, R. A. Fastnacht, and J. E. Graebner, Physica C 173, 73 (1991).
[9] R. B. van Dover, E. M. Gyorgy, L. F. Schneemeyer, J. W. Mitchell, K. V. Rao, R. Puzniak, and J. V. Waszczak, Nature 342, 55 (1989).
[10] R. B. van Dover, E. M. Gyorgy, A. E. White, L. F. Schneemeyer, R. J. Felder, and J. V. Waszczak, Appl. Phys. Lett. 56, 2681 (1990).
[11] B. Rosa, B. Hensel, G. Saemann-Ischenko, and L. Schultz, Appl. Phys. Lett. 54, 1051 (1989).
[12] R. F. Cook, T. R. Dinger, and D. R. Clarke, Appl. Phys. Lett. 51, 454 (1987).
[13] K. Char, A. D. Kent, A. Kapitulnik, M. R. Beasley, and T. H. Geballe, Appl. Phys. Lett. 51, 1370 (1987).
[14] H. C. Li, G. Linker, F. Ratzel, R. Smithey, and J. Geerk, Appl. Phys. Lett. 52, 1098 (1988).
[15] P. Chaudhari, R. H. Koch, R. B. Laibowitz, T. R. McGuire, and R. J. Gambino Phys. Rev. Lett. 58, 2684 (1987).
[16] X. D. Wu, A. Inam, T. Venkatesan, C. C. Chang, E. W. Chase, P. Barbox, J. M. Tarascon, and B. Wilkens, Appl. Phys. Lett. 52, 754 (1988).
[17] G. W. Crabtree, J. Z. Liu, A. Umezawa, W. K. Kwok, C. H. Sowres, S. K. Malik, B. W. Veal, D. J. Lam, M. B. Brodsky, and J. W. Downey, Phys. Rev. B 36, 4021 (1987).
[18] U. Welp, W. K. Kwok, G. W. Crabtree, K. G. Vandervoort, and J. Z. Liu, Appl. Phys. Lett. 57, 84 (1990).
[19] C. J. Dolan, G. V. Chandrashekhar, T. R. Dinger, C. Feild, and F. Holtzberg, Phys. Rev. Lett. 2, 207 (1989).
[20] L. J. Moeckly, S. E. Russeck, D. K. Lathrop, R. A. Buhrman, Jian Li, and J. W. Ekin, Appl. Phys. Lett. 57, 1687, (1990).
[21] C. B. Eom, J. Z. Sun, K. Yamamoto, A. F. Marshall, K. E. Luther, T. H. Geballe, and S. S. Laderman, Appl. Phys. Lett. 55, 595 (1989).
[22] C. Blue and P. Boolchand, Appl. Phys. Lett. 58, 2036 (1991).

[23] M. G. Norton, S. R. Summerfelt, and C. B. Carter, Appl. Phys. Lett. **56**, 2246 (1990).
[24] C. B. Eom, A. F. Marshall, S. S. Laderman, R. D. Jacowitz, and T. H. Geballe, Science Rep. **249**, 1549 (1990).
[25] M. G. Norton, L. A. Tietz, S. R. Summerfelt, and C. B. Carter, Appl. Phys. Lett. **55**, 2348 (1989).
[26] C. P. Bean, Rev. Mod. Phys. **36**, 31 (1964).
[27] W. A. Fietz and W. W. Webb, Phys. Rev. **178**, 657 (1969).
[28] T. R. Dinger, T. K. Worthington, W. J. Gallagher, and R. L. Sandstrom, Phys. Rev. Lett. **58**, 2687 (1987).
[29] M. D. Lan, J. Z. Liu, and R. N. Shelton, Phys. Rev. B **44**, 233 (1991).
[30] T. R. McGuire, T. R. Dinger, P. J. P. Freitas, W. J. Gallagher, T. S. Plaskett, R. L. Sandstrom, and T. M. Shaw, Phys. Rev. B **36**, 4032 (1987).
[31] T. W. Peterson and R. B. Goldfarb, IEEE Trans. Magn. MAG-**27**, 1809 (1991).
[32] V. R. Karasik, N. G. Vasil'ev, and V. G. Ershov, Zh. Eksp. Teor. Fiz. **59**, 790 (1970) [Sov. Phys. JETP **32**, 433 (1971)].
[33] H. Kupfer, I. Apfelstedt, R. Flukiger, C. Keller, R. Meier-Hirmer, B. Runtsch, A. Turowski, U. Wiech, and T. Wolf, Cryogenics **29**, 225 (1989).
[34] B. Oh, M. Naito, S. Arnason, P. Rosenthal, R. Barton, M. R. Beasley, T. H. Geballe, R. H. Hammond, and A. Kapiltunik, Appl. Phys. Lett. **51**, 852 (1987).
[35] M. Tinkham, Helv. Phys. Acta **61**, 443 (1988); M. Tinkham, *Introduction to Superconductivity* (Krieger, Melborne, 1975).
[36] J. Mannhart, P. Chaudhari, D. Dimos, C. C. Tsuei, and T. R. McGuire, Phys. Rev. Lett. **61**, 2476 (1988).
[37] N. Savvides, Physica C **165**, 371 (1990).
[38] P. G. deGennes, Rev. Mod. Phys. **36**, 225 (1964).
[39] N. R. Werthamer, Phys. Rev. **132**, 2440 (1963).
[40] J. Clarke, Proc. R. Soc. London Ser. A **308**, 447 (1969).
[41] P. W. Anderson and Y. B. Kim, Rev. Mod. Phys. **36**, 39 (1964).
[42] G. Deutscher and K. A. Muller, Phys. Rev. Lett. **59**, 1745 (1987).
[43] S. Senoussi, M. Oussena, G. Collin, and I. A. Campbell, Phys. Rev. Lett. **37**, 9792 (1988).
[44] H. R. Kerchner, R. Feenstra, J. O. Thompson, J. R. Thompson, D. K. Christen, S. T. Sekula, and L. A. Boatner, in Proceedings of the Materials Research Society Symposium, edited by D. Christen, J. Narayan, and L. Schneemeyer, 1989, Vol. 169, p. 903.
[45] W. Schindler, J. Appl. Phys. **70**, 1877 (1991).
[46] L. Civale, A. D. Marwick, M. W. McElfresh, T. K. Worthington, A. P. Malozemoff, F. H. Holtzberg, J. R. Thompson, and M. A. Kirk, Phys. Rev. Lett. **65**, 1164 (1990).
[47] C. Blue and P. Boolchand (unpublished).
[48] A. M. Campbell and J. E. Evetts, Adv. Phys. **21**, 199 (1972).
[49] M. D. Lan, J. Z. Liu, and R. N. Shelton, Phys. Rev. B **44**, 2751 (1991).
[50] C. W. Hagen and R. Griessen, Phys. Rev. Lett. **62**, 2857 (1989).

In situ preparation of superconducting $Y_1Ba_2Cu_3O_{7-\delta}$ thin films by on-axis rf magnetron sputtering from a stoichiometric target

C. Blue and P. Boolchand[a)]
Department of Electrical and Computer Engineering, University of Cincinnati, Cincinnati, Ohio 45221

(Received 15 October 1990; accepted for publication 10 February 1991)

Superconducting $Y_1Ba_2Cu_3O_{7-\delta}$ thin films have been fabricated *in situ* by *on-axis* rf reactive magnetron sputtering from a single stoichiometric 1-2-3 target. By using high total sputtering pressures (>400 mTorr) and low oxygen pressures (<10 mTorr), negative ion resputtering is almost eliminated and high quality oriented films on (100)MgO are realized with excellent reproducibility. Such films display zero resistance T_c's as high as 88 K with transition widths ΔT_c (90%–10%) of about 2 K, residual resistivity ratios $R(300\ K)/R(100\ K)$ of 2.5, and critical current densities greater than 10^6 A/cm^2 at 14 K.

Currently there are several methods for the growth of high temperature superconducting thin films including sputtering,[1,2] evaporation,[3,4] and laser ablation.[5] Although thin films are produced using each of these techniques, reactive magnetron sputtering using a single composite target has become more popular due to its simplicity. In conventional low pressure (5–10 mTorr) reactive magnetron sputtering the composition of the deposited film is known to be quite different from that of the target. This is due to resputtering of the film by negative ions formed at the cathode (target) during the sputtering process. In the case of YBCO, barium is preferentially removed from the film, followed by copper, and the resulting film can have substantial compositional deviations from the 1-2-3 stoichiometry.[6] This resputtering problem has been solved by various groups using different methods, such as placing the substrate in an off-axis configuration,[7,8] or dc sputtering at very high pressures.[2,9] These methods in general result in rather low deposition rates of about 300 Å/h. To offset this disadvantage, we have chosen to work at very high sputtering pressures, but in an on-axis geometry yielding rather high deposition rates as discussed in this work. Most groups fabricating *in situ* films by conventional rf magnetron sputtering in an on-axis geometry use an off-stoichiometry target (copper rich) to compensate for copper resputtering.[10,11] This latter approach is restrictive in that it requires optimizing the cathode target composition to achieve the desired film composition.

To our knowledge, the present effort constitutes one of the first of its kind to fabricate high quality *in situ* YBCO thin films using conventional rf sputtering from a stoichiometric target in an *on-axis* geometry. We show that by using high total sputtering gas pressures ($P_T>400$ mTorr), low oxygen gas pressures [$P(O_2)<10$ mTorr], and low rf power (<100 W), oxygen resputtering can be nearly eliminated in a conventional rf magnetron *on-axis* deposition configuration. Furthermore, such a method provides rather high deposition rates of 1800 Å/h. We have fabricated smooth, *c*-axis oriented *in situ* thin films of YBCO on MgO substrates with T_c onsets between 90 and 92 K and transition widths ΔT_c (90%–10%) around 2 K. The critical currents of the films are found to be above 10^6 A/cm^2 at 14 K.

Stoichiometric $Y_1Ba_2Cu_3O_{7-\delta}$ targets either fabricated in-house or supplied by Superconductive Components Inc. were used. The magnetron sputtering gun (US Gun) housed in a stainless-steel bell jar is typically evacuated to a base pressure of 10^{-7} Torr using a CT-8 CTI cryopump. Substrates are polished (100)MgO single crystals and are heated during deposition to $T_s=600$–700 °C using a Conductus 2 in. high-temperature substrate heater. In all experiments, the substrates are mounted directly centered above the target in an on-axis geometry with a target to substrate distance of 4 cm.

Typical sputtering conditions for films deposited at total sputtering pressures P_T in the range $200<P_T<600$ mTorr with an oxygen pressure of $P(O_2)=10$ mTorr are a substrate temperature (T_s) of 700 °C, an rf power of 60 W, and a dc bias on the target ranging from -100 V (for the 200 mTorr case) to -25 V (for the 600 mTorr case). This gave deposition rates ranging from 2500 to 1500 Å/h, respectively. After each deposition, argon is evacuated from the sputtering chamber and an atmosphere of oxygen is introduced. The substrate temperature is reduced to 500 °C where it is held fixed for approximately 30 min. The substrate heater is then shut off and the samples allowed to cool to room temperature. The samples are then removed from the chamber. The appearance of the films is black and mirror-like with some rougher areas along the edges of the substrates. These films are then analyzed without any post-annealing.

The thickness of the films is measured using an Alpha Step 200 profilometer over 5–50 μm wide lines fabricated using standard photoresist lithography with dilute phosphoric acid as the etchant. Resistance versus temperature behavior is determined using a conventional four-point probe configuration in an exchange gas system using pressed indium contacts. For resistivity measurements, Ag pads are thermally evaporated onto 5–50 μm wide patterned lines. The crystal structure is examined by theta-two theta x-ray diffraction. Rutherford backscattering spectroscopy and energy dispersive x-ray analysis (EDX) are used to determine the composition of the films and scanning

[a)]Also Professor, Department of Physics, University of Cincinnati, Cincinnati, OH 45221

 0003-6951/91/182036-03$02.00 © 1991 American Institute of Physics

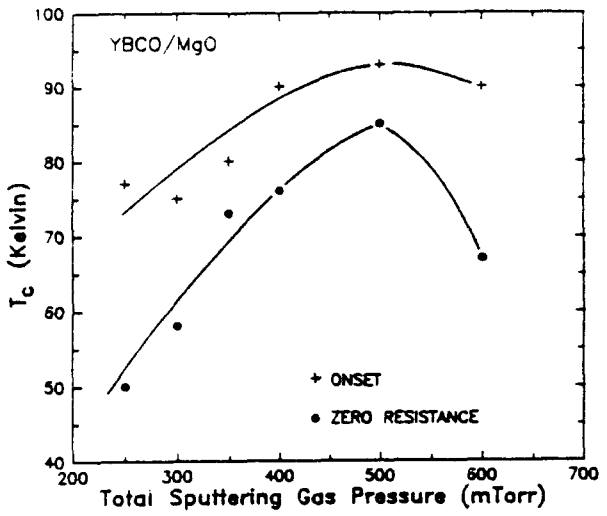

FIG. 1. Total sputtering pressure dependence of T_c(onset) and T_c(zero resistance) for YBCO thin films grown on (100)MgO for case 1. The oxygen gas pressure was kept fixed at 5–10 mTorr.

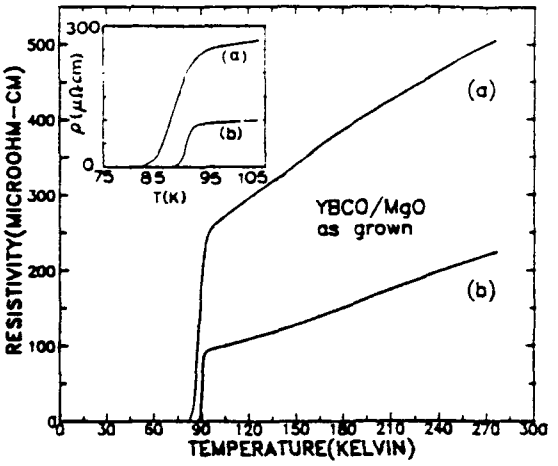

FIG. 2. Resistivity vs temperature of (a) YBCO thin film deposited on (100)MgO for case 1 and (b) YBCO thin film deposited on (100)MgO for case 2. Both films were grown under the optimum conditions of $T_s = 700$ °C and $P_T = 500$ mTorr. Inset affords a better comparison of the resistive transition near T_c.

electron microscopy (SEM) to investigate the surface morphology. A EG&G PAR model 4500 vibrating sample magnetometer coupled to a closed-cycle refrigeration system is used to study the magnetic properties of the films as a function of temperature.

The film quality of magnetron-sputtered films is generally sensitive to the sputtering parameters, such as the substrate temperature, sputtering gas pressure, power, etc. When sputtering in an on-axis geometry, as is our case, the film quality is especially dependent upon the total sputtering gas pressure and the ratio of the argon to oxygen gas pressure. Furthermore, the position at which oxygen enters in relation to the cathode (target) can effect the film quality largely because when oxygen is localized near the substrate, there is a lower probability for it to be ionized and accelerated away from the cathode toward the substrate. It is well known[6] that O^- ions formed at the cathode are accelerated away from the negatively biased cathode and are quickly neutralized in the plasma. The now neutral but energetic oxygen can travel through the plasma and impinge on the substrate where it can resputter material from the growing film. This resputtering effect can be greatly reduced by increasing the plasma pressure which better thermalizes the neutral oxygen by increasing the collision frequency. Also, an increased plasma pressure reduces the negative bias required on the target thus imparting a lesser kinetic energy to the formed O^- ions at the cathode. For these reasons, we investigated two cases in our work. In case 1 the argon and oxygen gases are mixed prior to inlet into the sputtering chamber, while in case 2 the sputtering gas (argon) is localized at the target (cathode) and the reactive gas (oxygen) is localized at the substrate using injection rings.

Figure 1 shows the dependence of T_c on the total sputtering pressure for films grown on (100)MgO for case 1 in which the gases are mixed. The substrate temperature was fixed at $T_s = 700$ °C and only 5–10 mTorr of oxygen was present in each deposition. Films grown at pressures $P_T < 200$ mTorr exhibited semiconducting behavior and showed no T_c down to 14 K (the lower temperature limit of our system). EDX revealed that these films are Ba and Cu deficient most likely due to resputtering by negative oxygen ions formed at the cathode. The highest T_c was obtained for films grown at a total sputtering pressure $P_T = 500$ mTorr. Increasing the pressure beyond this actually degrades film quality (i.e., decreases T_c). The reasons for this are not clear at present. At the optimum pressure of 500 mTorr, the amount of oxygen gas present during sputtering had to be kept very low (5–10 mTorr). Even the presence of only 10% of oxygen (50 mTorr) results in a decreased deposition rate and Ba and Cu deficient films (with T_c's around 60–65 K).

Figure 2(a) shows that R vs T behavior of our best film grown at the optimum conditions ($P_T = 500$ mTorr, $T_s = 700$ °C) for case 1 in which the gases are mixed prior to inlet into the sputtering chamber. The zero resistance T_c is 83 K with a somewhat broad transition width ΔT_c(90%–10%) of 5 K. The residual resistivity ratio ($R_{300\ K}/R_{100\ K}$) of this film is about 2.1 and the resistivity at 100 K is 260 $\mu\Omega$ cm. Figure 2(b) displays the R vs T behavior of a film also grown at the same optimum conditions ($P_T = 500$ mTorr, $T_s = 700$ °C) but for case 2 in which the oxygen is localized near the substrate and the argon near the target. The zero resistance T_c of this film is 88 K with a narrower transition width of 2 K. The residual resistivity ratio is 2.5 and the resistivity at 100 K is 100 $\mu\Omega$ cm.

Figure 3 compares typical x-ray diffractograms for films grown when the gases are mixed [case 1, Fig. 3(a)] and when the oxygen is localized [case 2, Fig. 3(b)] around the substrate. In both cases only (00l) reflections are prominent indicating that both films are highly c-axis ori-

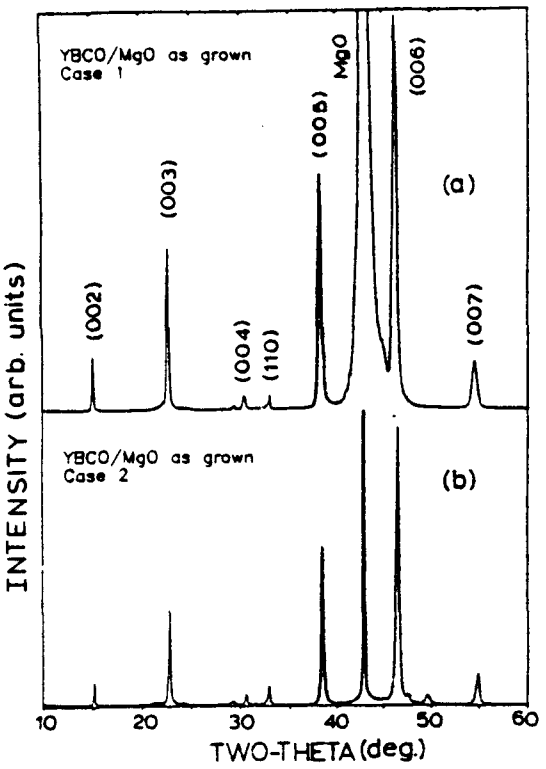

FIG. 3. Typical x-ray diffraction scans for YBCO thin films grown on (100)MgO for (a) case 1, and (b) case 2. Both films were grown under the optimum conditions of $T_s = 700$ °C and $P_T = 500$ mTorr.

ented with the c-axis normal to the substrate. However, a fit of the data shows that the c-axis of the film grown in case 1 is 11.74(1) Å, while that of the film grown in case 2 is 11.69(1) Å. The c-value expected for a high quality film should be nearly that of the bulk material of ~11.68 Å. The larger c-axis of the film grown in case 1 was found not to be due to oxygen deficiency, but rather crystal defects (i.e., stacking faults) resulting from the nonoptimal *in situ* growth. This probably is the reason for the somewhat larger ΔT_c(90%–10%) of 5 K observed for even our best films grown for case 1. Films grown at lower pressures ($P_T = 200$ mTorr) which did not show a T_c continued to display a diffraction pattern characteristic of a mostly c-axis oriented 123 film at $T_s > 700$ °C. The x-ray diffraction peaks of these films are shifted to lower two-theta values giving an even longer c-axis of ~11.9 Å. Overall, we observe that the c-cell length parameter of our films systematically decreases as the total sputtering pressure is increased. The resulting systematic increase of T_c (and overall film quality) with decreasing c-axis length that we observe is very similar to that observed by Muroi *et al.* in their work on rf-sputtered thin films.[12] By localizing the oxygen at the substrate (as in case 2), presumably fewer negative oxygen ions are formed and accelerated across the sheath where they are neutralized and eventually bombard the film. Also, more oxygen is supplied to the film enhancing *in situ* crystal growth.

The critical currents of films grown in case 2 were determined from magnetization measurements using a vibrating sample magnetometer. With an applied magnetic field directed along the c-axis, the critical current density J_c(A/cm^2) was deduced from the magnetization difference Δm at a given field following the Bean critical state model.[13] The zero-field critical current densities for our films at 14 K are found to be $\sim 3\times 10^6$ A/cm^2 and do rapidly decrease near T_c. The value at 77 K was found to be 4×10^4 A/cm^2. The critical currents of these films display a weak field dependence however, and drop by less than a factor of 2 from zero to 1 T.

The surfaces of all our films (those grown in both cases) are smooth and mirror-like. The surface roughness of our films measured with an Alpha Step 200 surface profilometer was less than 25 nm and could be easily patterned to 5 μm linewidths using standard photoresist lithography. SEM investigation of several *in situ* films grown on (100)MgO showed that the surfaces of these films are much smoother than post-annealed films with no apparent granular structure

In summary, we have fabricated high quality *in situ* YBCO thin films on MgO substrates using a conventional *on-axis* rf magnetron sputtering technique from a stoichiometric target. Typical deposition parameters included: $T_s = 700$ °C, $P_T = 500$ mTorr, $P(O_2) = 5$–10 mTorr, rf power of 60 W, and a target dc bias of -30 V. The deposition rates of 2500–1500 Å/h achieved in our approach are significantly higher than those reported by a comparable dc sputtering method or an off-axis rf sputtering method. Our films are found to be smooth and highly oriented with T_c onsets around 92 K and zero resistance T_c's as high as 88 K. The critical current densities are greater than 10^6 A/cm^2 at 14 K.

We are grateful to Professor Ronald Cappelletti, Professor David Ingram, Professor Darl McDaniel, J. R. Gaines Jr., Craig A. Blue, and Mark Phillips for assistance in this work. This work was supported by NSF grant DMR-89-02836.

[1] K. Char, A. D. Kent, A. Kapitulnik, M. R. Beasley, and T. H. Geballe, Appl. Phys. Lett. 51, 1370 (1987).
[2] H. C. Li, G. Linker, F. Ratzel, R. Smithey, and J. Geerk, Appl. Phys. Lett. 52, 1098 (1988).
[3] P. Chaudhari, R. H. Koch, R. B. Laibowitz, T. R. McGuire, and R. J. Gambino, Phys. Rev. Lett. 58, 2684 (1987).
[4] M. Naito, R. H. Hammond, B. Oh, M. R. Hahr, J. W. P. Hsu, P. Rosenthal, A. F. Marshall, M. R. Beasley, T. H. Geballe, and A. Kapitulnik, J. Mater. Res. 2, 713 (1987).
[5] X. D. Wu, A. Inam, T. Venkatesan, C. C. Chang, E. W. Chase, P. Barbox, J. M. Tarascon, and B. Wilkins, Appl. Phys. Lett. 52, 754 (1988).
[6] S. M. Rossnagel and J. J. Cuomo, AIP Conf. Proc. 165, 106 (1988).
[7] W. Y. Lee, J. Salem, V. Lee, C. T. Rettner, G. Lim, R. Savoy, and V. Deline, A.I.P. Conf. Proc. 165, 95 (1988).
[8] C. B. Eom, J. Z. Sun, K. Yamamoto, A. F. Marshall, K. E. Luther, T. H. Geballe, and S. S. Laderman, Appl. Phys. Lett. 55, 595 (1989).
[9] J.-M. Triscone, M. G. Karkut, O. Brunner, L. Antognazza, M. Decroux, and O. Fisher, Physica C 158, 293 (1989).
[10] K. Tanabe, D. K. Lathrop, S. E. Russek, and R. A. Buhrman, J. Appl. Phys. 66, 3148 (1989).
[11] T. Murakami, Y. Enomoto, and M. Suzuki, Physica C 153-155, 1690 (1988).
[12] M. Muroi, T. Matsui, Y. Komuma, Y. Okamura, K. Tsuda, M. Nagano, and K. Mukae, J. Mater. Res. 4, 781 (1989).
[13] T. R. Dinger, T. K. Worthington, W. J. Gallagher, and R. L. Sandstrom, Phys. Rev. Lett. 58, 2687 (1987).